Dissertation

CELLULAR & MOLECULAR REACTIONS OF PRE-OSTEOBLASTS TO DIFFERENT MAGNESIUM IMPLANTS

Submitted by

Sepideh Mostofi

for the Academic Degree of

Doctor of Philosophy (PhD)

at the

Medical University of Graz
Department of Orthopedics and Orthopedic Surgery

under the Supervision of

Prof. Dr. Ute Schäfer
Assoc. Prof. Dr. Annelie-Martina Weinberg

2016

Dissertation

Zelluläre und molekulare Reaktionen von Prä-Osteoblasten auf unterschiedliche Magnesium-Implantate

eingereicht von

Sepideh Mostofi

zur Erlangung des akademischen Grades

Doktor (in) der Philosophie (Ph.D)

an der

Medizinischen Universität Graz

ausgeführt am / an der

Institut / Universitätsklinik für Orthopädie

unter der Anleitung von

Prof. Dr. Ute Schäfer
Assoc. Prof. Dr. Annelie-Martina Weinberg

2016

Statutory Declaration

I hereby declare that this thesis is my own original work and that I have fully acknowledged by name all of those individuals and organizations that have contributed to the research for this dissertation. Due acknowledgement has been made in the text to all other material used. Throughout this thesis and in all related publications I followed the "Standards of Good Scientific Practice and Ombuds Committee at the Medical University of Graz".

Some of the results which are used in this thesis have been already published in Plos one Journal by ***Mostofi et al*** under title of "Effects of Corroded and Non-Corroded Biodegradable Mg and Mg Alloys on Viability, Morphology and Differentiation of MC3T3-E1 Cells Elicited by Direct Cell/Material Interaction.

(Date, Place) (Sepideh Mostofi)

Graz, 21.11.2016

Acknowledgments

I would like to kindly appreciate

Uni.-Prof. Dr. Ute Schäfer who made the accomplishment of my PhD possible and encouraged my new ideas and brought new ideas to my project.

Assoc. Prof. Dr. Annelie Weinberg for being my supervisor and guiding me with valuable information regarding clinical aspects.

Uni.-Prof. Dr. Berthold Huppertz for helping me to continue my studies in the Molecular Medicine PhD program and guiding me with fruitful comments.

Prof. Dr. Regine Willumeit-Römer, head of the Metallic Biomaterials division at Helmholtz-Zentrum Geesthacht for running a project in a very efficient way, organizing workshops and company visits to help us with our carrier development, holding precious discussions related to our project, guiding us in how to work in a team, and for involving us in the most important decisions for our project.

Mag. Ulrike Zefferer who was always reachable, fast, intelligent and a helpful person in our group. I owe a lot to you.

Dr. Scient. med. Clemens Kittinger & his team who let me work in the hygiene department and helped me with technical support and effective discussions.

Prof. Dr. Peter J. Uggowitzer & Dr. Joelle Hofstetter who provided me with a better understanding of material science through their constructive and innovative ideas.

My lab mates Univ.-Ass. Priv.-Doz.- Dr. Silke patz, Muammer Üçal, Dr. Christa Trattnig, Sriveena Srinivasaiah for being nice to me and for their technical and mental support.

Dr. Karin Pichler who deeply supported me with practical work at the beginning of my PhD.

Ehsan Bonyadi Rad who helped me with Western Blot experiments.

Dr. Fernando Warchamico & Dipl.-Ing. Claudia Ramskogler who helped me with scanning electron microscopy analysis in the Department of Material science at Graz Technical University.

Dr. techn. Dipl.-Ing. **Helmar Wiltsche** who helped me with inductively coupled plasma atomic emission spectroscopy in the Institute of Analytical Chemistry and Food Chemistry at Graz Technical University.

Special Thanks to **M. Eng. Björn Wiese** who helped me with material experiments.

Assoc. Prof. Dr. Gerd Leitinger & BSc. Elisabeth Pritz for helping me to perform scanning electron microscopy in the Histology department at Graz Medical University.

The entire staff of the Orthopedic Department, Graz Medical University, especially **Univ.-Prof. Dr.Leithner and Mrs. Paulitsch** and the staff at the ZMF, with special thanks to **Markus Absenger-Novak** for his support, assistance and help with LSM.

Dr. Johannes Eichler & Dr. Elisabeth Martinelli who gave me valuable information from a clinical perspective.

My colleagues within the European Marie-Curie Training Network, with special thanks to **Gabor, Nezha, Maria, Frantisek, Marian, Andrea, Inigo, Silvia, Francesca and Olga** for making my life more beautiful and supporting me with their outstanding knowledge.

Mrs. Regina Rossman for most of the difficult administrative works and for her patience.

My wonderful uncle & aunt **Armand & Jaleh** whose loyal advice made me stronger.

My wonderful friends **Rokhsareh, Elmira, Mahshid, Neda and Farnaz** who supported me in my good and bad moments.

My father-in-law and my mother-in-law **Saeed & Minoo** for their continuous support.

My special thanks to my parents **Enayat & Akram** and my unique brother **Keyvan** for their endless support and love. Thank you for believing in me.

Finally the deepest thanks to my lovely husband **Dr. Siavash Dezfouli** for his endless support. You always inspired me throughout the project.

Table of contents

Abbreviations and Definitions

2-D	**Two-dimensional**
3-D	Three-dimensional
AFM	Atomic force microscopy
ATP	Adenosine triphosphate
ALP	Alkaline phosphatase
B-actin	Beta actin
BMPs	Bone morphogenetic proteins
BSP	Bone sialoprotein
BSE	Back-scattered electrons
cDNA	Complementary deoxyribonucleic acid
CO2	Carbon dioxide
Co-Cr	Cobalt-chromium
CPD	Critical point drying
Col I	Collagen I
DAPI	2-(4-Amidinophenyl)-1H-indole-6-carboxamidine
DMEM/MEM	Dulbecco's modified eagle medium
DNA	Deoxyribonucleic acid
ECM	Extracellular matrix
ECL	enhanced chemiluminescence
EDX	Energy-dispersive X-ray spectroscopy
FBS	Foetal bovine serum
FGFs	Fibroblast growth factors
GAPDH	Glyceraldehyde 3-phosphate dehydrogenase
GPa	Grade point average
HA	Hydroxyapatite
HMSC	Human mesenchymal stem cells
hFOB	Human foetal osteoblasts
HBS	Hank's Balanced Salt Solution
HUCPV	Human umbilical cord perivascular
HRDSR	high ratio differential speed rolling (HRDSR)
ICP-OES	Inductively coupled plasma spectroscopy
IL-1	Interleukin-1
IL-6	Interleukin-6
IIGF-I	Insulin-like growth factor 1
IGF-III	Insulin-like growth factor 3
ISO 10993	International Standardization Organization
µCT scans	Specimens micro-computed tomography scanners
LDH	Lactate Dehydrogenase
L929	Fibroblast L929 mouse cell line
LAE442	Mg-4%Li-3.6%Al-2.4%RE, in wt. %
LB broth	Lysogenic broth
Mg-Al	Magnesium-Aluminum
MC3T3-E1	Mouse osteoblastic cell line
Mg-Ca	Magnesium-calcium
Mg-Cd	Magnesium-cadmium
Mg2Ag	Magnesium-silver
Mg4Y3RE	Magnesium-yttrium-rare-earth

Mg10Gd	Magnesium-gadolinium
Mg10Gd1Nd	Magnesium-gadolinium -Neodymium
Mg-Sr	Magnesium-Strontium
Mg-Zn	Magnesium-Zinc
Mg-Zn-Zr	Magnesium-Zinc-Zirconium
MG63	Human Osteosarcoma cell line
MSCs	Mesenchymal stem cells
MTT	3-(4,5-Dimethylthiazol-2-yl)-2,5-diphenyltetrazolium bromide
MMP 1	Matrix metalloproteinase 1
NaCl	Sodium chloride
NF-kB	nuclear factor kappa-light-chain-enhancer of activated B cells
OP	Osteopontin
OPG	Osteoprotegerin
PVDF	polyvinylidene difluoride
PDGF	Platelet-derived growth factor
PBS	Phosphate Buffered Solution
PTH	Parathyroid hormone
Pure Mg	Pure Magnesium
PBMC	peripheral blood mononuclear cell
RANKL	Receptor activator of nuclear factor kappa-B ligand
RPM	Revolutions per minute
REE	Rare earth elements
RIPA	Radio immunoprecipitation assay
RNA	Ribonucleic acid
RT-PCR	Real-time polymerase chain reaction
RT	Room Temperature
RAW 264.7	Cell Line murine Macrophage from blood
RUNX2	Runt-related transcription factor 2
SF_6	Sulfur hexafluoride
Sa	arithmetical mean height
Saos2	Sarcoma osteogenic cell line
SEM	Scanning electron microscopy
SDS-PAGE	sodium dodecyl Sulphate polyacrylamide gel electrophoresis
Sq	Root mean square height
SP7	Osterix
SBF	Simulated Body Fluid
TNF-α	tumor necrosis factor alpha
TGF-β	Transforming growth factor beta
VEGF	Vascular endothelial growth factor
V/S	Volume/Surface
U2OS	Bone osteosarcoma
Wt%	Weight Percent
WZ21	Magnesium-Zinc-Calcium-Manganese-Yttrium
ZX 50	Magnesium-Zinc-Calcium-Manganese
Zro_2	Zirconium Dioxide

Chemical elements symbols

Ag	Silver
Ar	Argon
Ca	Calcium
Ca-P	Calcium-Phosphate
$CaCl_2$	Calcium chloride
$CaCO_3$	Calcium carbonate
$Ca_3(PO_4)_2$	Calcium Phosphate
Cl	Chlorine
Ce	Cerium
Dy	Dysprosium
Gd	Gadolinium
HCO_3	Carbonate
K	Potassium
KCl	Potassium chloride
La	Lanthanum
Mg	Magnesium
Mn	Manganese
$MgCl_2$	Magnesium chloride
$Mg(OH)_2$	Magnesium hydroxide
MgO	Magnesium Oxide
$MgCO_3$	Struvite
$MgSO_4$	Magnesium Sulphate
$Mg_3(PO_4)_2$	Magnesium Phosphate
$NaHCO_3$	Sodium bicarbonate
Na_2HPO_4	Disodium phosphate
Na_2CO_3	Sodium carbonate
Na	Sodium
Nd	Neodymium
$NaHCO_3$	Sodium bicarbonate
P	Phosphorus
Pr	Praseodymium
PO_4	Phosphate
Sr	Strontium
Zr	Zirconium
Y	Yuittrium

List of Figures

List of Tables

Zusammenfassung

Hintergrund: Hintergrund: Aufgrund ihrer exzellenten klinischen Resultate werden für orthopädische Anwendungen für gewöhnlich konventionelle Implantate wie beispielsweise Kobaltchrom, rostfreier Stahl oder Titan verwendet. Der größte Nachteil dieser konventionellen Implantate ist jedoch, dass sie wieder entfernt werden müssen. Die für die Entfernung der Implantate notwendige zweite Operation ist oftmals mit Komplikationen, wie beispielsweise einem gehäuften Auftreten von pädiatrischem Trauma oder Infektionen, verbunden, die in Folge weitere operative Eingriffe notwendig machen. Konventionelle Implantate besitzen zwar ausreichende mechanische Eigenschaften, können jedoch aufgrund ihres unterschiedlichen Elastizitätsmoduls im Vergleich zum natürlichen Knochen „stress shieldig effects“ verursachen. Um diese Komplikationen zu vermeiden, werden neue Implantate benötigt, die nach dem Heilungsprozess vom Körper resorbiert werden können. Unter diesen biologisch abbaubaren Implantaten zeigen Magnesium-basierte Implantate aufgrund ihrer mechanischen, physikalischen, chemischen und biologischen Eigenschaften das größte Potential. Diesen positiven Attributen stehen jedoch große Nachteile wie rasche Korrosion oder die massive Freisetzung von Wasserstoffgas gegenüber. Um die Korrosionsrate Magnesium-basierter Implantate kontrollieren zu können, stehen Methoden wie Legieren, Oberflächenbeschichtung, Prä-Korrosion oder Hitzebehandlung zur Verfügung. In der aktuellen Studie wurden prä-korrodierte Magnesium-basierte Proben verwendet, um zu evaluieren, ob die an der Oberfläche geformten Korrosionsablagerungen die Korrosionsrate verlangsamen und ob chemische und strukturelle Oberflächenveränderungen für die umliegenden Zellen von Vorteil sind.

Material und Methoden: Die Abbauprofile von pure Mg, Mg2Ag und Mg10Gd wurden in Zellkulturmedium mit 10% FBS untersucht. Die Korrosionsrate wurde über die Freisetzung von Magnesium-Ionen über die Zeit mittels ICP-OES analysiert. Veränderungen der Oberflächenmorphologie und der chemischen Oberflächenzusammensetzung wurden mittels Rasterelektronenmikroskopie mit EDX bestimmt. Der Effekt der Oberflächenmodifikation auf die Zellviabilität wurde durch Kultivierung von MC3T3-E1 Zellen auf 1, 2 oder 3 Tagen korrodierten Proben untersucht. Die Zellmorphologie auf diesen Oberflächen wurde mittels F-actin Färbung und Rasterelektronenmikroskopie analysiert. Die stimulierenden und inhibitorischen Effekte der von den pure Mg, Mg2Ag und Mg10Gd Extrakten stammenden Magnesium-Ionen auf Prä-Osteoblasten wurden mittels MTT Assay mit und ohne pH-Wert Anpassung untersucht. Die Expression zweier osteogenen Marker (Collagen I und Runx2) wurde

auf nicht-korrodierten Proben mit längerer Immersionszeit (bis zu 12 Tagen) mittels Western Blot und Immunozytochemie evaluiert. Die antibakterielle Aktivität von Mg2Ag, Mg4Ag und Mg6Ag wurde unter Verwendung der beiden verbreitetsten Mikroben-Spezies (*S. aureus und S. epidermidis*) für bis zu 3 Tagen Kultur mit dem Bio-Screen Gerät gemessen.

Resultate: Sowohl Mg2Ag als auch Pure Mg zeigten ein ähnliches Korrosionsverhalten. Nadelförmige Kristalle konnten nach 3 Tagen Immersion auf der Oberfläche des Implantats gefunden werden und bedeckten die gesamte Oberfläche beider Materialien nach 8 Tagen vollständig. Auf der Oberfläche von Mg10Gd gab es zu keinem Immersionszeitpunkt einen Hinweis auf Kristallbildung. Der hohe Prozentsatz von Calcium und Phosphor, die sich an der Oberfläche dieses Materials (Mg10Gd) anlagern, kann diese Kristallbildung unterdrücken. **Ionenausstoss:** Die Kristalle, welche sich nach 3 und 8 Tagen auf den pure Mg and Mg2Ag Implantaten bildeten, wurden als stabile Korrsionsprodukte gewertet, welche das Material aktiv vor weiterer Korrosion schützen können. Auf dem Mg10Gd Implantat konnte diese Ionenfreisetzung nicht beobachtet werden, da ein kontinuierlicher Mg-Ionen Ausstoß während der ganzen Immersionszeit stattfand. **Zelluläre Reaktionen:** Die Prä-Korrosion des Materials verbesserte das Zellverhalten (Viablilität oder Morphologie) im Vergleich mit dem nicht-korrodierten Material nicht. Eine verlängerte Prä-Korrosion (3 Tage) führte speziell auf der Oberfläche von pure Mg und Mg2Ag zu einem erhöhten Zelltod. **Metabolische Aktivität:** Eine geringe Konzentration von Mg, welche bei allen Implantatsorten vorhanden war, hatte einen stimulatorischen Effekt auf MC3T3-E1 Zellen, während eine hohe Konzentration einen negativen Effekt hatte. **Genexpression:** Die Zellen zeigten im Vergleich zur Kontrolle eine stetige Hinunterregulierung, wenn sie bis zu 12 Tage auf pure Mg und Mg2Ag kultiviert wurden. Eine ähnliche Hinunterregulierung wurde auch bei Kultivierung auf Mg10Gd beobachtet, allerdings erreichte am Tag 12 das oesteogenische Potenzial der Zellen den Normalwert vergleichbar mit jenem der Kontrollzellen. **Antibakterielle Aktivität**: Alle Silber-enthaltenden Mg-Implantate zeigten eine gute, antibakterielle Aktivität schon in niedrigen Konzentrationen, jedoch zeigten gesteigerte Silberkonzentrationen keine gesteigerte antibakterielle Aktivität.

Schlussfolgerung: Mg10Gd Legierungen zeigten den homogensten Abbau. Außerdem war es das vielversprechendste Material in Bezug auf Biokompatibilität.

Abstract

Background: Due to the excellent clinical out-come of conventional bone implants such as Cobalt chromium, Stainless steel and Titanium, they are commonly used in orthopedic applications, however the need of implant removal can be pointed out as their major drawback. Secondary operation for implant removal might be associated with some clinical disorders such as increased occurrence of pediatric trauma and post-operational infections which might highlight inquiry for surgical interventions. Although these implants possess sufficient mechanical poperties but due to the noticeable difference between their elastic modulus as compared to the natural bone they have high tendency toward so called "stress shielding effects". In order to avoid these complications during bone surgeries, new set of implants which can resorb after accomplishment of healing process is needed. Among biodegradable implants, Magnesium based implants showed suitable potential, due to their proper mechanical, physical, chemical and biological properties. However, in spite of their adequate qualification as bone implants, their fast corrosion rate and vast hydrogen gas release can be considered as a big disadvantage. Several methods such as alloying elements, surface coating, pre-corrosion and heat treatment can be applied in order to control the corrosion rate of these implants. In this study, Mg based samples were experienced pre-corrosion, in order to be further evaluated whether corrosion deposits form on the surface can slow down the corrosion rate and also chemical and structural alteration of the surface can be beneficial for the cells.

Material and methods: Degradation profile of Pure Mg, Mg2Ag and Mg10Gd was studied in cell culture medium supplemented with 10% FBS. The corrosion rate was analysed based on evaluation of Mg ion release over time with ICP-OES method. Alteration in surface morphology and surface chemical elemental composition was determined by scanning electron microscopy equipped with EDX. Effect of surface modification on viability of the cells was identified by cultivation of MC3T3-E1 cells on 1, 2 and 3 days corroded specimens. Moreover morphology of the cells were analysed on these surfaces by F-actin staining and scanning electron microscopy. The stimulatory and inhibitory effect of Mg ions derived from Pure Mg, Mg2Ag and Mg10Gd extracts on pre-osteoblast cells were analysed by MTT assay with and without pH adjustment. Expression of two osteogenic markers (Collagen I and Runx2) was evaluated on non-corroded specimens at longer immersion times (up to 12 days) by western blot and Immunocytochemistry. Antibacterial activity of Mg2Ag, Mg4Ag and Mg6Ag was assessed towards two most prevalent microbial species (*S.aureus* and *S. epidermidis*) up to 3 days of culture with Bio-screen device.

Results: Both Mg2Ag and Pure Mg were shown similar pattern of corrosion. Needle shape crystals were detected at day 3 of immersion which were covered the surface of both materials entirely at day 8. There was no evidence of crystal formation on the surface of Mg10Gd at any immersion time. High atomic percentage of Calcium and Phosphor adsorbed to the surface by this material (Mg10Gd) can suppress the surface from crystal formation**. Ion release:** Crystals formed on the surface of 3 and 8 days corroded Pure Mg and Mg2Ag was considered as stable corrosion products which can actively protect the surface from further corrosion. This ion release pattern was not observable in Mg10Gd as a result of continuous Mg ion release during the whole immersion time. **Cellular Reaction:** pre-corrosion of materials in cell culture medium did not improve cellular behavior (viability and morphology) as compared to the non-corroded control. Prolonged pre-corrosion (3 days) resulted in significant cell death especially on the surface of Pure Mg and Mg2Ag. **Metabolic activity:** Low concentration of Mg derived from all specimens had stimulatory effect on MC3T3-E1 cells, while high concentration seemed negatively influence the cells. **Gene expression**: The cells showed steady down-regulation as compared to the control when cultured on Pure Mg and Mg2Ag up to 12 days. Although similar down-regulation was observed when the cells were cultured on Mg10Gd, but at day 12, the osteogenic potential of the cells came back to the normal level (comparable to the control). **Antibacterial activity:** all silver containing Mg implants exhibited suitable antibacterial properties at low dilutions; however increase in silver content did not result in increase of antibacterial activity.

Conclusion: Mg10Gd alloy showed the most homogenous degradation. Furthermore it was the most promising material in respect of biocompatibility.

1. Introduction

Biomaterials in clinical applications

Increased occurance of clinical problems such as pediatric trauma and postoperative infections elevated the requirement for suitable medical implants which can assist the healing process of the bone (1, 2).

Other clinical disorders such as Trauma, arthritis and tumors can cause bone defects requiring surgery to replace or remove lost bone (3-6). Several methods, including autografting, allografting and bone graft replacement, help surgeons to repair regions of bone loss (7-9). It is also possible to eliminate diseased bone and instead insert metallic implants (prostheses) (10). Implants used to replace diseased bone must remain in the body permanently (10). Implants used to facilitate healing, in contrast, remain in the body only temporarily until completion of the healing process (11).

In general, implants which are used for orthopedic applications must possess key mechanical properties, including hardness, elastic modulus, tensile strength and fatigue strength (12-15). They must, furthermore, exhibit high corrosion resistance (16), biocompatibility (17, 18) and provide a favorable platform for new bone formation (19, 20).

Implants for medical applications can be polymers, ceramics, composites or metals. Polymer-based implants generate good bioactivity and biocompatibility, but, due to their inappropriate mechanical properties, cannot be considered as suitable material in orthopedic applications (21, 22). Metals have high impact among other implants due to their suitable mechanical properties and optimum strength and can therefore be used in orthopedic and maxillofacial applications (23). They can also be applied as fixation devices, such as bone plates and screws, joint replacements, dental implants and coronary stents (24, 25). Two types of metal implants are commonly used in clinical applications. Implants of the first of these types are made using non-biodegradable conventional biomaterials. Cobalt-Chromium, stainless steel, Titanium and Titanium alloy implants are the most widely used non-resorbable implants in bone surgeries (26-31). Whilst these implants possess excellent mechanical properties, their high elastic modulus which can cause stress shielding effects, might be considered to be their major weak point (Table 1). These implants can, moreover, also release toxic ions, which can cause problems including advanced inflammatory reactions, neurological disease and implant instability (32-38). The high risk of inflammatory reactions resulting from the release of toxic ions, and stress shielding effects in many cases necessitate implant removal (37, 38). The associated secondary operation is

however costly and life threatening, especially for older people. These drawbacks of non-resorbable biomaterials have spurred the development of a new generation of implants (39). Alternative biodegradable implants exhibiting a high level of biocompatibility and possessing osteointegration properties have become a topic of interest over last decades (40, 41). These biodegradable implants must, moreover, possess mechanical and anti-corrosive properties comparable to the non-resorbable implants.

Biodegradable implants undergo gradual corrosion in the body and eventually disappear after completing their task of assisting the bone healing process (42). These implants must therefore largely comprise of elements which can be easily metabolized by, and generate suitable corrosion properties in the body. Recently developed biodegradable metals are largely based on three principle metals, namely Magnesium, Iron and Zinc. The work presented in this thesis focused on biodegradable Magnesium implants.

1.1 Biodegradble Magnesium implants

1.1.1 History of Biodegradable Mg implants

The history of bioresorbable Magnesium implants extends back to 1833 when Michael Faraday produced metal implants by electrolysis of dried $MgCl_2$ (43). Later, in 1852, Robert Bunsen produced Mg commercially using a similar method (43). In 1878, Edward C. used Mg wires as as tourniquet in order to cease bleeding of vessels in a few patients and concluded that degradation of Mg proceeded more slowly under in vivo conditions. He furthermore reported that complete degradation of Mg wires is dependent on specimen size. Another clinician who introduced bioresorbable Mg implant to the vast surgical area was Erwin Payr from Graz, Austria. In 1898 he received different types of biodegradable Mg implants in the form of plates, sheets, wires and nails from the Rohrbeck Company in Vienna. In 1900 he conducted clinical studies with these implants in-vivo and concluded that tissue oxygen and water levels, $C0_2$ level, cellular chemical mechanisms and blood soluble salt content are the main factors controlling degradation of Mg in-vivo. Albin Lambotte developed animal investigations and clinical trials of Mg implants. He observed rapid corrosion of pure Mg plates used to fix a cortical bone fracture in combination with steel screws and massive release of Hydrogen gas bubbles, but confirmed the biocompatibility of pure Mg. He discovered that using Mg implants with other metallic implants such as iron and stainless steel cause electrolytic corrosion (43). As his next step he decided to treat supracondylar fractures using Mg implants. Assisted by his colleague Jean Verbrugge he

operated on 4 children (aged 7-10). Apart from a formation of gas cavities which disappeared after several weeks, he did not recognize any other complications in the healing process of the fractures (43). McBride, continuing the survey of Jean Verbrugge in 1938 observed higher corrosion resistance of Mg screws compared to Mg plates, since the shape of these implants enables tighter fixation in the cortical bone (43, 44). In 1948, Troitski and Tsitrin, working on materials made of Mg-Cd alloys used Mg-Cd screws and plates to treat pseudarthrosis and observed appropriate callus bone formation with complete implant resorption (43, 45). Whilst most of the mentioned investigations revealed that Mg-based alloys do not exhibit any cytotoxic effects and stimulate the healing process of the bone, the rapid corrosion of pure Mg and combined alloying elements make it incompatible with the time required for bone healing (minimum 12 weeks). Further studies focused on increasing the corrosion resistance by optimizing the type and concentration of the alloying elements in Mg implants are therefore needed (46). The ultimate aim of all in vitro and in vivo studies is to provide a material with appropriate mechanical properties and optimized degradation behavior which can be used in medical applications. Usage of Biodegradble Mg implants in human clinical trials started in 2015. In a survey conducted by Plaas et al, 22 patients with Hallux valgus deformity and a distal metatarsal osteotomy were treated using Mg implants (MAGNEZIX screw, Syntellix GmbH) (47). All cases exhibited fast healing, except for one with traumatic dislocation of the osteotomy. Although Mg-based implants have been used in clinical trials, further studies addressing the mechanism of degradation at the implantation site as well as the physiological effect of degradation must be further analyzed.

1.1.2 Why Magnesium has been used as a main element in the composition of biodegradable implants

1.1.2.1 Role of Mg in the body

Magnesium is one of the important cations and ranks as the fourth most abundant cation in the body (48). Half of the total Mg in the normal human body is located in the soft tissues and the rest in the bone (48). Magnesium is essential for several physiological activities in the body, including, for example, energy-production processes (49). ATP is the major unit of energy in human cells (50). Cells require ATP for activities such as protein synthesis, cell division and transportation of substances across cell boundaries (50). Without sufficient Magnesium, our bodies are unable to convert nutrients such as fatty acids, glucose and amino acids to energy units usable by cells. Nadler et al reported regulation of the LTRPC7 divalent cation channel (required for cell viability) by Mg-ATP which shows an important role of Magnesium in cell viability (51). Enzymes are responsible for most of the important chemical reactions in the body. Magnesium is a cofactor of around 300 enzymes in the body (48, 52, 53). It has been reported that Mg plays an important controlling role in both the Krebs cycle and glycolysis (52). In its role as cofactor, Mg regulates the initiation and inhibition of multiple enzymatic reactions, including DNA, RNA, and protein synthesis and the metabolism of glucose and fat (50). Mg is furthermore able to sustain the integrity of DNA (54), the bodies genetic code which plays a central role in cell replication and production of proteins (55). Preservation of DNA stability prevents mutations that can have detrimental effects on cellular behavior. Should mutations, however, occur, Magnesium serves as a cofactor for the repair of the underlying DNA damage (54). Magnesium moreover plays a role in the maintenance of cellular hemostasis (56). Magnesium ions can control the activity of cellular Sodium-Potassium pumps (57). Mg deficiency results in the deterioration of these Sodium-Potassium pumps, which can result in Potassium deficiency (hypokalemia) through Potassium efflux from the cells and excretion of these ions in urine (58). Mg is moreover known to be a Ca^{2+} antagonist able to maintain cellular hemostasis by inhibiting the activity of calcium channels which are mostly present in smooth and skeletal muscle cells (59).

1.1.2.2 Role of Mg in bone metabolism

Mg plays an important role in metabolism of bone matrix and the mineralization process during bone formation, since more than half of the body's total Mg is located in the bone (53, 60).

Mg deficiency can occur in multiple ways, including through decreased intake, reduced intestinal and tubular absorption and the usage of drugs and alcohol (61). Rude et al studied the effect of Mg deficiency on bone metabolism using mouse models. They closely tracked the influence of low Mg levels on mouse metabolism. Their results revealed an increased Ca^{2+} level in mice with Mg deficiency compared to the control group without significant changes in the level of PTH hormone. They further showed a decrease in growth plate diameter and columns of chondrocytes suggesting that Mg deficiency can reduce bone growth (62). They moreover observed a decrease in the size of trabecular bone in the metaphysis region and a significant decrease in the number of the osteoblasts, as well as a noticeable increase in the number of osteoclasts. They also detected a significant increase in inflammatory cytokines such as IL-1 and TNF-α in osteoclasts at days 3 and day 12 respectively, accounting for bone resorption by osteoclasts in mice with Mg deficiency (62). In another study, Bulluci et al reported the effect of Mg deficiency on bone metabolism around titanium implants (63). In their study, Mg deficiency resulted in increased Ca^{2+} and PTH hormone levels. They also reported a significant reduction in bone density in the group with Mg deficiency compared to the control group (63) as well as a noticeable reduction in thickness of cortical bone at the bone-implant interface, showing a marked effect of Mg on bone growth and bone metabolism (63).

1.1.3 Advantage of using biodegradble Mg implants

Bioresorbable Mg implants are deemed a suitable material for orthopedic applications by virtue of their appropriate properties. One of the most important criteria that metallic implants must meet is that their mechanical properties are compatible with those of the target tissue, which is bone in the present case (64). Mg raised great interest amongst orthopedic surgeons due to its appropriate mechanical properties (65). The elastic modulus of Mg implants is 40GPa, which is close to elastic modulus of cortical bone (10-30 GPa)(Table 1), meaning that Mg can therefore be used in orthopedic applications without the risk of stress shielding (66, 67). Stress shielding is a clinical complication which results in implant loosening (68). It can also impair bone healing and, more importantly, induce inflammatory reactions (68, 69).

Table 1. Mechanical properties of various biomaterials and bone tissue.

	Tensile strength[MPa]	Young's Modulus[GPa]	Density [g/cm^3]
Cortical bone	35-283	5-23	1.8-2.0
Cancellous bone	1.5-38	0.01-1.57	1.0-1.4
Stainless steel (316L)	290	193	7.9
Cobalt-Chrome alloy (ASTM F-75)	450	210-250	8.3
Titanium alloy (Ti6Al4V)	895-930	110-114	4.43
Pure Mg	90	44	1.74
WE43	250-277	44-46	1.84
Mg10Gd	69.1-85.4	-	1.88
Mg6Zn	277-281	42.3	1.84
Mg1Ca	75-240	-	1.73

Note: Table compiled using data from references (47, 64, 65)

Metallic implants should not induce cytotoxic reactions in tissues and cells. In general, Mg implants exhibit sufficient biocompatibility; their rapid corrosion rate must, however, be controlled (70-74). Another advantage of using bioresorbable Mg based implants is that Mg is able to stimulate new bone formation (75), as illustrated by a study demonstrating new bone formation around Mg-Zn rods by Hematoxylin and Eosin staining (76). Another study conducted by Li et al, observed formation of new bone around Mg1Ca pins after 90 days by radiographic analysis. Osteocytes and osteoblasts, furthermore, showed high activity around these Mg1Ca pins, demonstrating a positive impact of Mg and Mg alloys on bone cell activity (77). The same findings were made in an in vivo study performed by Kraus et al. who used two Mg alloys, ZX50 and WZ21 (with fast and slow corrosion rates respectively), to evaluate the interaction of bone tissue with Mg implants in the skeleton of growing rats during the degradation period. With ZX50, despite massive Hydrogen gas formation, the bone recovered promptly after complete absorption of the pin with evidence of callus formation. Furthermore, no significant disturbance in function of the bone in direct contact with these implants was detected. As well as maintaining its integrity for more than one month, WZ21 generated appropriate osteo-conductive properties

by increasing bone formation at the implantation site. Hydrogen gas formation, moreover, did not negatively influence tissue formation (Fig 1) (78).

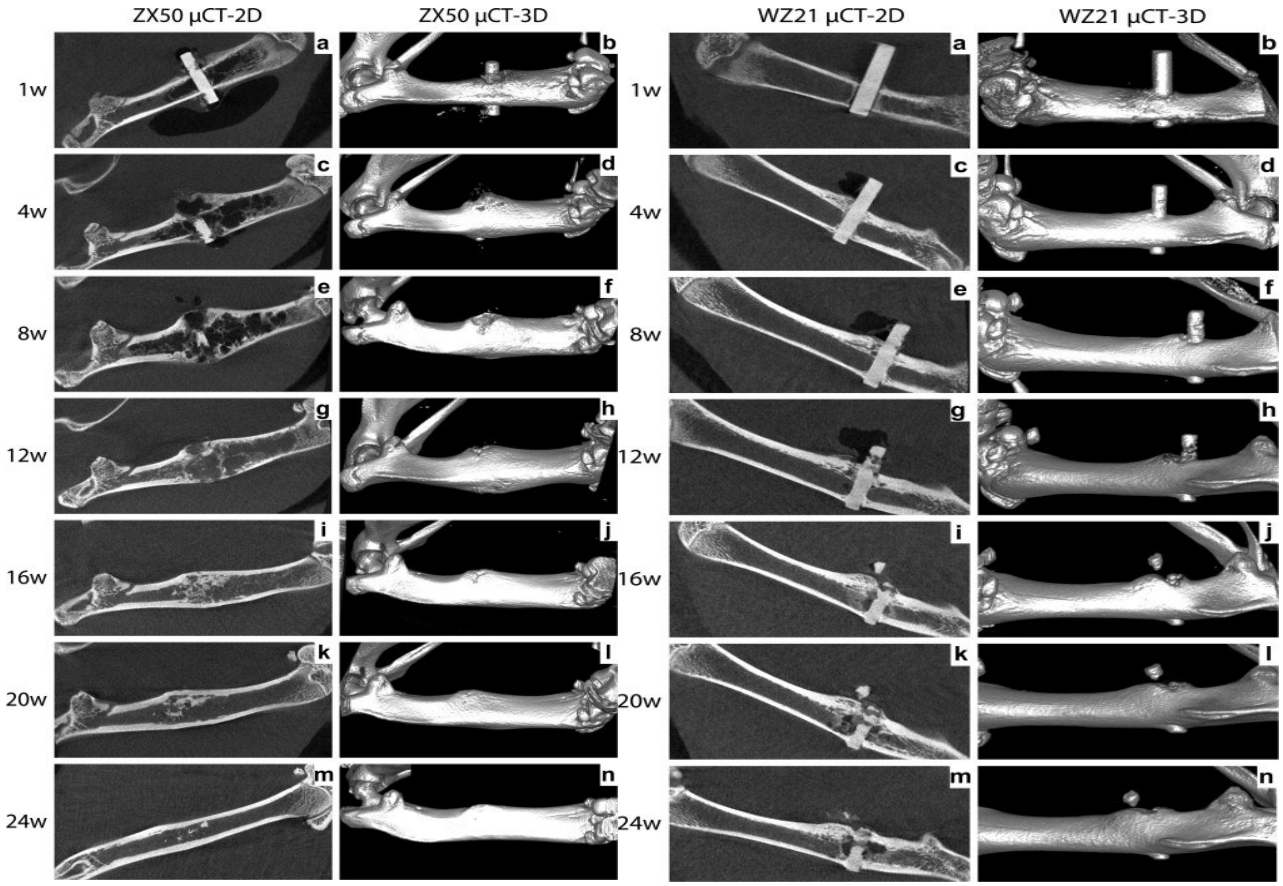

Fig 1. µCT scans demonstrating the degradation process of ZX50 and WZ21 (left and right sides respectively) in both 2D and 3D forms. The bone recovered entirely after complete resorption of ZX50 at week (16 and 24). Despite incomplete resorption of WZ21 even 24 weeks post implantation, the bone recovered fast and completely, with the permission of Acta Biomaterialia Journal (78).

Choosing suitable implants which can undergo self-degradation is of great importance, since it is thereby possible to avoid secondary operations and surgical interventions which might associated with surgical complications such as increased contamination rate and elevated therapy costs. This issue is especially important for children. Whilst broken bones in children heal better and faster than in adults through a process called remodeling, some fractures can induce serious problems for children and block their bones from further growth (79). Any kind of damage caused by fracture of or injury to the growth plate in children can potentially stop the bone from further development and change its function. Children must therefore be treated more carefully in terms of surgical interventions by choosing appropriate implants.

1.1.4 Limitations of using Mg-based biodegradable implants in clinical applications

1.1.4.1 Hydrogen gas production:

Bone is a unit of the skeletal system which mechanically backs up muscles and soft tissues and enables bodily movements (80). Bone furthermore maintains hemostasis of the minerals in the body and participates in energy metabolism (80). When bone is exposed to extensive pressure and stressed conditions exceeding its tolerance level, fractures happen. Several processes are involving in bone healing procedure. The first reaction after bone fracture is the development of blood clots in vessels which attract inflammatory cells including neutrophils, macrophages, lymphocytes and plasma cells (81, 82). Beside their phagocytic role at the fracture site, macrophages play an important role in release of inflammatory cytokines and growth factors such as TGF-β, VEGFs, PDGF, FGFs, IL-1, IL-6, TNF-α, BMPs, IGF-I, IGF-II and macrophage colony stimulating factor. Release of these factors facilitates transportation of mesenchymal stem cells from the periosteum and bone marrow (83-87) and prompt their differentiation into fibroblast, chondroblasts, osteoblasts and angioblasts (84, 85, 87, 88), cells that are essential for tissue reconstruction and regeneration. At the repair stage, growth factors stimulate formation of granulation tissue (81, 88) which is later replaced by avascular cartilaginous callus. Chondrocytes located in this region are able to proliferate and cross the hypertrophic zone and mineralize the cartilaginous matrix (88). Vascularization by endothelial cells and angiogenesis are necessary for the healing process (81, 86, 89). After calcification of the cartilage matrix this is substituted by woven bone (83, 90). At the final stage of healing process, woven bone is remodeled to form cortical and trabecular bone (91, 92) accompanied by continuing neovascularization with the aim of recovering normal bone integrity (see Fig 2) (92).

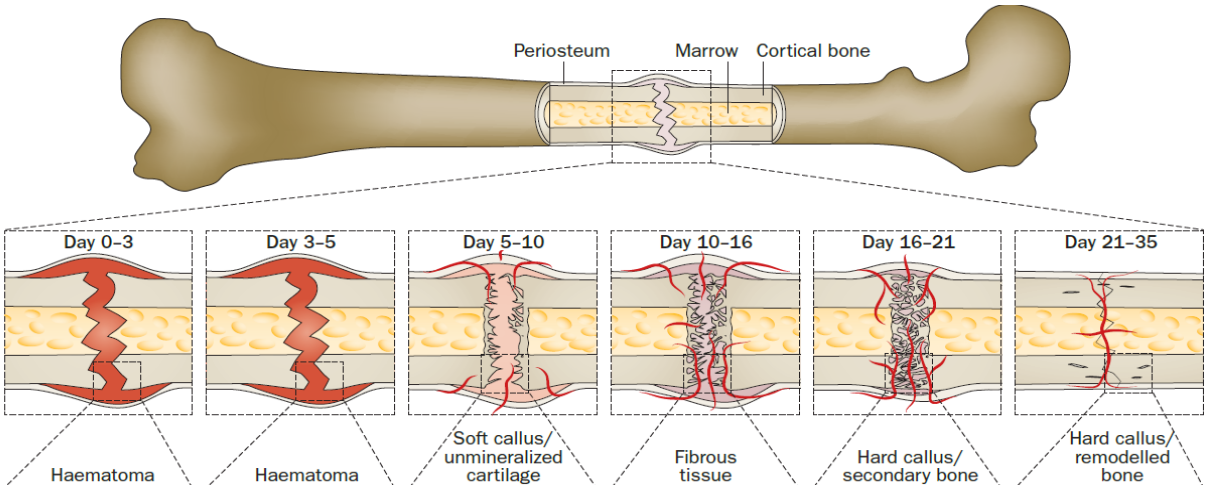

Fig 2. Bone healing phases including hematoma formation, fibrocartilage callus formation, bony callus formation and bone remodeling, with the permission from Nature Reviews Rheumatology Journal (93).

Several factors influence the bone healing process, such as the type of fracture, biomaterials used to fix bone defects and the method of fracture fixation (83, 90). As biomaterials used to fix bone defects, Mg based implants exhibit sufficient osteoinductive properties (94). Mg-based implants are also known to be a proper material for the induction of new bone formation and stimulation bone healing. These implants however undergo corrosion within the body and thereby produce massive amounts of Hydrogen gas which can negatively influence adjacent cells and surrounding tissue (95). Navonia et al conducted a study in order to analyze the effects of Hydrogen gas formation resulting from the degradation of pure Mg implants on the morbidity of rats carrying these implants in their femoral bone for up to 18 days (96). They further analyzed the ability of the rat's body to remove gas bubbles from the implantation site. As an outcome of their study, they concluded that the rat body cannot tolerate rapid, continuous formation of gas cavities. Rat survival declined sharply at day 7 post-implantation and after 18 days of post implantation no rats survived. Rapid H_2 gas release leading to subcutaneous emphysema and modification of the blood cells were considered as the main reasons for the high morbidity between these rats (96). In another study conducted by Wang et al, formation of gas pockets resulting from corrosion of Mg-Zn-Zr implants in cancellous bone of the rabbit did not have any negative effects on bone formation at 12 and 24 weeks post implantation. These cavities were observed to be later filled by new bone and cartilage tissue (97). Myrissa et al detected Hydrogen gas formation in the intramedullary cavity one week after implantation with Pure Mg, Mg2Ag and Mg10Gd implants. Despite a significant decrease in the level of Hydrogen gas formation in bones implanted with Pure Mg and Mg2Ag specimens and new bone formation, 4 and 12 weeks after implantation, the implants did not show any degradation during the entire experimental period (Fig 3) (98).

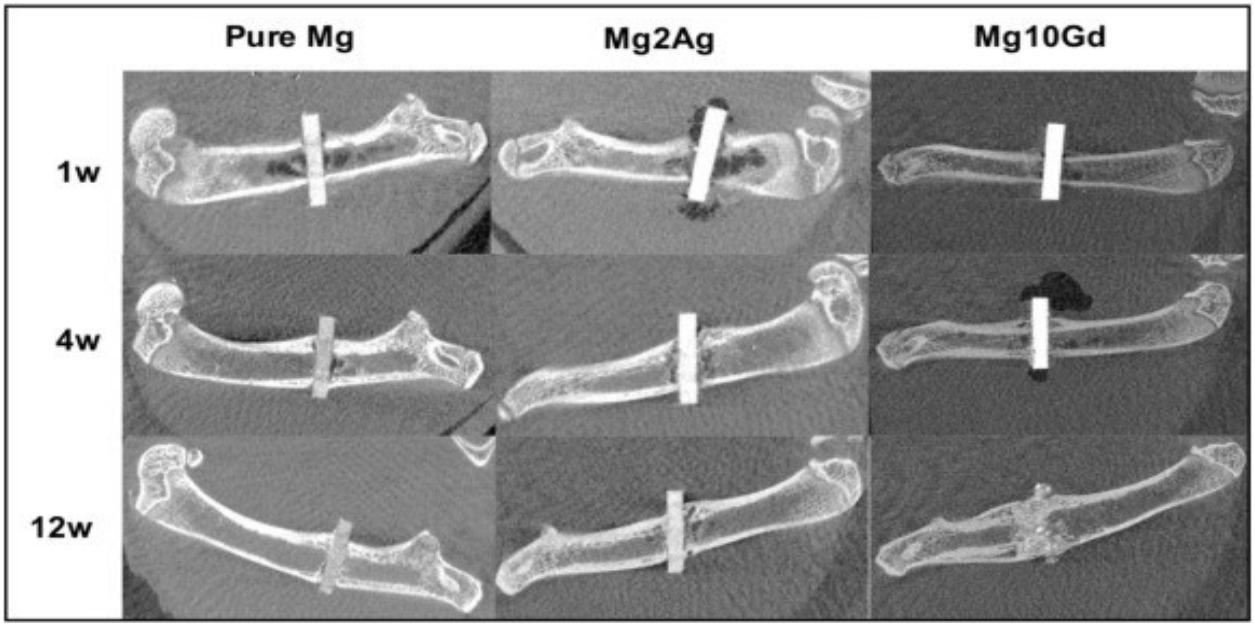

Fig 3. μCT scans (two-dimensional slices) showing the degradation process in the femur bone of Sprague–Dawley® rats at 1, 4 and 12 weeks after implantation, with permission from ELSEVIER (98).

1.1.4.2 Corrosion products

Corrosion products such as $Mg(OH)_2$ derived from the reaction of Mg with water can dramatically increase pH and thereby affect the growth of adjacent cells and surrounding tissue (99-101). $Mg(OH)_2$ is not stable in aqueous solutions and can easily dissolve into Mg ions and hydroxyl groups (65). Positive Mg ions tend to combine with negative chlorine ions and form $MgCl_2$ which is highly soluble (102). It has been reported that chlorine ions are able to break down the passive layer which forms on the surface of biomaterial through corrosion and penetrate into the structure of the metal and cause pitting corrosion (103). The occurrence of pitting corrosion of Mg based implants can result in implant instability.

$$Mg_{(s)} + 2\,H_2O_{(aq)} \rightleftharpoons Mg(OH)_{2\,(s)} + H_{2\,(g)} \quad (1)$$

This overall reaction may include the following partial reactions:

$$Mg_{(s)} \rightleftharpoons Mg^{2+}_{(aq)} + 2\,e^- \text{ (anodic reaction)} \quad (2)$$

$$2\,H_2O_{(aq)} + 2\,e^- \rightleftharpoons H_{2\,(g)} + 2\,OH^-_{(aq)} \text{ (cathodic reaction)} \quad (3)$$

$$Mg^{2+}_{(aq)} + 2\,OH^-_{(aq)} \rightleftharpoons Mg(OH)_{2\,(s)} \text{ (product formation)} \quad (4)$$

(65)

Mg implants that exhibit a slow rate of corrosion within the body are considered to be desirable implants able to exist in the body throughout the entire bone healing process. Since hard tissues like bone require at least 12 weeks to heal, designing an implant which does not absorb before

this, and which exhibit high biocompatibility are therefore crucial (77). The rate of corrosion of Mg implants can be controlled by several processing methods such as applying alloying elements, surface coating and heat treatments (104-119). Pre-corrosion of Mg implants in cell culture medium is moreover known to be beneficial by decreasing the initial corrosion rate of Mg implants (118, 120, 121).

1.1.5 Current modifications of Mg implants designed to control rapid corrosion

1.1.5.1 Alloying

A combining of Mg with other alloying elements can reduce corrosion rate and increase the corrosion resistance of Mg implants. The effect of alloying elements on implant biocompatibility must however be seriously considered (66, 122). Calcium, Zirconium, Zinc, Strontium, Manganese, Silver and rare earth elements are the most common alloying elements used in combination with Mg (123).

Calcium

Calcium is an essential element which exists mostly in the bone. Use of calcium as an alloying element can therefore be predicted to have favorable effects on bone healing after implantation (124). Zhang E et al reported a decrease in grain boundaries of Mg-Zn-Mn alloys by increasing the amount of Ca from 0.3 to 1 Wt. % which subsequently resulted in increased corrosion resistance of Mg-Zn-Mn-Ca alloys (125). Binary Mg-Ca alloys with 2-3 Wt. % of Calcium fabricated by high ratio differential speed rolling (HRDSR) and post-rolling annealing, exhibited smaller grain sizes as well as slower corrosion rate compared to pure Mg (124). Zijian li et al reported high cell viability and fine cellular morphology of cells immersed in 10, 50 and 100% of extracts derived from Mg1Ca implants, which might contribute to the positive effects of Ca^{2+} ions on cell viability (72).

Zinc

Zinc is another fundamental element in the body. This element is normally used in combination with Aluminum in Mg alloys (126). Addition of the Zinc to Mg-Al alloys resulted in a decreased melting point of the Mg-Al binary system which enhanced the corrosion resistance of these materials (127). Several studies have reported a significant decrease in grain size by increasing Zinc content which resulted in increase of corrosion resistance in Mg alloys (128-130). Pompa et al reported a high viability of MC3T3-E1 cells (more than 75%) towards AZ31 and AZ91 extracts which revealed a high biocompatibility of the Zn-containing alloys (131).

Zirconium

Addition of zirconium to Mg implants tends to refine grain sizes (132). It can provide finer microstructure in the binary system of Mg-Zr alloy compared to pure Mg. In terms of biocompatibility, Li et al concluded that addition of Zr to Mg implants can promote cell viability (133). In their study, Mg5Zr demonstrated higher cell viability compared to pure Mg (133).

Strontium

Strontium can induce osteointegration and promote osteoblast differentiation. Addition of Sr has been reported to cause grain refinement (133, 134). Gu et al reported a decrease in grain size of a binary Mg-Sr alloy by addition of 0-5 wt. % Strontium (66). Another study from Li et al however reported that addition of 2-5 wt. % Strontium resulted in adverse effects such as larger grain sizes and reduced corrosion resistance (133). In the study conducted by Gu et al, MG63 cells showed high viability in Mg1Sr and Mg2Sr extracts, showing that these materials exhibit sufficient biosafety. In contrast, the viability of MG63 cells was reduced by treatment with extracts of Mg3Sr and Mg4Sr due to fast ion release and elevated pH resulting from a rapid corrosion of these materials (66).

Manganese

Manganese is a non-toxic element which can be used in combination with Mg due to its grain refinement properties. Young et al reported decreased grain sizes by increasing Mn content up to 3 Wt. % (135) which enhanced the corrosion resistance of these implants.

Rare earth elements

Addition of rare earth elements to Mg implants improves their mechanical strength and enhances their corrosion resistance. The potential toxicity of REE elements and their systemic effects on surrounding tissue must, however, be taken into consideration before addition of these elements as alloying elements to Mg implants and use in clinical applications (136). In order to evaluate whether Mg alloy implants containing rare earth elements exhibit toxic effects on MG63, RAW 264.7 and HUCPV cells, Feyerabend et al prepared chloride forms of the following rare earth elements (Y, Nd, Dy, Pr, Gd, La and Ce) and added different concentrations of these extracts to cells. Notable cell-dependent effects of rare earth containing chlorides were detected in their study. HUCPV cells were recognized to be the most resistant cell line and RAW 264.7 macrophages the most sensitive. Among all examined elements, Ce and La exhibited the highest cytotoxicity, whilst Gd and Dy demonstrated more acceptable results compared to Y (137).

In another study, Elmar Wilbold et al studied the viability of MC3T3-E1 cells after treatment with 10, 50 and 100% dilution of Mg-Ce, Mg-Nd and Mg-La. Mg-Ce extracts were found to impair cell viability of the cells, showing the toxic potential of Ce as a rare earth element. Higher cell viability was detected when cells were treated with Mg-Nd extracts compared to Mg-La. The cytotoxic potential of these implants was moreover detected under in vivo conditions. There was no evidence of systematic disorders and health problems in the animals carrying these implants in their bones. In addition, REE-containing materials did not stimulate any inflammatory reactions. The applied materials showed homogeneous degradation in vivo and no gas cavities were detected during the implantation time (136). In another study, Witte et al, who examined four Mg implants (AZ31, AZ91, WE43 and LAE442) in guinea pig femurs, reported a notable increase in bone mineralization around Mg implants, 6 and 18 weeks post implantation (46)

Alloying elements used in this study

Silver

Silver is able to enhance the mechanical properties and corrosion resistance of Mg implants. In a study conducted by Die tie et al, addition of silver to a binary alloying system (Mg2Ag, Mg4Ag and Mg6Ag) followed by T4 heat treatment, increased corrosion resistance compared to pure Mg (138, 139). Addition of the silver to the cast and T6 treatment, however, generated diametrically opposed results.

Biosafety of Silver

Soluble silver compounds are absorbed more readily than metallic and non-soluble silver compounds (140, 141), and thus exhibit a marked tendency to cause adverse effects on human body in this form (142). Silver normally exists in human tissue only in a trace amounts. Exposure of the body to silver ions may result in acute symptoms such as reduced blood pressure, diarrhea, stomach irritation and decreased respiration (142). Prolonged intake of silver salts at a low dosage result in fatty degeneration of the kidney and the liver, and cause alterations in blood cells (142). In addition, long term consumption of soluble silver compounds can cause argyria or argyrosis (143-145). Silver in different forms is considered not to be toxic for the immune, nervous, reproductive and cardiovascular systems, and it is thought not to be carcinogenic (146). Exposure to both metal and soluble compounds forms of silver is however recommended to be limited to 0.01 mg/m^3 (147).

Silver possesses antibacterial potential which can avoid bacterial contamination during and after orthopedic surgery (138) Silver ions can penetrate bacterial membranes and cause bacterial cell

death by interacting with key proteins and enzymes. As well as possessing antibacterial properties, Silver-containing implants also exhibit good biocompatibility (138). Die Tie et al reported high viability of MG63 cells on Mg2Ag; Mg4Ag and Mg6Ag implants after 72hrs of immersion, showing high biocompatibility of these materials (138). In another study, Cheryova et al reported a beneficial effect of Mg2Ag on cell viability, differentiation and morphology (148).

Gadolinium

Several studies have reported that Gadolinium can be used as a suitable alloying element to adjust the mechanical properties of a vast range of alloy compositions and heat treatments due to its high solubility and capacity to form intermetallic phases. In a study conducted by Hort et al, gradual addition of Gd (2, 5, 10 and 15 wt %) to the binary alloying system Mg-XGd resulted in significantly enhanced mechanical properties. Corrosion behavior is, however, another important factor which must be taken into consideration besides optimum mechanical properties. Hort et al reported improved corrosion behavior with up to 10% Wt Gd. Mg specimens with 15 Wt% Gd exhibited a marked increase in corrosion rate (149).

Biosafety of Gadolinium

Gadolinium is a rare earth element and one of the chemical metal elements of the Lanthanide series. Lanthanides are known as bone seekers due their marked tendency to deposit in bone (150, 151). Gd^{3+} possesses a similar ion radius to that of Ca^{2+} and is able to compete with Ca^{2+} in most of the biological systems which need Ca^{2+} to function appropriately (152). Although many studies have reported a cytotoxic effect of Gd on mammals, the acute toxicity of this element is moderate (153, 154). In a study conducted by Feyerabend et al, Gd was not cytotoxic for osteoblast-like cells showing that Gd can be considered to be an appropriate material for clinical applications (155). In another study conducted by Cecchinato et al, Mg10Gd and Mg4Y3RE were deemed appropriate materials which can positively affect the attachment of HUPCV cells and result in the formation of healthy and well-developed cellular structures (156). Their study, furthermore, documented better cellular distribution and cell morphology on these materials compared to pure Mg (156).

Whilst alloying elements can partially control the high corrosion rate of Mg implants, initial rapid corrosion of Mg remains a problem in the orthopedic field. The designing of new alloying systems, application of novel fabrication and production methods, and increased basic knowledge concerning chemical reaction and degradation of Mg based implants under physiological conditions, are therefore needed (100).

1.1.5.2 Surface coating

Rapid corrosion of Mg implants can also be modulated by coating (157). The main objective of coating is an enhanced corrosion resistance of Mg implants, taking into account the need to simultaneously provide highly biocompatible and bioactive surfaces (157). The many available coating methods include Fluoride coating, Ca-P coating, Ca-P hydroxyapatite coating, $CaMgSi_2O_6$ diopsid coating and ZRO_2 coating (157).

Whilst the aforementioned coatings are highly biocompatible and improve corrosion resistance, sustainability of these coatings on the surface of the materials for longer immersion times is needed in order to maintain the corrosion rate at a desirable level during the corrosion process, necessitating further fundamental studies of the coating methods and of the reaction of the materials with the coating layer (158, 159).

1.1.5.3 Pre-corrosion

Immersion of Mg-based implants in corrosion medium (cell culture medium or SBF) can result in the formation of a passive protective layer able to naturally and actively decrease the initial corrosion rate of Mg and Mg alloys by protecting the surface from further corrosion (118, 120, 121). Pre-corrosion has been reported to decrease the rate of corrosion of pure Mg and Mg10Gd1Nd implants (118). Pre-corroded Mg10Gd1Nd specimens exhibited clearly lower pH compared to non-pre-corroded specimens, whilst there were no noticeable differences between the pH of pure Mg with and without pre-corrosion, showing that the formation of a protective layer cannot absolutely protect the surface from further corrosion (118).

Whilst Ostrowski et al pointed out the positive role of a protective passive layer in reducing corrosion rate, they also admitted that a passivation layer could be attacked by chloride ions which exist in corrosion medium and become subsequently dissociated (158). In this case, corrosion will continue until the next passivation layer forms on the surface and will negatively influence the surrounding cellular and tissue environment (158). Willumeit et al reported that pre-corrosion of Mg-based implants in cell culture medium for 6hrs resulted in the formation of desirable surfaces able to efficiently improve cellular attachment and proliferation. Longer pre-corrosion times (up to 72hrs) provided a beneficial surface for the cells in their study (Fig 4) (118). As in the previously mentioned study, Keim et al concluded that pre-corrosion of Mg samples in cell culture medium (DMEM) can result in the formation of the layer which is highly protective and can elevate the population of Hela cells on the material (160). Cecchinato et al observed similar improvements in terms of cellular responses on Mg10Gd, Mg2Ag and

Mg4Y3RE specimens which were pre-corroded for 48 hrs. (156). Pre-corrosion of Mg samples does not, however, always result in the formation of a fully protective layer. Lorenz et al detected optimum primary cellular attachment on Mg samples pre-corroded in m-SBF medium due to the appropriate surface roughness and Ca-P layer which formed as a protective layer on the surface. They, however, found out that this layer can partly hinder further surface corrosion and that consequent Mg ion release from areas without corrosion deposits was not desirable for long term cell survival (161). As in the study from Lorenz et al, Ngueyen et al detected no significant differences between corrosion performance of D-Mg specimens (pre-corroded for 24h in mTeSR1) and untreated metallic Mg (M-Mg), showing incomplete coverage of the surface with a corrosion layer unable to decrease corrosion rate (162). In another study, Witte et al detected no impact of pre-corrosion on viability of MG63 cells cultured on AZ91D samples compared to non-pre-corroded samples (163). Razavi et al have another theory about the effect of passivation layers and corrosion products on cellular behavior. They deem corrosion products to be a factor which can have detrimental effects on cellular behavior and believe that consequent release of corrosion products from the corroded surface does not provide a favorable surface for cellular attachment due to the marked discrepancy between the corrosion layer and the substrate (117).

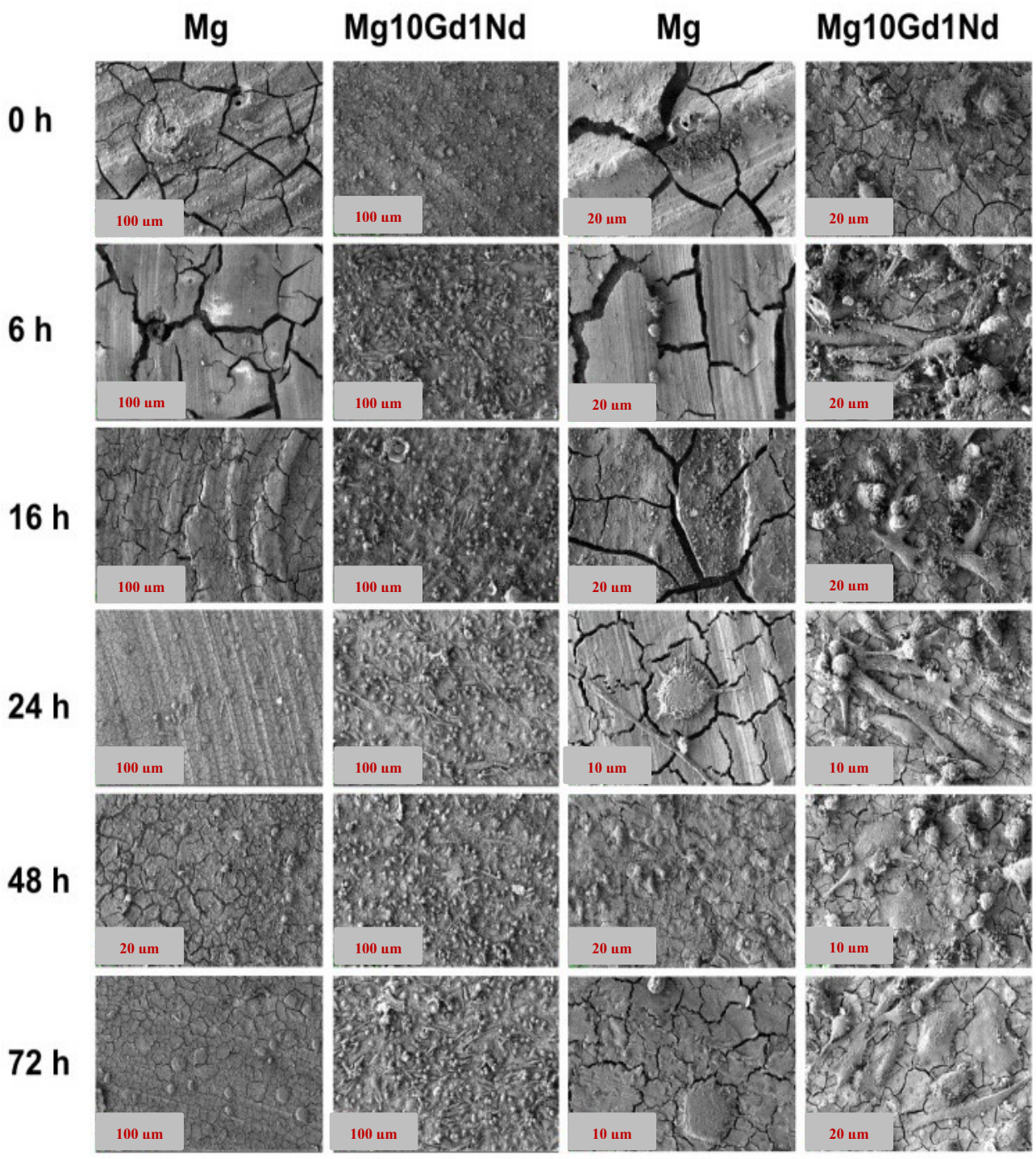

Fig 4. SEM images of Saos-2 cells cultivated on pure Mg and Mg10Gd1Nd with different pre-incubation times, with permission from International journal of medical science (118).

1.1.5.4 Heat treatment

Metal microstructure can be modified by heat treatment. This technique is of great interest since it can markedly alter grain size as well as the formation and/or distribution of intermetallic phases and subsequently enhance corrosion resistance. Smaller and finer grain sizes are known to improve the mechanical properties and decrease the rate of corrosion of Mg-based implants (117). Gu et al applied three different alkali solutions ($NaHCO_3$, Na_2HPO_4 and Na_2CO_3) to Mg-Ca alloys and afterwards heat treated these alloys for 12 hrs. The results of their study demonstrated that alkali and heat treated Mg specimens exhibited higher corrosion resistance than non-treated control specimens. Heat treated Mg-Ca alloys, furthermore, exhibited slower and more homogeneous corrosion. L929 cells treated with extracts of alkali heat treated materials moreover exhibited no evidence of cytotoxicity (164).

1.2 Corrosion and factors which can influence corrosion

1.2.1 Immersion system

Several studies have reported a slower rate of corrosion of Mg-based implants under in vivo conditions than in vitro studies, which can be attributed to the buffering capacity and circulation of the blood inside the body (24, 165, 166). These properties of blood result in the removal of the corrosion products from the implantation site in the body and maintain a physiological pH which can further result in more normal and homogenous degradation (166). The multiple methods available for immersion of Mg-based implants include static, semi static and dynamic systems which can effectively influence the corrosion rate of Mg specimens (104, 122, 167-169). In the static immersion system, the amount of corrosion medium is calculated according to ISO 10993–12 based on the ratio of the surface volume to the surface area (V/S) with a pre-determined medium volume. This set-up is far removed from actual conditions in the body and may result in a significant increase in local pH, saturation of the corrosion medium due to rapid, continuous ion release and precipitation of the corrosion products on the surface. All of these factors can potentially cause discrepancies between in vitro and in vivo results (170). In the semi static corrosion system, part of the corrosion medium is replaced with new medium every few days. Whilst this type of immersion does not faithfully mimic in vivo conditions, it can nevertheless partially avoid corrosion medium loss by evaporation and massive formation of corrosion products on the surface as a result of rapid ion release into the medium (171). Soaking Mg-based implants in a flowing solution is called dynamic immersion. This system of immersion is able to

better mimic the in vivo situation than static immersion. Zhe et al analyzed the corrosion behavior of a Mg-3Sn-0.5Zn alloy under static and dynamic immersion system in Hank's solution. Using the static immersion system, the pH rose to 11 after 5 days and afterwards remained at the same level for up to 30 days of immersion. Similar pH values obtained for specimens in the dynamic immersion system showed that there are no significant differences between static and dynamic immersion systems in this respect. They also detected similar corrosion products ($Mg(OH)_2$ and $CaCO_3$) on the surface of the Mg-3Sn-0.5Zn in both static and dynamic systems. The corrosion layers on the surface of the specimens immersed under flow conditions were, however, more compact and subject to less corrosion attack compared to those on statically immersed specimens. Ion release and weight loss results further confirmed milder and more uniform corrosion of dynamically immersed specimens. Dynamic flow can remove corrosion products which are weakly attached to the surface and leave compact homogeneous corrosion products in place. This layer can protect the matrix of the material from deep pitting corrosion. Dynamic flow immersion can furthermore maintain the pH and chloride ion equilibrium which block the surface from pitting corrosion (172).

1.2.2 Corrosion medium

One of the most important challenges in modeling in vivo conditions is to find an electrolyte solution able to appropriately mimic body fluid (66, 173, 174). Simulating body fluid (SBF), Hank's solution, DMEM, PBS and 0.9% NaCl solution are most widely used as corrosion media in in vitro experiments (175). Mg-based implants have been reported to exhibit divergent corrosion behavior in different corrosion media. Song et al reported higher corrosion current density for AZ91 immersed in Hank's solution than that reported by Yao for 0.9% NaCl solution (176, 177). In another study, AZ91 exhibited different current corrosion densities in similar corrosion medium (m-SBF) showing that even different batches of the same medium can influence the corrosion rate of Mg specimens (178, 179). The study conducted by Yamamoto et al evaluated the degradation behavior of pure Mg in 6 different corrosion media (NaCl, HEPES buffered NaCl, $NaHCO_3$ buffered NaCl, Earle (+), E-MEM and E-MEM supplemented with FBS). The highest ion release was observed in HEPES buffered NaCl and the lowest Magnesium dissolution in E-MEM supplemented with FBS. Formation of insoluble salts on the surface of Mg implants due to the presence of inorganic salts in the corrosion medium is one of the mechanisms which can effectively delay the corrosion of Mg-based implants (175).

1.2.3 Corrosion environment

Another factor which has a significant impact on the rate of corrosion of Mg-based implants is corrosion environment. Yang et al conducted a study in order to elucidate the effect of corrosion environment on the corrosion behavior of Mg-Dy alloys (168). They immersed Mg-Dy alloys in 0.9 NaCl and DMEM+10% FBS at room temperature (RT) under cell culture conditions (21% O_2, 37°C, 5% CO_2) and atmospheric conditions (21% O_2, 37°C, 0.043% CO_2). The lowest corrosion rate in the samples immersed in cell culture medium was observed under atmospheric conditions. Buffering system, addition of proteins and various physiological conditions (such as temperature, amount of O_2 and CO_2) were listed as important factors able to determine the corrosion mechanism in their study (168). Fabrication of the material, sterilization methods, preparation techniques such as sealing, polishing and immersion time of the specimens are other factors which can influence the rate of corrosion and mechanical properties of Mg-based materials (160, 180-183).

1.3 Effect of corrosion on cell viability

Corrosion of Mg-implants is associated with a massive release of ions and elevated pH which can influence cell viability (101, 102). Surface modifications and topographical features which occur during metal corrosion can furthermore affect cellular behavior (116, 184-186). In many studies, cell viability is dependent on the concentration of Mg ions released into the medium during corrosion (187-190). Hanzi et al for example reported that a Mg concentration above 10mM significantly reduces MC3T3-E1 cell viability (189). Similar observations were made with MC3T3-E1, BMSc, U2OS and L929 cells at Mg concentrations of 5mM, 5mM, 35 mM and 15 mM respectively (115, 185, 187, 191, 192). In another study conducted by LL Wu, PBMC cell viability was increased by elevating Mg concentration from 0-25 mM (193). In contrast to the study of LL Wu, Cipriano et al reported that an increase in Mg ion concentration (0-27.6 mM) did not noticeably affect BMSc cell viability. High local pH and intrusive alterations in surface topography were deemed to cause the reduction in cell viability observed in their study (185).

The ways in which cells react to corroding implants does not just depend on the level of Mg ions released into the medium. The type of cells used is also an important factor affecting viability results (192, 194). In the study conducted by Wang et al for example, L929 cells and osteoblasts exhibited optimal viability at a Mg concentration of 35mM derived from pure Mg extracts, whilst the safety level for MC3T3-E1 cells was 15mM (192). Burmester et al observed reduced growth

of osteoblasts, SaoS2 and U2Os at Mg concentrations of 5mM, 10mM and 20mM respectively, showing variable sensitivity of these cells to Mg ions (194).

Medium pH has an important effect on cellular behavior under in vitro condition. In many studies a high rate of corrosion of Mg-based materials resulted in elevated pH levels which is deemed to reduce cell viability (101, 185, 189, 195, 196). F. Seoss et al detected a marked decrease in viability of Hela cells at a pH of 10. They furthermore detected no viable cells at a pH higher than 10, showing a detrimental effect of high pH on cell viability (101). Jiali Wang et al observed similar outcomes with osteoblasts and L929 cells at pH values higher than 8.5. This high pH value, however in contrast, appeared to have stimulatory effect on the growth of MC3T3-E1 and BMSc cells (197).

1.4 Osteogenic differentiation of precursor cells

Mesenchymal stem cells, which exist in bone marrow and the periosteum, are able to differentiate into osteoprogenitor cells which can further differentiate to the osteoblasts. The differentiation process can be divided into three phases, namely cell reproduction, ECM maturation and matrix mineralization. Multiple signaling pathways and factors orchestrate the bone cell differentiation process (Fig 10) (198-200). ECM proteins such as Collagen I, OP, BSP, MMP1, ALP and OPG, as well as transcription factors Runx2 and SP7 are expressed by MSCs during osteogenic lineage development (201-203).

The MC3T3-E1 cell line used in the present study originated from newborn mouse calvarias, and has the ability to differentiate into osteoblasts and undergo mineralization at later stages under in vitro conditions (204). MC3T3-E1 cells (pre-osteoblasts) can express low levels of the early osteogenic markers which are extensively expressed by immature osteoblasts (204). Increased expression of these markers by pre-osteoblasts is an indication of ongoing differentiation (205).

Runx2, an early differentiation marker, is a transcription factor and member of the Runx family. This marker can drive multipotent stem cells to differentiate along the osteoblast lineage at an early stage. It can furthermore enhance the function of ALP and the osteoblast mineralization process (206). Runx2 is able to interact with the promoters of genes such as MMP1, OC, ALP, OP, RANKL, ALP and regulate the expression of these genes (207, 208). The transcription factor Sp7 also plays an important role in the regulation of the osteoblastic genes (208) and has a similar function to Runx2.

ALP is a marker of differentiation which facilitates the mineralization of extracellular matrix (ECM) (203). During the early differentiation phase (up to 14 days), elevated expression of ALP is detectable, whilst at later stages (during mineralization) expression of this marker declines significantly (209). Collagen I constitutes the organic unit of the ECM. Whilst collagen I is found in tissues other than bone, it is one of the dominant constituents of bone extracellular matrix. Expression of this marker by osteoblasts is an indication of mineralized bone matrix and can be considered to be one of the primitive activities of mature bone cells (210-212). Osteopontin and osteocalcin are two non-collagenous ECM proteins. These markers are used as early and late differentiation markers respectively (203, 213). Osteopontin cannot be recognized as a particular bone protein, but plays an important role in cellular attachment and cellular viability through its ability to bind to cell surface integrin (214). Osteocalcin, one of the most abundant proteins in bone, can facilitate bone mineralization by interconnecting to minerals (203). Osteoprotegerin is able to inhibit NF-kB activity by binding to RANKL as a decoy receptor. Interaction of OPG with RANKL can prevent further differentiation of osteoclast precursors to osteoclasts and regulate the resorption of these cells. This process occurs by impeding the interaction of stromal osteoclasts and precursor osteoblasts via RANKL-RANKL receptors (215).

1.5 Methods used to determine magnesium degradation rate in vitro

Evaluation of the pattern of corrosion of Mg implants under in vivo condition provides more detailed and accurate information about these implants than in vitro studies. The high cost of in vivo experiments and ethical issues, however, mandate analysis of the corrosion pattern of these implants under in vitro condition before performing animal studies. Methods for determining the rate of corrosion of Mg implants include potentiodynamic polarization and impedance measurements, hydrogen gas volume measurement, calculation of weight loss and measurement of Mg ion release. In this study, corrosion rate was measured by evaluation of Mg ion release. The correlation between Mg ion release and the rate of corrosion of Mg implants makes it possible to estimate corrosion rate by measuring the number of Mg ions released into the corrosion medium by methods such as inductively coupled plasma spectroscopy (ICP-OES) which is explained in detail in the Materials and Methods section. The influence of cells cultivated on the surface of Mg samples on the rate of corrosion was further evaluated with ICP-OES. Physiologic solutions pH has an important effect on the viability the surrounding cells and tissue. Because the reaction of Mg with water in aqueous solution elevates the pH, it is important to measure the pH at each incubation time point and evaluate the effects of pH on the cells and

tissues. Analysis of the alterations occurring on the surface of Mg implants, as well as detection of chemical elemental composition were performed using scanning electron microscopy equipped with EDX in this study. Factors which can influence material corrosion include corrosion medium, which consists of various proteins, sugars, organic and inorganic salts, and the immersion system employed. Cells can also influence the pace of corrosion (216). In order to ensure that cell cultivation on the surface of implants can influence corrosion rate, MC3T3-E1 cells were cultivated on Mg-based alloys (Pure Mg, Mg2Ag and Mg10Gd) and Mg ion release into the supernatant compared to the ion release by alloys without cells.

Immersion system

In order to measure corrosion rate and pH of the material in both cases (with and without cells), cell culture medium (DMEM) with other additives (including foetal bovine serum) and antibacterial agents (penicillin/streptomycin) were used. All immersion tests were performed under cell culture conditions (37°C, 20% O2, 5% CO2, 95% rel. humidity). The medium was not been changed during the immersion period. All the immersion tests performed in this study for the purpose of corrosion rate evaluation were done with non-corroded materials. Pre-corrosion of Mg samples in cell culture medium prior to cell cultivation has, however, been suggested by many studies, since this method is known to decrease the initial corrosion rate and to facilitate cellular attachment.

Cell Viability and morphology

In order to ensure the effect of corrosion products and surface morphology of the corroded materials on bone cells, Mg-based implants were pre-corroded in cell culture medium for 1, 2 and 3 days. The cells were cultivated on corroded surfaces and viability and morphology of the cells were evaluated by live-dead staining and scanning electron microscopy respectively. Non-corroded material was chosen as a control. Cell viability was also analyzed following longer incubation times (4, 8, 10 and 12 days) on non-pre-corroded samples.

Cell viability following treatment with different concentration of Mg contained within the supernatant of immersed Mg samples (Pure Mg, Mg2Ag and Mg10Gd) was evaluated using 3-(4,5-dimethylthiazol-2-yl)-2,5-diphenyltetrazolium bromide (MTT assay).

Gene expression

In order to evaluate the effect of different alloying systems and corrosion products on bone cell gene expression pattern, MC3T3-E1 cells were cultivated for different times on Mg-based

implants and expression of two of the most important osteogenic markers (Collagen I and Runx2) was evaluated by immunocytochemistry and western blot.

1.6 Bacterial infection

A principal complication of orthopedic surgery which can result in implant failure is bacterial contamination. Bacterial infection during orthopedic surgery may impair the mechanical properties, and eventually result in instability of the implant by loosening the material at the implantation site (217). In some cases of infection implants must be replaced and in severe cases there is a risk of ablation or morbidity (218).

S.aureus and *S.epidermidis* bacterial strains are responsible for a large proportion of implant-associated bacterial infections (219). It has been reported that more than 60% of implant associated infections involve these two strains (219). The ability of these bacteria to form biofilms renders them quite resistant to even the most effective antimicrobial agents (220, 221).

Infectious bacteria existing in surgery rooms, on surgical materials, in the body or on the skin of the patients are a potential source of bacterial contamination (222). Implant-associated bacterial infections are difficult to treat with antimicrobial agents because the most common bacteria in orthopedic surgeries are able to attach to the surface of the implant and form a biofilm at the implantation site (223). Accumulation of bacteria in biofilm structures is extremely life-threatening since they can enter the blood stream and cause chronic infections. Bacterial communities present in biofilms are highly resistant to even the most effective antibacterial agents. The host immune system furthermore struggles to eliminate bacteria present in biofilm form (224).

Generally speaking if infectious bacteria attach to the surface of the implant before completion of the healing process, the host defense system is unable to prevent colony formation and bacterial biofilm formation on the surface. Interception of implant-associated bacterial contamination is extremely important (225, 226).

Implants used for medical applications must possess several properties, including a favorable surface for optimal attachment of bone cells and antibacterial properties. Whilst Mg implants provide an appropriate surface for bone cell growth (186, 227), the antimicrobial activity of these implants needs to be improved (138). Addition of alloying elements to Mg based implants such as silver, which is known to possess adequate antimicrobial properties, can effectively enhance antibacterial activity. Addition of silver can moreover improve corrosion resistance and the mechanical properties of these materials (138).

Hypothesis

Magnesium is known to be a suitable element for the manufacture of bone implants. Due to its chemical reaction with water molecules in the body however it produces a lot of hydrogen gas, which is detrimental for surrounding cells and tissue. We hypothesize that addition of other alloying elements such as Silver and Gadolinium can enhance the corrosion resistance of pure Mg. We moreover expect addition of these elements to the Mg implants to have no adverse effects on bone cells and tissue. Addition of these alloying elements might furthermore enhance corrosion resistance and improve the cellular and molecular behavior of bone cells.

Another method applied in this study to control the corrosion rate was pre-corrosion in cell culture medium. We hypothesize that formation of corrosion products on the surface of the Mg-based implants can improve aspects of cellular behavior such as cell attachment and cell survival.

In this thesis we reason that there is a close correlation between surface chemical composition and cell behavior. We moreover hypothesize that the morphology of the corrosion layer formed on the surface can affect cell adherence and, consequently, cell survival.

Based on our literature search, we expected lower Mg ion release and reduced corrosion rate from Mg implants cultured with cells than from implants without cells on their surface.

Silver-containing Mg-based implants are known to possess antibacterial properties. In this study, we expected to observe a direct relationship between antibacterial activity and increasing implant silver content.

Aim

The principle aim of this thesis was to study the degradation profiles of Mg based implants. The effect of surface modifications on corrosion rate and biocompatibility was also investigated, as was the antibacterial role of silver-containing Mg-based implants.

Specific aims:

- Evaluation of degradation profile including surface modifications and surface chemical elemental composition of pure Mg, Mg2Ag and Mg10Gd under cell culture conditions
- Evaluation of Mg ion release and pH under cell culture conditions
- To evaluate whether pre-corrosion of Mg-based implants has a positive effect on controlling corrosion rate and enhances cell survival
- To study whether cultivation of the cells on the surface of Mg-based implants can reduce the corrosion rate and influence corrosion product formation
- Evaluation of selected short-term cellular response of osteoblasts to Mg-based alloys (cell viability, morphology and proliferation)
- Study the effect of different concentration of Mg and other elements released into cell culture medium during sample corrosion on viability and proliferation of pre-osteoblasts
- Evaluation of long-term cell gene expression responses of osteoblasts to Mg-based alloys
- Study the antibacterial properties of Mg2Ag, Mg4Ag and Mg6Ag versus two prevalent bacterial species (*S. aureus* and *S.epidermidis*)

2. Material and methods

2.1 Material Preparation

Pure Mg (99.99% Mg) and two Mg alloys Mg10Gd (10.5% Gd, Mg Bal.) and Mg2Ag (1.75% Ag, Mg Bal.) were utilized in this survey. The concentrations of Ag and Gd which were used as alloying elements were determined by X-ray fluorescence spectrometry according to weight percentage (Bruker AXS S4 Explorer, Bruker AXS GmbH., Germany) (Table 2).

Table 2. Composition of alloying elements in Mg-based implants, these findings have been published in an original article (216)

Alloy	Composition wt. %					
	Ag	Gd	Fe	Cu	Ni	Mg
Mg	-	-	0.0055	0.003	0.0018	Bal.
Mg10Gd	-	10.5	-	-	-	Bal.
Mg2Ag	1.75	-	0.0022	0.002	0.0013	Bal.

Samples were discs (10mm diameter and 1.5 mm height). Material production involved casting, heat treatment, extrusion, machining and cutting. Material casting was done in HZG-MagIC (Geesthacht, Germany) using pure materials; Mg (99.99%, XINXIANG JIULI MAGNESIUM CO.LTD, China), Gd (99.95%, Grirem Advanced Materials Co., Ltd., China) and Ag (99.99%, ESG Edelmetall-Handel GmbH & Co. KG, Germany). Mg2Ag and Mg10Gd were manufactured by constant mold gravity casting. After melting of pure Mg at a temperature of 720°C, pre-heated alloying elements (Ag and Gd) were added with steady shaking. The melt was then poured into a permanent steel mold treated with Boron Nitride which was pre-heated to a temperature of 550°C. SF6 and Argon mixture was used as a cover gas during the casting process. A 16h solution treatment at 440°C under argon atmosphere was applied to the alloys (T4 heat treatment). Alloys were homogenized with a T4 heat treatment prior to extrusion in an Argon atmosphere at 550°C (Mg10Gd) and at 420°C (Mg2Ag) for 6hr, and afterwards indirectly extruded with an extrusion ratio of 4/25. The temperature of the extrusion machine chamber was adjusted to 370°C and the billets (d = 30 mm) pre-heated for 1hr at 370°C and 430°C for Mg2Ag and Mg10Gd respectively. The extrusion pace was between 3 and 4.5 mm/s. Casting of pure Mg was performed by constant mold direct chill casting. The cast billet (d = 110 mm) was extruded indirectly with an extrusion ratio of 1/84. The extruded billets were afterwards machined and cut into discs.

2.2 Sterilization

The samples used for both corrosion and cytocompatibility tests were sterilized by γ-ray irradiation of 25 kGy. After sterilization and before performing the experiments, all samples were immersed in 70% ethanol for 10 minutes and immediately air dried.

2.3 Determination of material properties after machining

As explained above in part 2.1, the final step of material production was machining. The machine used to cut the Mg rods into plates can affect surface roughness and grain size. It can also cause the formation of secondary phases and segregation of elements and particles. These factors could subsequently influence corrosion rate, and it was therefore necessary to analyze these factors before performing cell and material experiments in order to show that all surfaces possessed more or less similar properties.

2.3.1 Determination of surface roughness

A Contour GT – K Bruker Profilometer using white light interferometry was utilized in order to measure surface topography and roughness specifications in close collaboration with HZG-MagIC (Geesthacht, Germany). Magnification of 5x with 10% overlap was used to enable stitching. [-150 µm to 150 µm] was set as the spectrum between length and back scan. Autoscan was activated in order to stop every stitch after 20 µm of measurement, following collection of 90% of the data. In order to expand the pixels, a threshold of 1% was applied. Software 5.41 was used in order to prepare the data for measurement. Nominal style of the surface was elevated by F-operator “cylinder and tilt”. 3 non-corroded specimens per condition with field of interest of 9.5 mm in diameter were analyzed.

The roughness of each alloy was similar. The surface of Mg10Gd was however slightly smoother than Mg2Ag and pure Mg. Alloying elements which increase hardness produce smoother surfaces, which might explain the slight surface differences between the specimens. In general, the cutting process seemed to be the same for all materials (Fig 5). These results have been published in an original article (216).

A

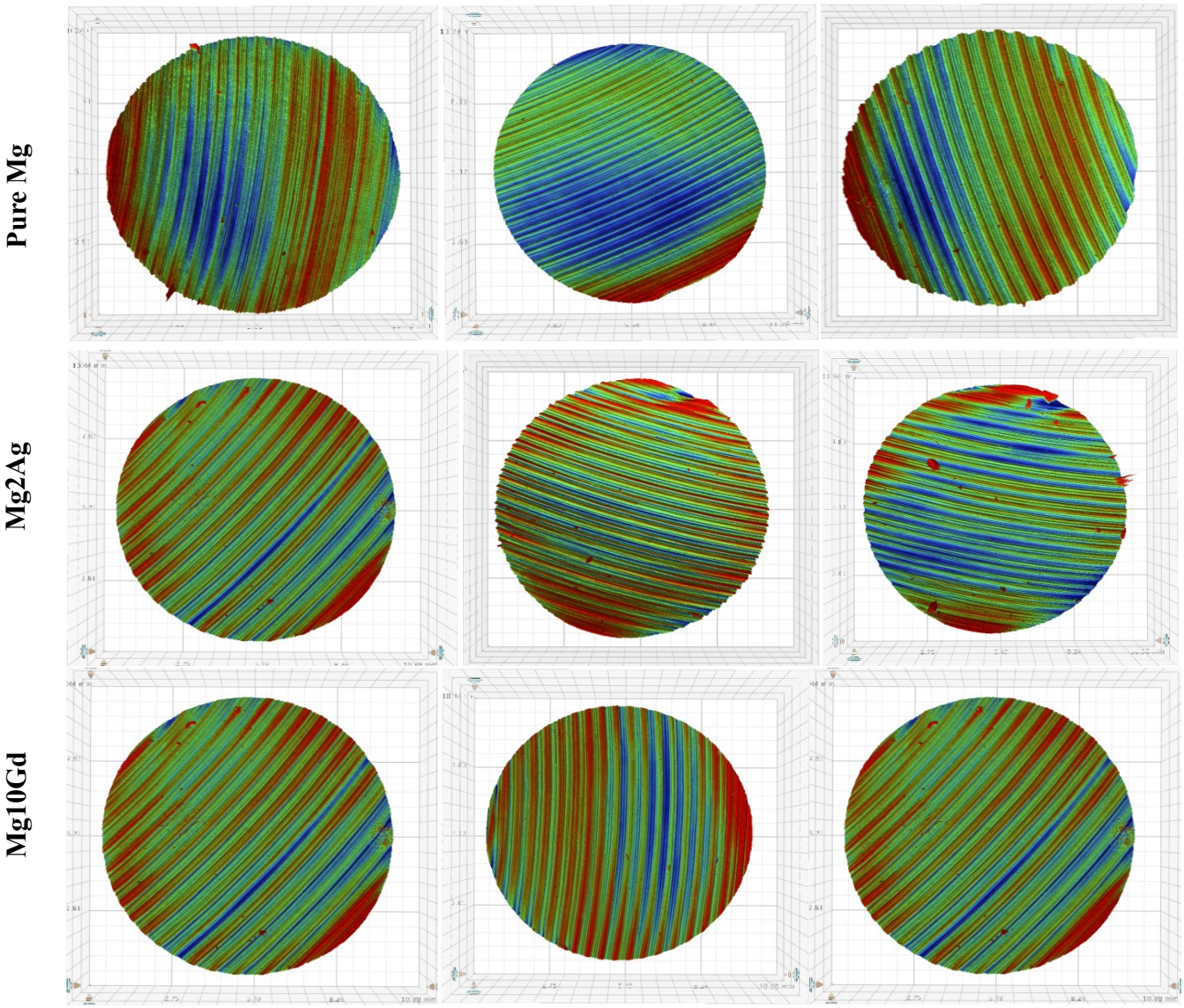

	Pure Mg		Mg2Ag		Mg10Gd	
Sample-Nr.	*Sa [µm]	**Sq [µm]	*Sa [µm]	**Sq [µm]	*Sa [µm]	**Sq [µm]
1	2.02	2.54	1.71	2.23	1.24	1.73
2	2.46	3.24	2.06	2.58	1.53	1.97
3	2.26	2.99	2.12	3.17	1.38	1.77
Average	2.25	2.92	1.96	2.66	1.40	1.83
Standard Deviation	0.22	0.35	0.22	0.47	0.12	0.17

B

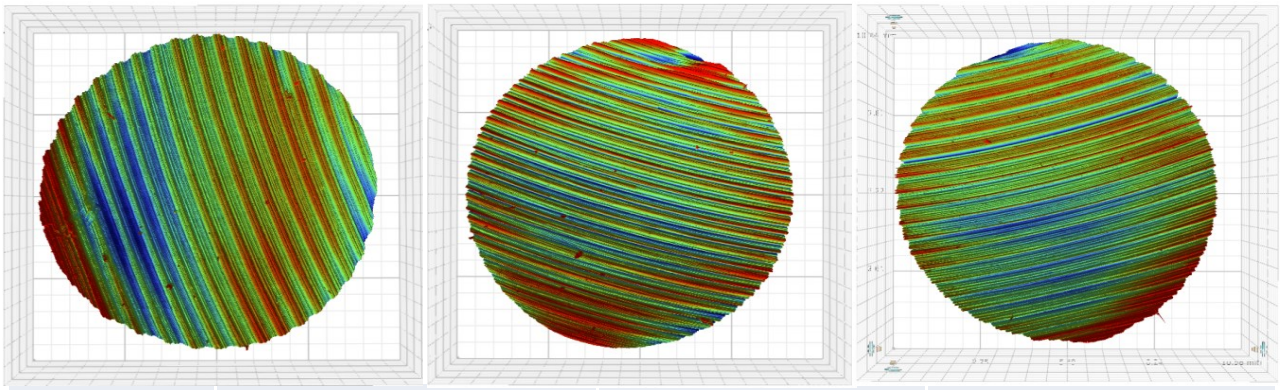

		*Sa [µm]	**Sq [µm]
Pure Mg	Average	2.25	2.93
	Standard Deviation	0.22	0.35
Mg2Ag	Average	1.97	2.67
	Standard Deviation	0.22	0.48
Mg-10Gd	Average	1.40	1.83
	Standard Deviation	0.12	0.13

Fig 5. Surface topography and roughness parameters of pure Mg, Mg2Ag and Mg10Gd discs. Roughness of each alloy was measured by a Contour GT – K Bruker Profilometer using white light interferometry (A) and surface roughness of all three alloys were compared to each other (B). *Sa known as a parameter which is used to define the surface roughness. It is the extension of Ra (arithmetical mean height of a line) to a surface. It shows an absolute value and the difference in height of each point compared to the arithmetical mean of the surface. ** Sq is identical to the standard deviation of heights. It shows the root mean square value of a line. These results have been published in an original article (216).

2.3.2 Determination of grain sizes

Samples for scanning electron microscopy analysis were embedded in epoxy resin, ground with 220-2500 grit Sic paper and polished using a 3 µm diamond suspension, followed by 1µm diamond and an anhydrous OPSTM suspension. An etchant consisting of 140 ml ethanol, 30 ml deionized water, 7 ml glacial acetic acid and 8 g picric acid was used to etch the samples before washing them in ethanol and air drying. An optical microscope equipped with a digital camera was used to observe and record microstructures. Grain sizes were determined by line intercept method. Mean square grain diameter for pure Mg was 38 ±1 µm and similar to Mg2Ag with 40 ±1 µm. For Mg10Gd, the square grain diameter was smaller (27 ±1 µm), but of the same order of

magnitude. All three alloys were compatible in terms of grain sizes (Fig 6). These results have been published in an original article (216).

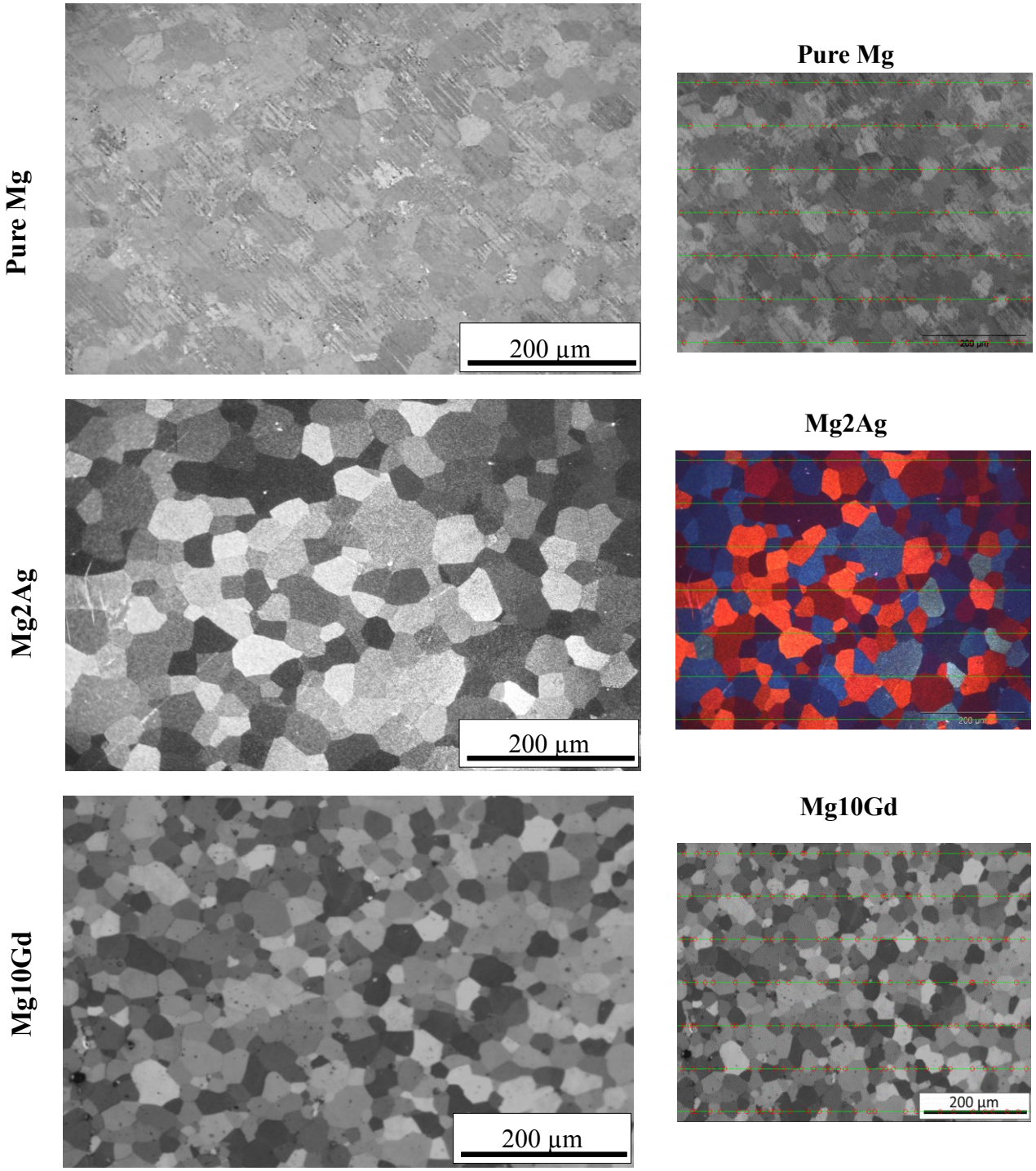

Fig 6. Microstructure of pure Mg, Mg2Ag and Mg10Gd. Microstructures were observed using an optical microscope with a digital camera. Grain size was determined using the line intercept method to calculate the middle square grain diameter. Mg2Ag and pure Mg exhibited similar grain sizes, whilst Mg10Gd showed smaller middle square grain diameter, these results have been published in an original article (216).

2.3.3 Determination of the properties of microstructures

Specimens were prepared for scanning electron microscopy using a procedure similar to that described in part 2.1. Microstructures were investigated with a scanning electron microscope (SEM) in back-scattered electrons (BSE) equipped with energy dispersive X-ray spectroscopy (EDXS) at a working voltage of 20 keV. In SEM-BSE mode and with EDXS, no secondary phases, segregation of elements or particles were detected in pure Mg and Mg2Ag samples. Mg10Gd, however, exhibited an irregular distribution of Gd, visible in SEM-BSE figures as contrast differences (Fig 7). The bright areas in the microstructure contained 10.2 ± 1.1 wt. % Gd and the dark areas 4.5 ± 1.2 wt. % Gd. These results have been published in an original article (216).

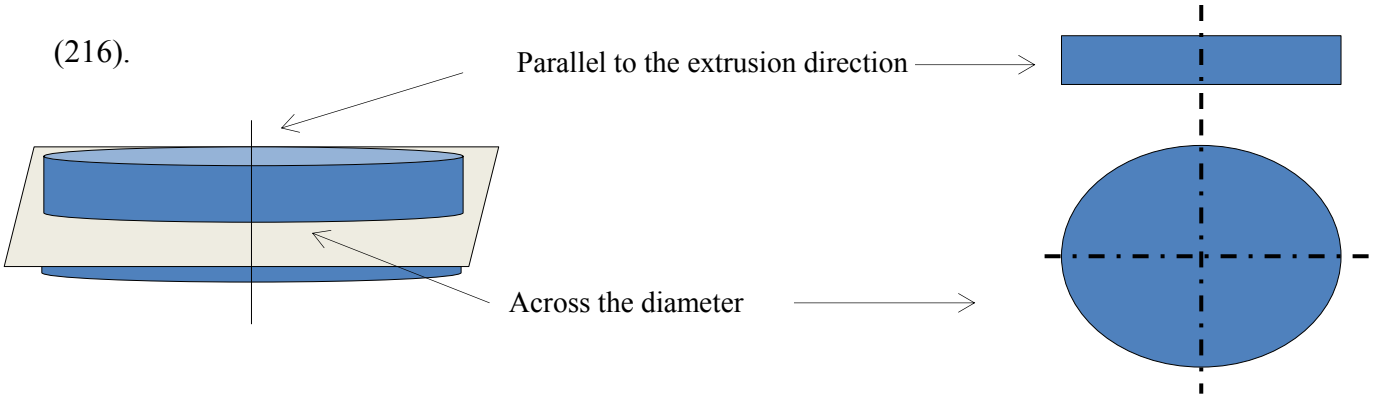

Pure Mg

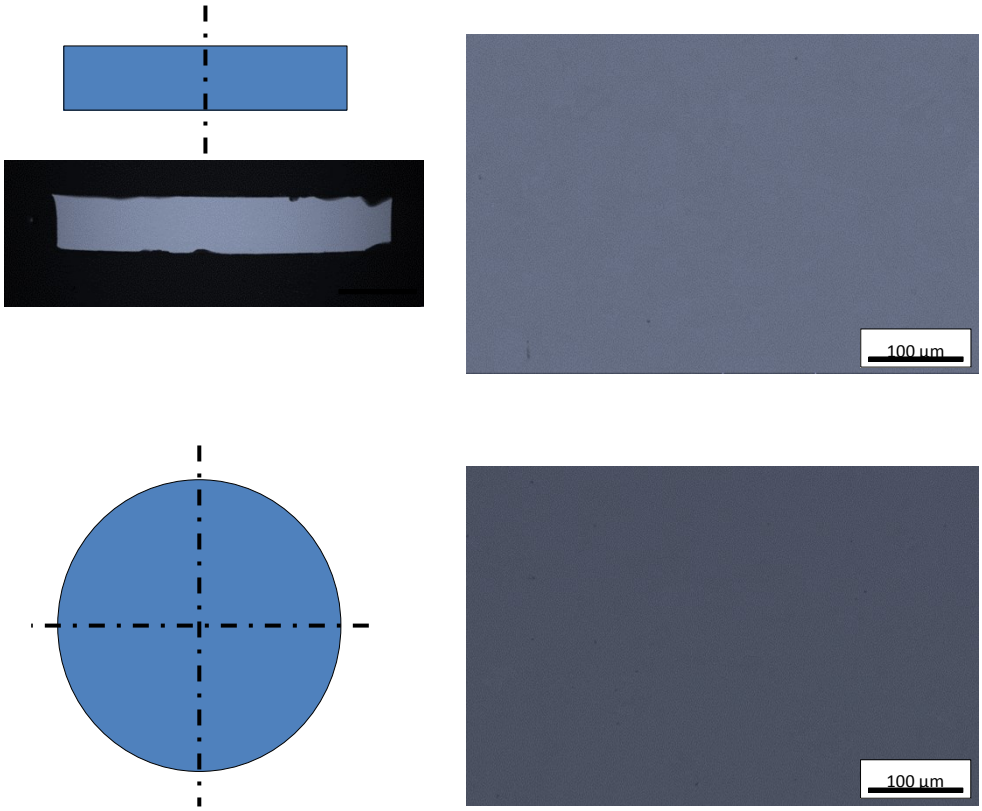

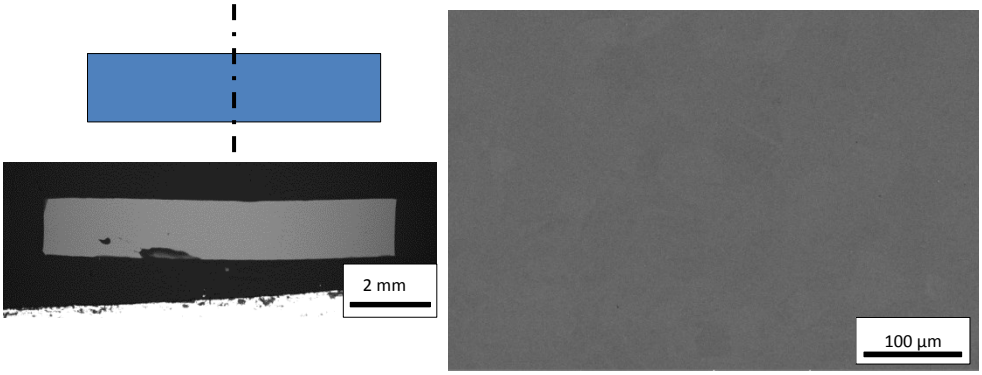

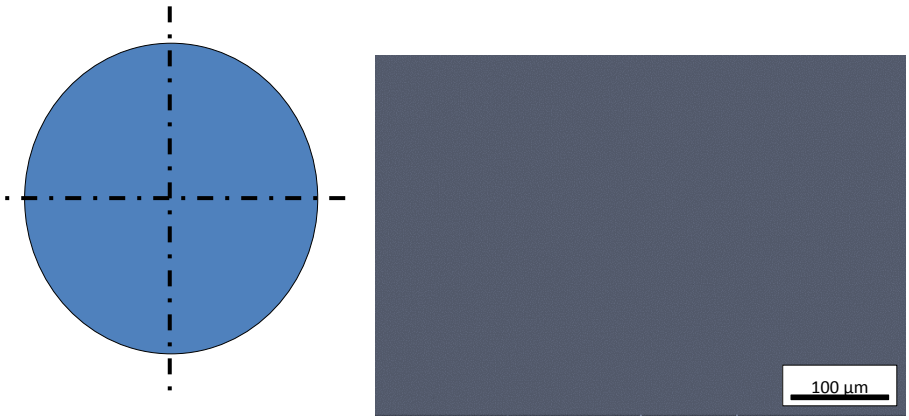

C

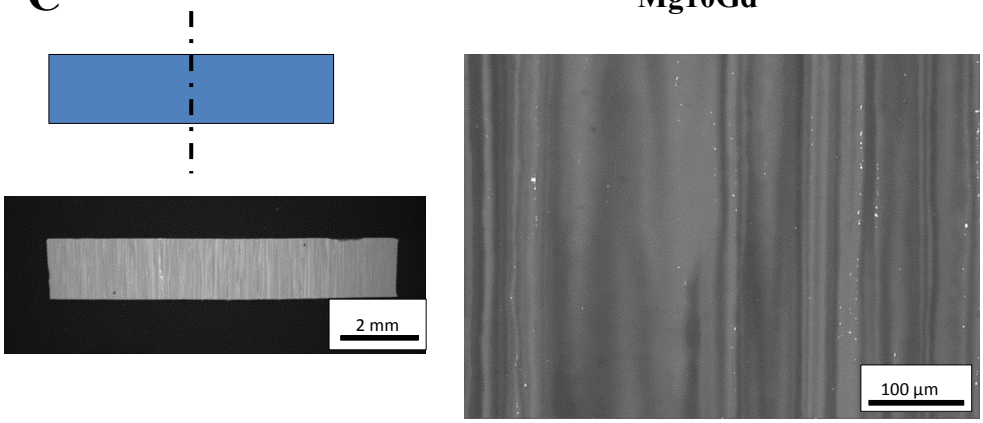

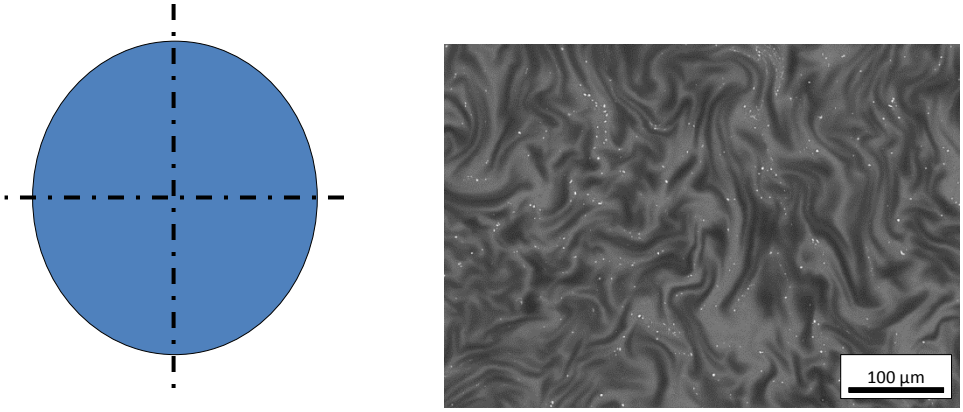

Fig 7. Microstructures of pure Mg, Mg2Ag and Mg10Gd. Microstructures were observed with scanning electron microscopy (SEM) with back-scattered electrons (BSE) equipped with energy dispersive X-ray spectroscopy (EDXS), these results have been published in an original article (216).

2.4 Corrosion measurement

2.4.1 Immersion test

Corrosion rates were determined in this study by immersion testing, which was performed according to ISO 10993 standards with slight modifications. Specimens were immersed for 1, 2, 3 and 8 days in 4 mL Dulbecco's Modified Eagle's Medium (Invitrogen, Carlsbad, CA, USA) supplemented with 10% fetal bovine serum (Sigma-Aldrich, St. Louis, MO, USA). The immersion system was a so-called static system, i.e. the corrosion medium was not changed throughout the entire immersion period. The corrosion profiles of the specimens were evaluated by measuring Mg ion release into the supernatant of the immersed samples at defined time points. Supernatants from 3 day immersed samples were also used for later cell viability experiments. Dilutions were prepared for analysis based on the highest concentration of Mg ion detected after 3 days of immersion.

In order to evaluate Mg ion concentration, supernatants from immersed samples were centrifuged for 10 minutes at 4500 rpm to remove precipitates which might exist in the supernatants. A simultaneous, axially viewed inductively coupled plasma optical emission spectrometer (ICP-OES; Ciros Vision EOP, Spectro, Germany) equipped with a cross-flow nebulizer, a Scott type PFA spray chamber and a standard ICP torch with a 2.5 mm injector diameter was used to measure Mg ion concentration. ICP-OES is an instrument which is can be used to determine the levels of different elements in both solid and liquid samples. In this system, samples are exposed to intense heat which leads to the formation of a cloud of hot gases containing free atoms and ions of the element of interest as a result of sample decomposition. Remarkable levels of collisional excitation and ionization occur at high temperatures. These atoms and ions with a high excitation level have the potential to fall to the lower state through thermal or emission energy transmission. Radiated light of particular wavelengths is then measured and utilized in order to identify the concentration of the element of interest (228). In this study the selected plasma conditions were 1350WRF power, 12.5 L/min outer gas flow, 0.6 L/min intermediate gas flow and 0.83 L/min nebulizer gas flow. The 280.270 nm Mg emission lines were used. Calibration standards (0–10 mg/L) were prepared from a multi-element stock solution (100 mg/L, 28 element

stock solutions, Roth, Germany). A 1 mg/L internal standard (Sc) was used to compensate for instrument drift. Normal cell culture medium was used as a control.

Mg ion release was also measured following cultivation of MC3T3-E1 cells on non-corroded Pure Mg, Mg2Ag and Mg10Gd for 1, 2 and 3 days. The release rate was compared to samples without cells.

2.4.2 Determination of pH

Supernatant used to determine Mg ion concentrations were also utilized for measuring pH values. pH values were measured using a normal pH meter (HANNA instruments, GmbH, Austria) at specific time points.

2.4.3 Determination of surface characterization and chemical elemental composition

In order to further analyze degradation profile and the formation of corrosion deposits on the surface, Mg discs were immersed in 4ml cell culture medium supplemented with 10% FBS for 1, 2, 3 and 8 days under cell culture conditions (37 °C, 5 % CO_2, and 95 % humidity). The medium was not changed throughout the entire immersion period. At each established time point, Mg discs were removed from 6 well plates and dried at room temperature. Analysis of surface structure and chemical elemental composition was performed using a LEO 1450VP scanning electron microscope (ZEISS, Oberkochen, Germany) equipped with an EDS detector (BRUKER QUANTAX 400) with an accelerating voltage of 15 kV. Energy-dispersive X-ray spectroscopy (EDX) is a technique for determination of sample elemental composition. In this system, the sample is exposed to the X-ray beam which excites the outer electrons layer of the atoms. The electrons then move from the high energy inner layer to the low energy outer layer, releasing energy in the process in the form of X-rays. By measuring this amount of energy the amount of elements in the EDX spectrum can be determined (229).

2.5 Cytocompatibility assays

2.5.1 Cell culture

MC3T3-E1 cells (pre-osteoblasts) obtained from ECACC (Salisbury, UK; catalogue number 99072810) were used as a cell model in this study since this cell line has the capacity to differentiate into mature osteoblast cells. Eagle's minimum essential medium (Sigma-Aldrich, St. Louis, MO, USA) was utilized as basal medium and supplements including 10% fetal bovine serum (Sigma-Aldrich), 100 U/mL penicillin, 100 μg/mL streptomycin and 2 mM glutamine (all

reagents, Invitrogen, Carlsbad, CA, USA) were added to this medium. Cell cultivation was performed under cell culture conditions at 37°C, 5% CO_2 and 95% humidity. MC3T3-E1 cells (5×10^4) were cultivated on corroded and non-corroded Mg and Mg alloys specimens. In order to analyze the effect of surface modifications on cellular behavior, corroded surfaces needed to be provided. For this purpose the specimens were immersed for 1, 2 and 3 days in cell culture medium (DMEM supplemented with 10% FBS). At each planned immersion time, cell culture medium was taken and the specimens were transferred to new 24 well plates using plastic forceps. The samples were transferred from the side in order to avoid manipulation of the surface of the specimens. 5×10^4 cells in 50 µL suspension were seeded promptly on to the surface of the specimens. The samples were incubated for 30 minutes in a cell culture incubator in order to allow initial cell adherence. 2 mL of cell culture medium (MEM supplemented with 10% FBS) was then added gently to the cells from a side to fully submerge the samples. MC3T3-E1 cells were cultivated for 24h on corroded and non-corroded Mg and Mg alloys.

2.5.2 Live dead staining assay

After culturing the cells for 24h on corroded and non-corroded Mg based samples, cell viability was determined by live-dead staining (Invitrogen). In another set of experiments, the cells were cultivated only on non-corroded specimens for longer immersion times (4, 6, 8 and 12 days). In this set of experiments, cell culture medium was changed every second day.

In order to perform live-dead staining, (for both short and long incubation times) each sample was washed three times in phosphate buffer solution (PBS, Gibco, Invitrogen). 5 µL of Calcine and 20 µL of Ethidium homodimer-1 were added to 10 mL of PBS and mixed properly in a dark room. 2 mL of this staining solution was then added to each well and the specimens were incubated for 30 minutes at room temperature in the dark. The specimens were afterwards washed three times with PBS without $CaCl_2$ and $MgCl_2$ (PBS, Invitrogen). An Inverted fluorescent microscope (Olympus) was used to visualize and photograph the stained cells. The pictures so obtained were merged using microscope software.

2.5.3 F-Actin staining

Rhodamine-phalloidin staining was used to stain the cytoskeleton of MC3T3-E1 cells cultured on corroded and non-corroded Mg and Mg alloys in order to determine the influence of surface modifications on cell morphology. For this purpose the cells were first fixed for 10 minutes with

4% Paraformaldehyde (Merck, Darmstadt, Germany). The cell membranes were then permeabilized for 5 minutes with 0.3% Triton-X100 (Sigma-Aldrich). All of the above processes were done at room temperature. A stock solution of Rhodamine-phalloidin (Invitrogen) was prepared in methanol with a final concentration of 6.6 μM (300 U/mL). 5μL of the prepared stock solution was diluted in 200 μL of PBS and incubated for 20 minutes at RT. 4',6-Diamidino-2-Phenylindole, Dihydrochloride (DAPI) counterstaining (Invitrogen) was used to stain cell nuclei. A 300nM working solution was prepared from a 10.9 mM stock solution. F-actin bundles and cell nuclei were visualized by means of laser scanning microscopy (Zeiss LSM 510) at wavelengths of 540/565 nm and 358/461nm respectively.

2.5.4 Scanning electron Microscopy

The same samples used for F-actin staining were analyzed by scanning electron microscopy in order to provide better images of the cells in the absence of background fluorescent staining. MC3T3-E1 cells were fixed for 30 minutes in 2% Paraformaldehyde/2.5% Glutaraldehyde in 0.1M Cacodylate buffer (Fluka BioChemika GmbH, Buchs, Switzerland). The specimens were then washed with 0.1M Cacodylate buffer (Merck) (pH 7.4) and afterwards dehydrated by immersion for 15 minutes at room temperature in increasing alcohol concentrations (30%, 50%, 70%, 80%, 90% and 96%). The samples were finally immersed twice in 100% ethanol for 15 minutes at RT before immersion in anhydrous acetone for 5 minutes. Before covering the samples with gold-palladium BAL TEC SCD500 (former BAL TEC, now Leica, Germany) for 60 sec, each sample was subjected to critical point drying with BAL TEC CPD 030 (formerly BAL TEC, now Leica, Germany). Scanning electron microscopy with a 15 kV acceleration voltages was utilized to take the pictures (Zeiss DSM950).

2.5.5 Indirect cytotoxicity assay (MTT assay)

The influence of corrosion deposits and especially Mg ion concentration and pH on the viability of MC3T3-E1 cells was evaluated by MTT assay. As explained above, Mg ion concentration in the supernatants of the specimens which were used for corrosion assays was measured by ICP-OES. The highest concentration of Mg^{2+}, released into the medium after three days of immersion was measured for all three materials (pure Mg, Mg2Ag and Mg10Gd), which were 1.52 mg/ml, 1.53 mg/ml and 1.47 mg/ml, respectively. Four different dilutions were prepared from each measured supernatant to assess the effects of different concentrations of Mg^{2+} (0.3, 0.6, 0.9 and

1.2 mg/ml) on MC3T3-E1 cell viability. Before addition of these extracts to the cells, pH was adjusted to physiological level. Cellular metabolic activity was also determined when cells were treated with extracts without pH adjustment.

4×10^4 MC3T3-E1 cells were seeded in 48-well tissue culture dishes (Costar; Corning, USA). The cells were treated with 250 µL of the sample extract 24h later in order to permit optimal attachment of the cells. After incubating the cells with sample extract for 24 h under cell culture conditions, the cell culture medium was removed and 25 µL MTT solution diluted 1:10 in cell culture medium was added to each well. The cell culture plates were then placed in a 37°C incubator for 4 hrs. MTT solution was then removed from the cells and 250 µL DMSO (Merck) was added to each well. 100 µL of the dissolved solution was then transferred to 96 well-plates and analyzed at a wavelength of 570 nm (Spectrostar-Ommega) by spectrophotometry. Cells treated with normal cell culture medium (MEM supplemented with 10% FBS) were used as a negative control.

2.5.6 Analysis of cell morphology following treatment with sample extract

The morphology of MC3T3-E1 cells was also analyzed after 24h treatment of the cells with different concentration of Mg^{2+} ions (0.3, 0.6, 0.9 and 1.2 mg/ml) derived from supernatants of pure Mg, Mg2Ag and Mg10Gd. The cells were cultured at a density of 2×10^4 on coverslips inserted in 6 well plates for 24h. Actin filaments and cell nuclei were stained using procedure similar to that described in section 2.5.3 and pictures were taken by laser scanning microscopy (Zeiss LSM 510).

2.5.7 Immunocytochemistry

MC3T3-E1 cells were seeded at a density of 5×10^4 on non-corroded pure Mg, Mg2Ag and Mg10Gd. The samples were incubated in cell culture medium (MEM supplemented with 10% FBS) under cell culture conditions 37°C, 5% CO_2 for 2, 4, 8 and 12 days. After certain incubation times, the media was removed and the samples were rinsed twice with PBS. The specimens were then fixed with 4% formaldehyde (Merck) for 10 minutes at room temperature. Afterwards the samples were washed twice with PBS and cell membranes were permeabilized for 5 minutes with 0.3% Triton X100 (Sigma-Aldrich) at RT and then washed three times in PBS, for 5 minutes. 1% Bovine serum albumin (Sigma-Aldrich) and 5% horse serum (Sigma-Aldrich) were combined in 0.3% Triton X100 (Sigma-Aldrich) in order to prepare fresh blocking solution. Polyclonal rabbit anti-collagen I (Catalogue number ab21286; Abcam, Cambridge, UK) was used as a primary

antibody and the samples were incubated with this antibody for 4 hours. The samples were then rinsed three times in PBS for 5 minutes. Highly cross-adsorbed anti-rabbit IgG (H+L) (Sigma-Aldrich) at a dilution of 1:200 was used as secondary antibody. The samples were incubated for 1h with this antibody and then washed three times with PBS for 5 minutes. Staining was visualized and documented by Laser scanning microscopy (Zeiss LSM 510).

2.5.8 Real time PCR

$5x10^4$ cells were cultured on the surface of all pure Mg. After 2, 4 and 6 days of immersion, the cells were detached by application of 2ml of Accutase. 8ml of cell culture medium was added subsequently. 6 specimens were pooled for each time point in order to obtain sufficient cells. Supernatants were centrifuged for three minutes at 4500 rpm and, after aspiration of the medium, the cell pellets were kept at -20 °C until PCR analysis. RNA was isolated using a Qiagen RNeasy Mini kit (catalogue number 74104) and measured by spectrophotometry. Since the RNA concentrations were low, these were measured using another method (Ribogreen RNA assay kit). RNA was converted to cDNA. cDNA synthesis from isolated RNA was done using a First Strand cDNA synthesis kit (Thermo Fischer Scientific Bioscience GmbH, St. Leonrot, Germany) according to the manufacturer's instructions. For one 20 µL reaction 5 µL diluted cDNA (1:20 cDNA from RNA), 10 µL master mix, 3 µL water and 2 µL forward/reverse primer mix were pipetted together in a white 96-well plate (Roche Applied Science, Vienna, Austria, catalog number: 4729692001). PCR was done by 7900 HT (fast real time PCR system). Negative controls were included in each experiment. The program used for mRNA expression analysis was as follows: Stage 1: 50°C 2min, Stage 2: 95°C 20 min, Stage 3: 95°C 15 Sec and 60°C 1 min, Stage 4: 95°C 15 Sec, 60°C 15Sec, 95° 15 Sec. Amplification was done for 40 cycles. 5 different housekeeping genes (GAPDH; 28S RNA; B-actin; 18S RNA and 36B4) were examined before investigation of osteogenic markers. Gene expression was evaluated using the $2^{-\Delta\Delta CT}$ method without PCR efficiency correction. Experiments were done 3 times in duplicate.

2.5.9 Western Blot

Non-corroded pure Mg, Mg2Ag and Mg10Gd were used in order to evaluate protein expression by MC3T3-E1 cells cultured for 2, 4, 6, 8, 10 and 12 days on these samples. $5x10^4$ cells were cultured on the surface of non-corroded Mg and Mg alloys for the designated time periods. Cells were immersed in cell culture medium supplemented with 10% FBS under cell culture conditions

and the medium was changed every second day. Cells were detached after the designated incubation times by addition of 2 mL Accutase for 10 minutes. The reaction was later stopped by addition of 8 mL of cell culture medium. The suspension containing floating cells was afterwards centrifuged at 4500 rpm for 5 minutes. After removing the medium, the cell pellets were resuspended in 1 mL MEM supplemented with 10% FBS. The resultant cell suspensions were then transferred into 1.5 mL Eppendorf tubes and centrifuged for 3 minutes at 1400 rpm (Micro centrifugation). RIPA buffer (Sigma) was used to prepare cell lysates for Immunoblotting (Radio Immunoprecipitation Assay). 10% sodium dodecyl Sulfate polyacrylamide gel electrophoresis (SDS-PAGE) was used to resolve the protein lysates (5µg/lane). Separated protein lysates were transferred to polyvinylidene difluoride (PVDF) membranes. Following transfer the membranes were cut and strips were incubated overnight with 1:4000 diluted Runx2 (D1L7F) rabbit monoclonal antibody (Cell Signaling, USA, catalogue number 12556S), 1:4000 diluted rabbit anti-Collagen I polyclonal (Abcam, catalogue number ab21286) and 1:500 diluted rabbit anti-B-actin (N21) polyclonal antibody (Santa Cruz, USA, catalogue number sc-130656;). A peroxidase-conjugated goat anti-rabbit secondary antibody (Santa Cruz, USA, catalogue number sc-2054) was used as secondary antibody at a dilution of 1:1000. ECL chemiluminescence reagents (Amersham) and exposure to X-ray films were used to detect protein bands. Band density for the proteins of interest was evaluated at each time point. The values so obtained were then normalized using the band density of housekeeping genes (B-actin). Protein expression levels were then compared to the biological control (cells cultured on a tissue culture plate).

2.6 Antibacterial properties

The antibacterial properties of Mg-Ag alloys were determined by evaluating the viability of bacterial populations following treatment with different dilutions of extracts derived from Mg-Ag alloys. Mg2Ag, Mg4Ag and Mg6Ag were immersed in LB Broth for 48h (broth volume calculated according to the surface ratio) and supernatant from each alloy was centrifuged for 10 minutes at 4500 rpm. Different dilutions of supernatants were subsequently prepared (10%, 25%, 50%, 75% and 100%). 200 microliter of each dilution (prepared from Mg2Ag, Mg4Ag and Mg6Ag extracts) was added to honey comb plates (specific for bio-screen device). *S. aureus* and *S. epidermidis* which are two abundant bacterial strains in orthopedic surgery were cultured on blood agar overnight. Appropriate dilutions of these bacteria were then prepared according to the McFarland standards (0.5). 2 microliter of each bacterial strain were added separately to each

well. LB broth with bacteria (without Silver extracts) was used a negative control. The plates were placed in the Bio-screen device and the antibacterial activity of the Silver-containing implants was measured every 10 minutes for three days.

2.7 Statistical Analysis

Statistical analyses were performed using SPSS software (SPSS Inc., Chicago, IL, USA). In order to evaluate normal and homogenously distributed data, a Shapiro-Wilk normality test was performed. One-way ANOVA used to compare mean values among homogenously distributed data was followed by a post-hoc Turkey test. In order to compare mean values from non-homogenously distributed data the non-parametric Kruskal-Wallis test was applied, followed by pair-wise comparisons using the Mann-Whitney U-test. Mean values of homogenous and non-homogenously distributed populations were generated as mean value± the standard deviation of the mean.

3. Results

3.1 Surface modifications of Mg and Mg alloys

3.1.1 Surface morphology and atomic % of chemical surface elements

Pure Mg

Scanning electron microscopy (SEM) equipped with Energy-dispersive X-ray spectroscopy (EDX) enables analysis of surface morphology as well as elemental composition. SEM and EDX analysis was applied to pure Mg samples following immersion in DMEM supplemented with 10% FBS for 1, 2, 3 and 8 days.

Results are summarized in Figs 8, 9 and 10 which show the alteration in surface morphology during corrosion, overview of the surface morphology during various immersion times and point analysis of the corrosion products formed on the surface respectively. Table 3 presents the chemical elemental composition of pure Mg after point analysis at days 1, 2, 3 and 8 of immersion. Fig. 8, shows the surface morphologies of pure Mg after 1, 2, 3 and 8 days of immersion in cell culture medium supplemented with 10% FBS. The white appearance in SEM images corresponded to the corrosion products, whilst the dark zones corresponded to deep corrosion pits. After 2 days of immersion in cell culture medium, the surfaces of pure Mg specimens exhibited pitting and localized corrosion. After 3 days of immersion, corrosion products in the form of needle crystals appeared, followed by complete coverage of the surface with similar crystals after 8 days of immersion. Fig 9, which provides an overview of the whole sample surface after various immersion times, indicates similar appearances. Pure Mg specimens exhibited more aggressive corrosion patterns over time compared to Mg10Gd.

EDX analysis, which originated from point analysis of the corrosion products formed on the surface of pure Mg at days 1, 2, 3 and 8 of immersion, indicated Mg, O and C to be the major elemental components of the corrosion layer, suggesting MgO, Mg $(OH)_2$ and $MgCO_3$ to be the main chemical constituents of the corrosion layer (Fig 10). Comparison of the elemental composition of the surface between days 1 and day 8 showed a decrease in atomic percentage of Ca and P and increase in Oxygen level (Table 3). It is however difficult to draw conclusions regarding the corrosion mechanism and the exact corrosion products since corrosion medium (DMEM) composition strongly affects corrosion product composition. These results have been published in an original article (216).

pure Mg_Day 1_50x	pure Mg_Day 1_200x
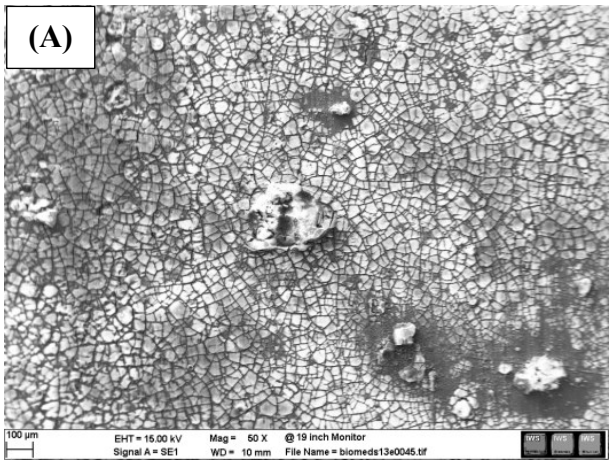	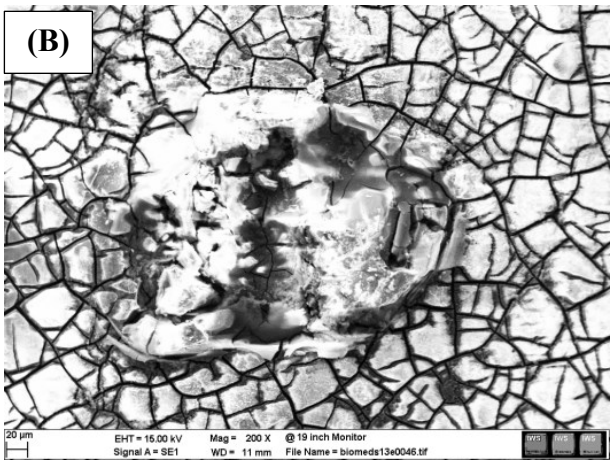
pure Mg_Day 2_50x	**pure Mg_Day 2_200x**
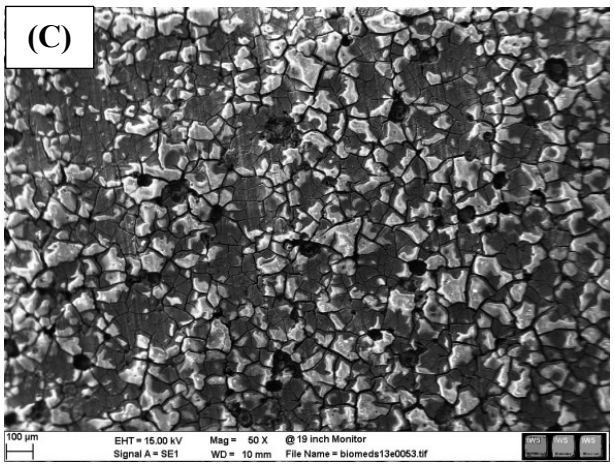	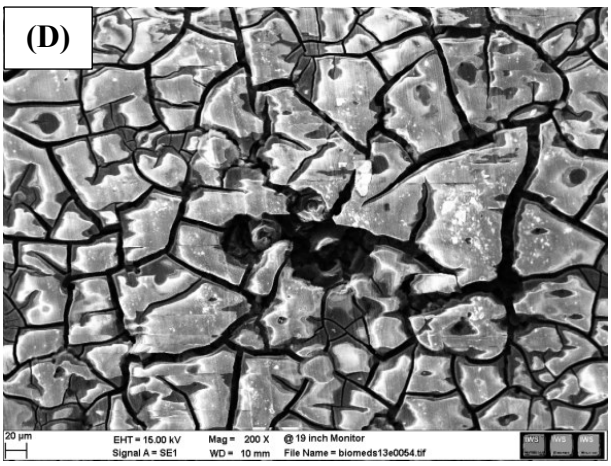

pure Mg_Day 3_50x	pure Mg_Day 3_200x
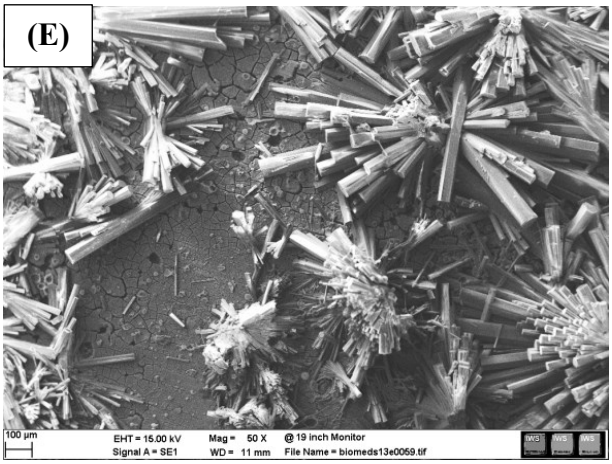	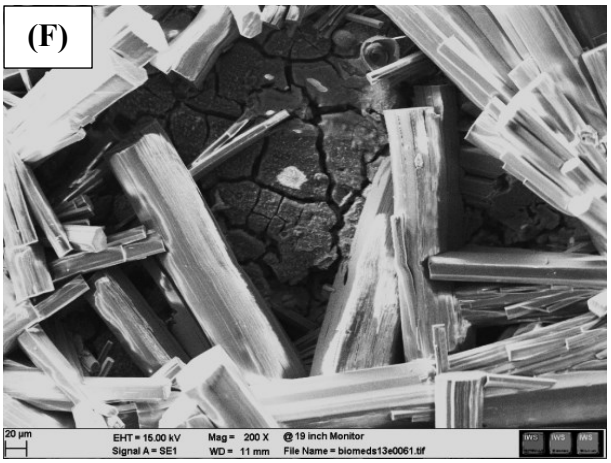
pure Mg_Day 8_50x	**pure Mg_Day 8_200x**
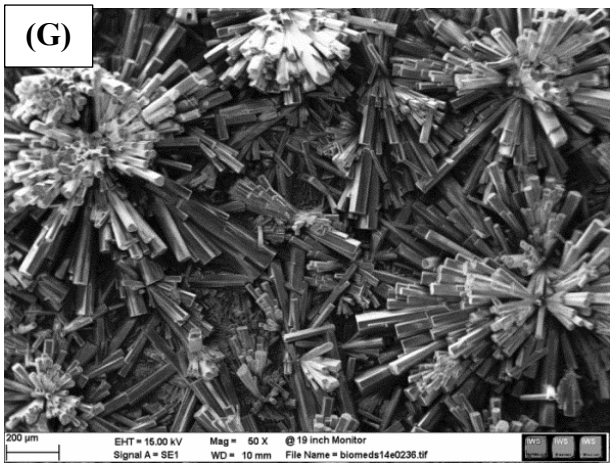	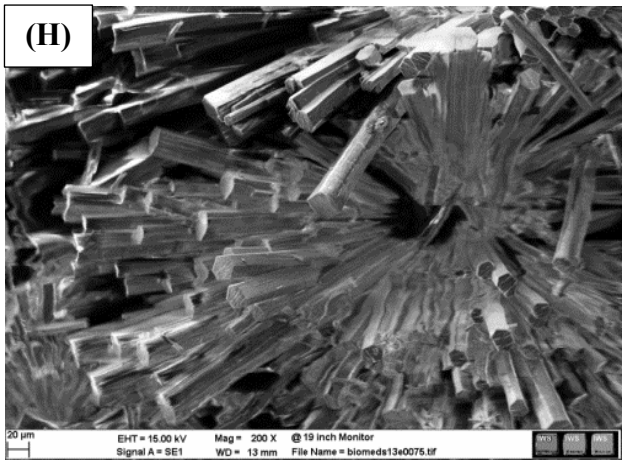

Fig 8. Changes in surface topography of pure Mg after 1, 2, 3 and 8 days of immersion (A-H) in DMEM with 10% FBS determined by scanning electron microscopy equipped with Energy-dispersive X-ray spectroscopy (EDS). Images were obtained at 200x and 50x. **Scale bars:** 100 µm & 20 µm, these results have been published in an original article (216).

Time	Day 1	Day 2	Day3	Day 8
pure Mg				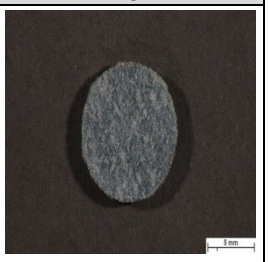

Fig 9. Overview picture of pure Mg specimens after 1, 2, 3 and 8 days of immersion in DMEM with 10% FBS. **Scale bars:** 5 mm

pure Mg_Day 1	Diagram Point A
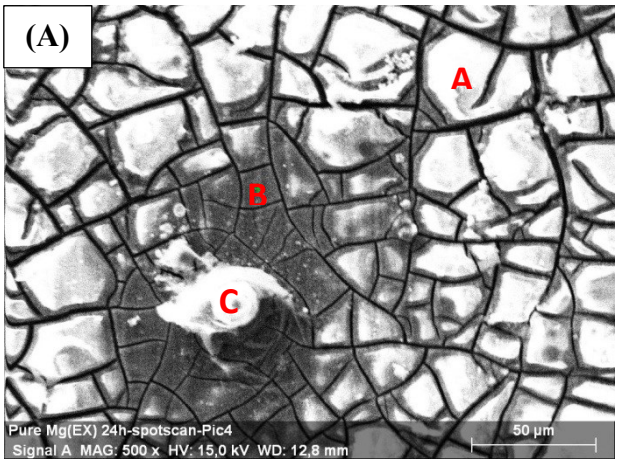	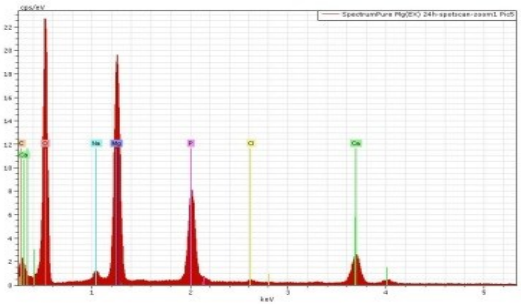
	Diagram Point B
	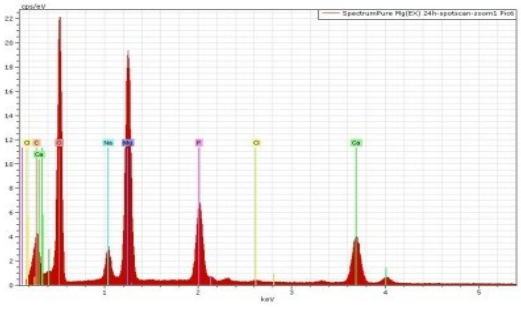
	Diagram Point C
	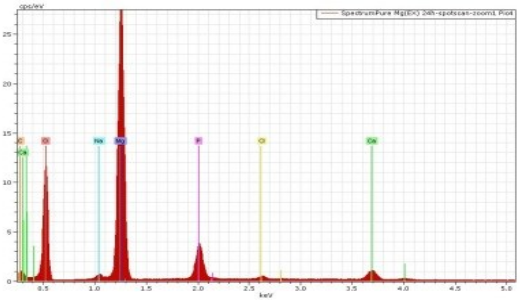

pure Mg_Day 2	Diagram Point A
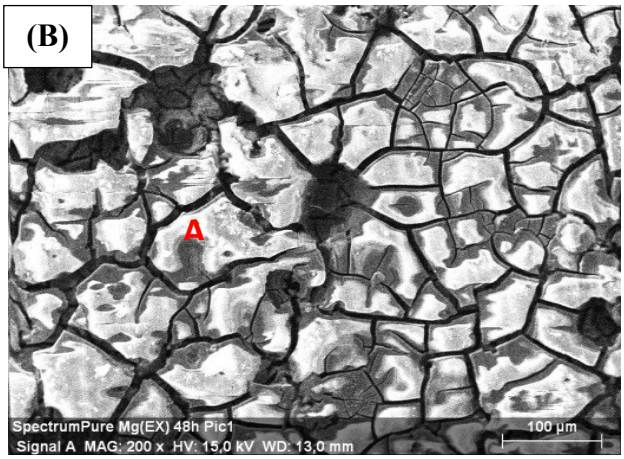	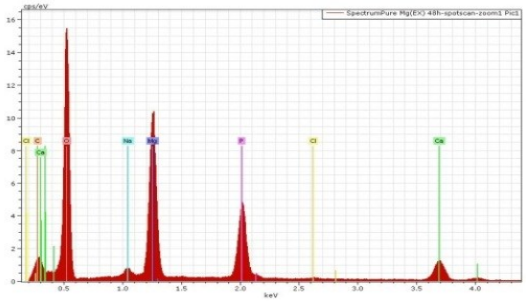
pure Mg_Day 3	**Diagram Point A**
	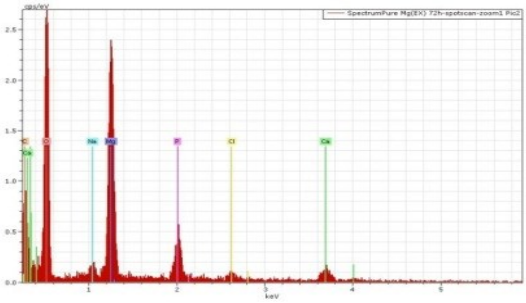
pure Mg_Day 8	**Diagram Point A**
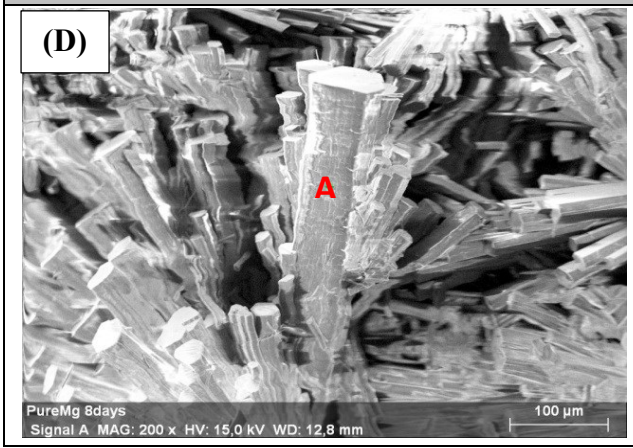	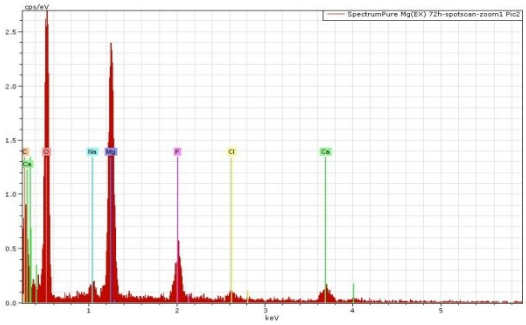

Fig 10. Scanning electron microscopy images with the corresponding energy dispersive x-ray spectroscopy analyses for pure Mg immersed in DMEM with 10% FBS for 1, 2, 3 and 8 days

immersion (A-D) respectively. **Scale bars:** 100 µm, these results have been published in an original article (216).

Table 3. Elemental composition of pure Mg after 1, 2, 3 and 8 days of immersion in DMEM with 10% FBS determined by Energy-Dispersive X-ray Spectroscopy (EDS).

Element	D1/Point A	D1/Point B	D1/Point C	D2/Point A	D3/Point A	D8/Point A
Oxygen	58.9	69.4	65.1	71.8	65.8	76.0
Calcium	1.0	3.2	5.0	2.7	2.3	0.48
Magnesium	30.2	14.9	12.4	12.4	10.4	11.9
Phosphorusus	3.1	4.8	4.2	4.7	2.1	0.04
Chlorine	0.2	0.1	0.09	0.13	0.5	0.05
Carbon	5.5	6.1	10.6	6.5	17.8	10.3
Sodium	0.6	1.06	2.2	1.50	0.70	0.9

Mg2Ag

As with pure Mg, Mg2Ag samples were immersed for 1, 2, 3 and 8 days in DMEM+10% FBS and micrographs were taken using SEM (Fig 11). Small cracks appeared on the surface of Mg2Ag after 1 and 2 days of immersion. Localized corrosion was observed with deposits of degradation products in the form of small, thin crystals after 3 days of immersion. Thick needle shaped crystals covered the entire surface of the material after 8 days of immersion. SEM images showed that Mg2Ag surface do not maintain integrity during the whole immersion time, which was evident from the formation of aggressive corrosion products (Fig 11). An overview picture of the whole surface of Mg2Ag confirmed these observations (Fig 12). According to point analysis and EDX data, crystal formation was accompanied by a noticeable increase in the atomic % of Oxygen, demonstrating that crystal formation is associated with enhanced oxidation (Fig 13 and table 4). Although crystal formation is highly correlated to Oxygen content, the increase in atomic % of Oxygen was not the only reason for crystal formation. Analysis of the Mg:O ratio on the surface of Mg2Ag and pure Mg (with crystals) demonstrated lower values than on the surface of Mg10Gd (without crystals) (Table 5). A significant decrease in Ca and P content (5-10 folds)

can be considered to be another reason for crystal formation (Table 4). Mg and C were detected as other major elements on the corroded surface (8 days of immersion). High C, Mg and O contents suggested formation of $Mg(CO_3)$ and $Mg(OH)_2$ corrosion products (Table 4). Since Mg2Ag generated similar corrosion products to those observed for pure Mg, it can be concluded that alloying of Mg with Ag did not noticeably affect the corrosion process. These results have been published in an original article (216).

Mg2Ag_Day 1_50X	**Mg2Ag_Day 1_200X**
(A) 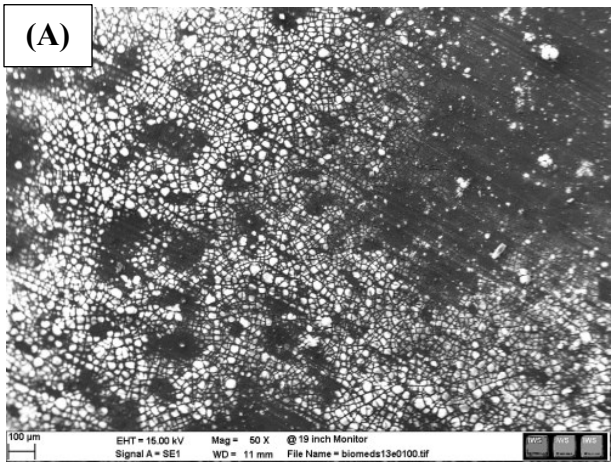	**(B)** 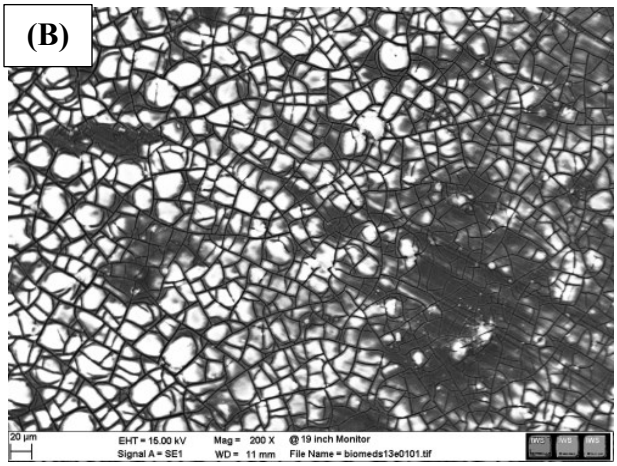
Mg2Ag_Day 2_50X	**Mg2Ag_Day 2_200X**
(C) 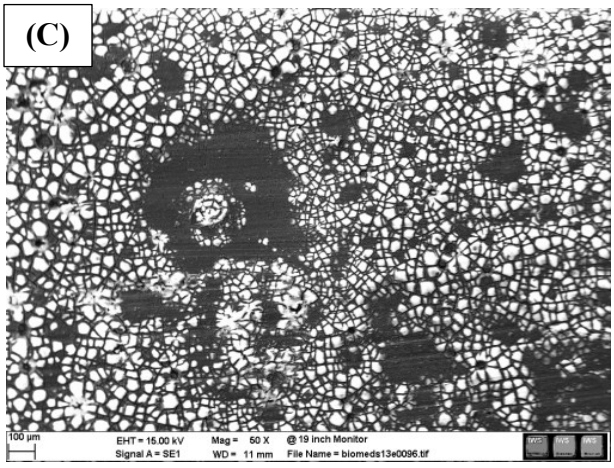	**(D)** 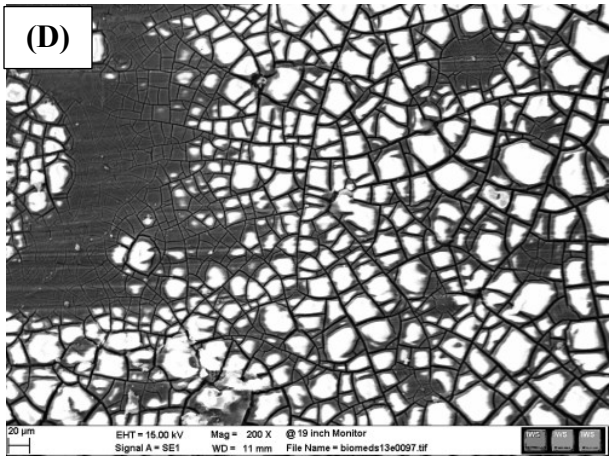

Mg2Ag_Day 3_50X	Mg2Ag_Day 3_200X
(E) 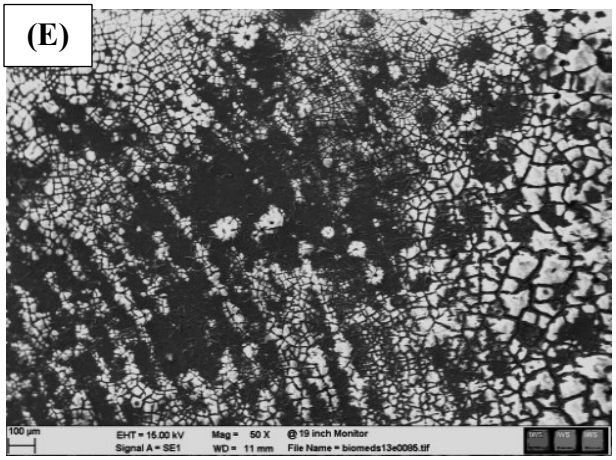	(F) 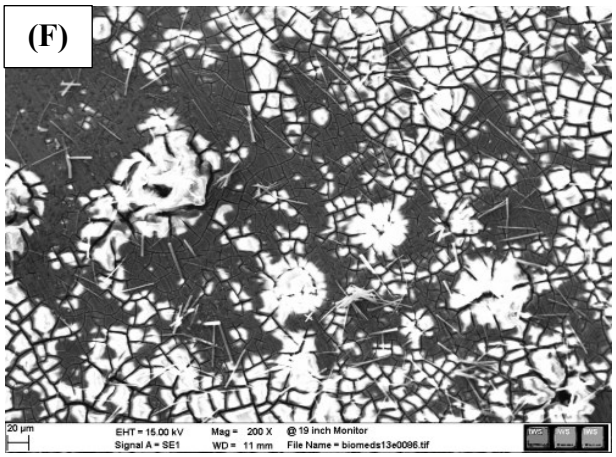
Mg2Ag_Day 8_50X	**Mg2Ag_Day 8_200X**
(G) 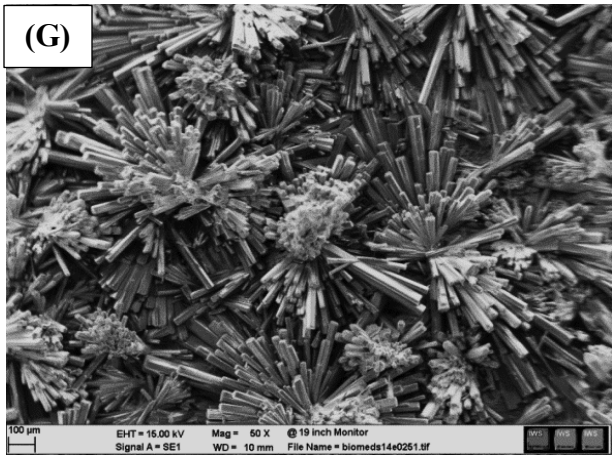	(H) 

Fig 11. Changes in Surface topography of Mg2Ag after 1, 2, 3 and 8 days of immersion (A-H) in DMEM with 10% FBS determined by scanning electron microscopy equipped with Energy-dispersive X-ray spectroscopy (EDS). Images were obtained at 200x and 50x. **Scale bars:** 100 µm & 20 µm, these results have been published in an original article (216).

Time	Day 1	Day 2	Day3	Day 8
Mg2Ag				

Fig 12. Overview picture of Mg2Ag specimens after 1, 2, 3 and 8 days of immersion in DMEM with 10% FBS (Left to right). **Scale bars:** 5 mm

Mg2Ag_Day 1	Diagram Point A
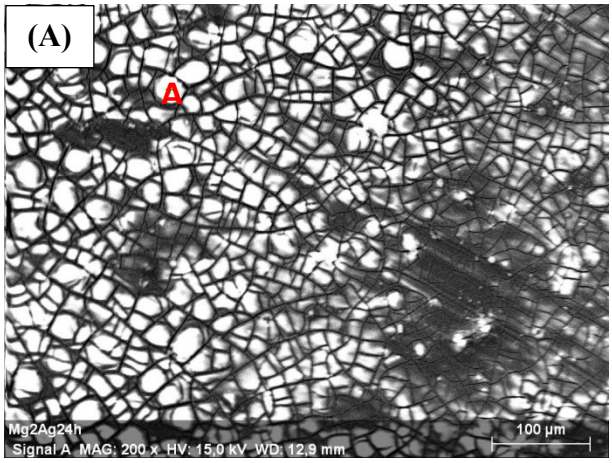	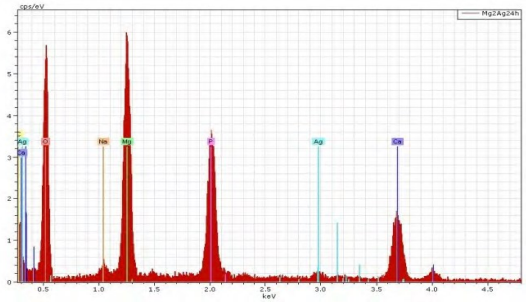

Mg2Ag_Day 2	**Diagram Point A**
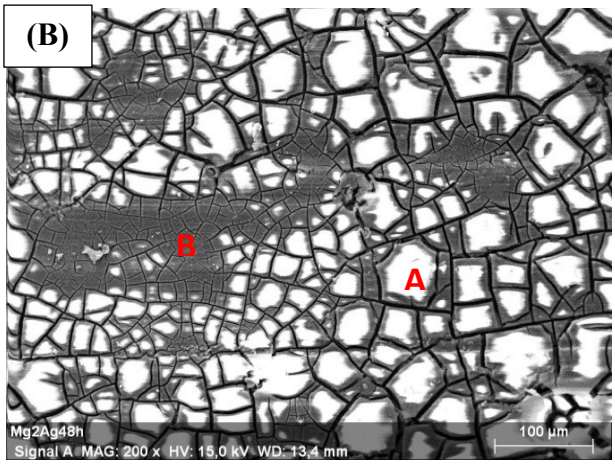	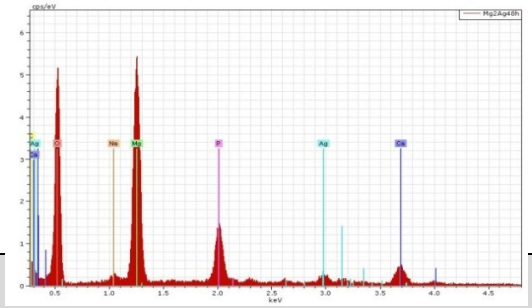 **Diagram Point B** 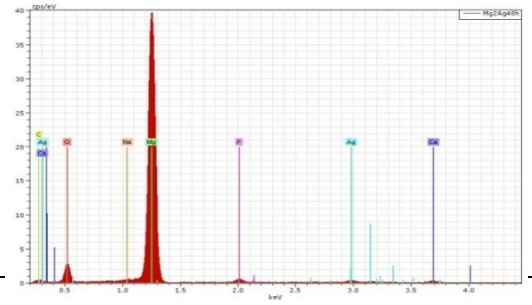

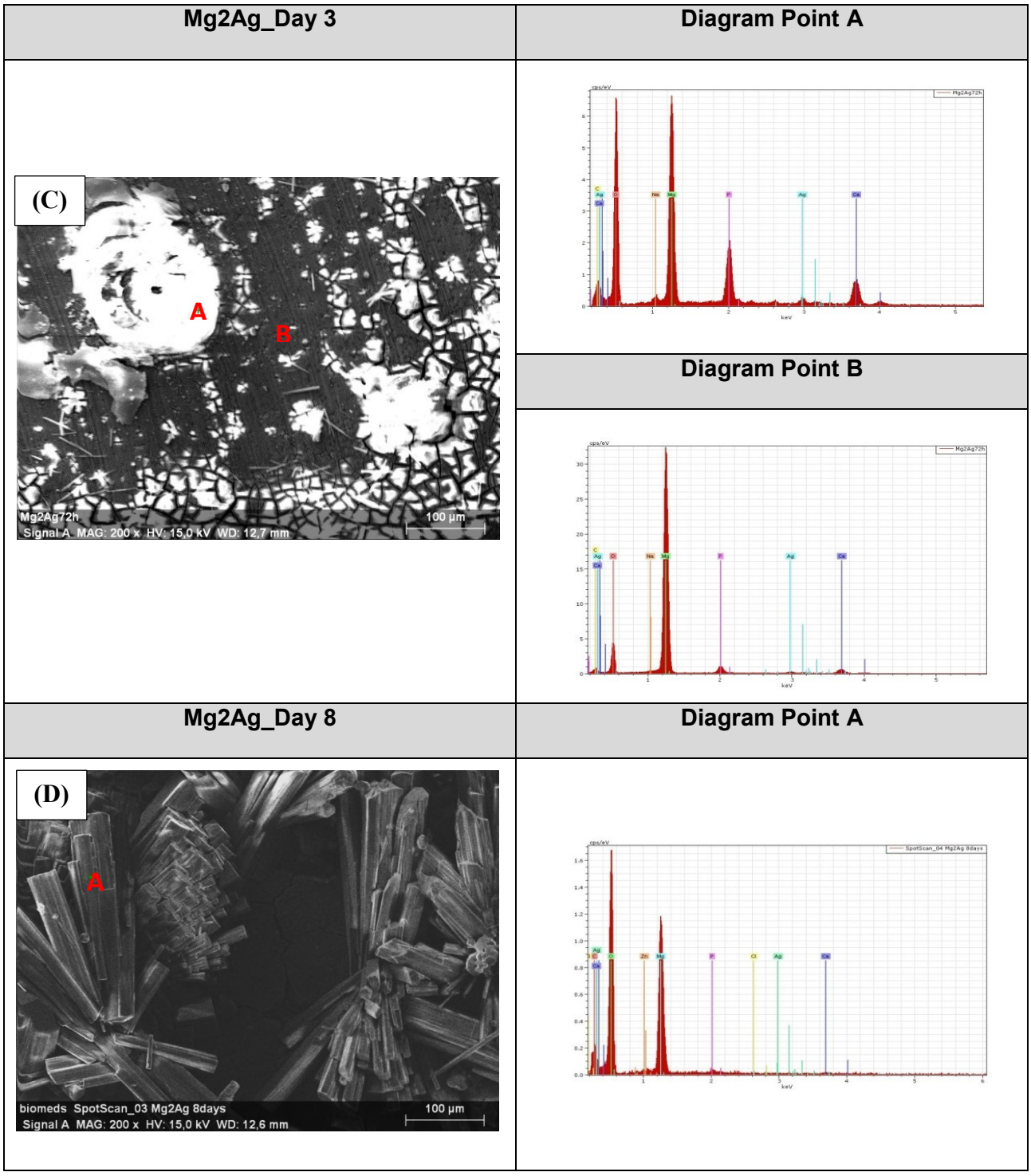

Fig 13. Scanning electron microscopy images with the corresponding energy dispersive x-ray spectroscopy analyses for Mg2Ag immersed in DMEM with 10% FBS for 1, 2, 3 and 8 days (A-D) respectively. **Scale bars:** 100 µm, these results have been published in an original article (216).

Table 4. Elemental composition of Mg2Ag following 1, 2, 3 and 8 days of immersion in DMEM with 10% FBS determined by Energy-Dispersive X-ray Spectroscopy (EDS).

Elements	D1/Point A	D2/Point A	D2/Point B	D3/Point A	D3/Point B	D8/Point A
Oxygen	65.4	29.8	68.6	40.3	68.1	81.8
Magnesium	10.1	61.1	16.7	46.6	15.9	9.3
Calcium	7.1	0.6	2.5	1.9	2.7	0.3
Silver	0.42	0.5	0.7	0.3	0.3	0.1
Phosphorus	6.8	1.1	3.9	2.08	3.9	0.3
Carbon	8.8	5.8	6.2	7.8	7.9	7.4
Sodium	1.1	0.7	1.0	0.6	0.9	0.1

Table 5. O: Mg ratio on the sample surface, these results have been published in an original article (216).

O:Mg Ratio	Day 1	Day 2	Day 3	Day 8
Pure Mg	4.6	4.8	6.3	6.3
Mg2Ag	4.6	4.1	4.2	8.7
Mg10Gd	4.6	8.9	6.9	12.5

Mg10Gd

Scanning electron microscopy images of Mg10Gd revealed massive light protruding grains and dark regions at all immersion time points (Fig 14). The surface morphology of Mg10Gd samples remained relatively smooth even after 8 days of immersion in cell culture medium. Whilst some small cracks appeared on all surfaces as a result of degradation during the immersion period, the corrosion product layer maintained its integrity (Fig 14). Overview pictures show no noticeable changes in surface morphology over time (Fig 15). EDX analysis originating from data point analysis revealed corrosion products to be composed mainly of Magnesium (Mg), Oxygen (O), Carbon (C), Calcium (Ca) and Phosphorusus (P) in all corrosion areas (dark grains and light protruding grains) and at all time points. Trace amounts of Gadolinium (Gd), Sodium (Na) and Chlorine (Cl) were detected at all time points (Fig 16). According to the SEM results, uniform corrosion attack without evidence of crystal formation were recognized in Mg10Gd samples (Fig 14). No significant changes in corrosion product composition were detected during three days of immersion. The outer layer is apparently composed of $Mg(OH)_2$ and $Mg(CO_3)$ based on high O, Mg and C contents. Calcium and Phosphor levels were below 5%, but noticeably higher than the corresponding levels for Mg2Ag and Pure Mg (Table 6). This could explain why no crystals were formed on the surface of Mg10Gd even after 8 days of immersion in cell culture medium. Potential adsorption of Ca and P by Gd can be raised in this context. These results have been published in an original article (216).

Mg10Gd_Day 1_50X	Mg10Gd _Day 2_50X
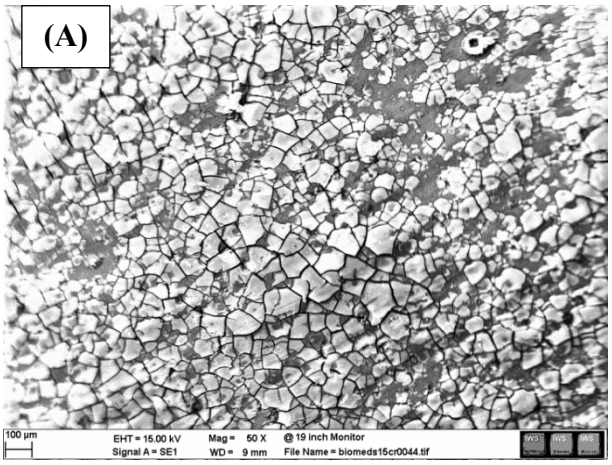	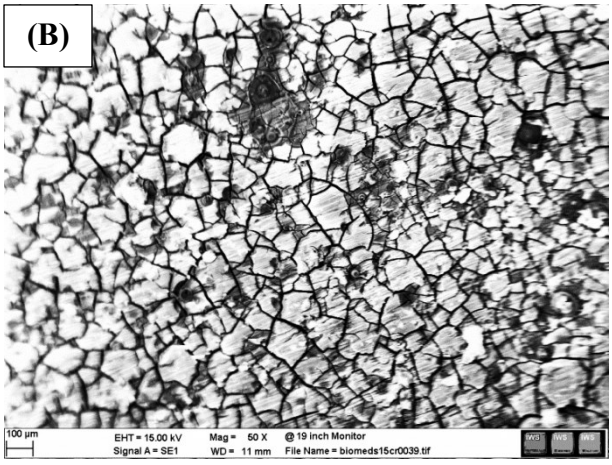
Mg10Gd _Day 3_50X	**Mg10Gd_Day 8_200X**
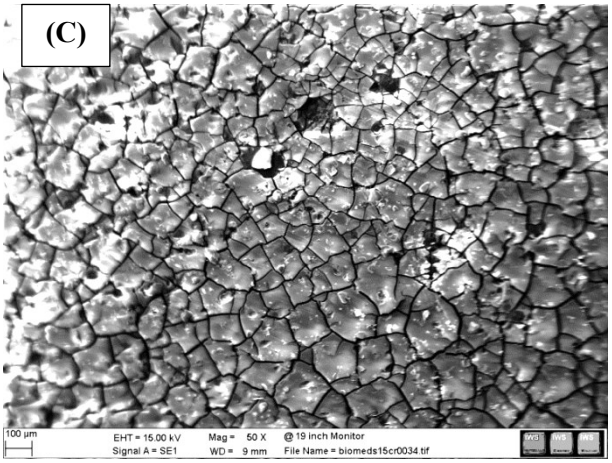	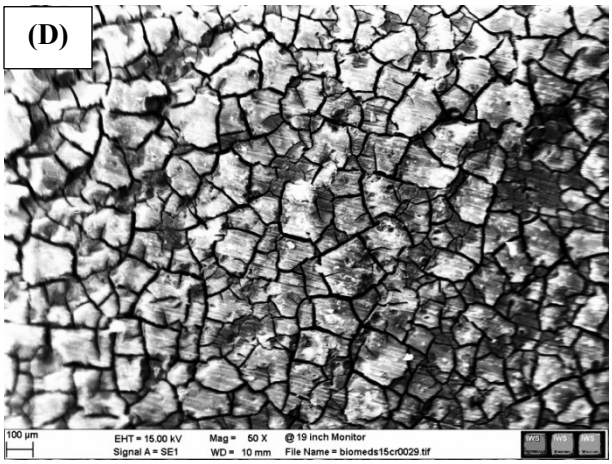

Fig 14. Change in Surface topography of Mg10Gd following 1, 2, 3 and 8 days of immersion (A-D) in DMEM with 10% FBS determined by scanning electron microscopy equipped with Energy-Dispersive X-ray Spectroscopy (EDS). **Scale bars:** 100 µm, these results have been published in an original article (216).

Time	Day 1	Day 2	Day3	Day 8
Mg10Gd			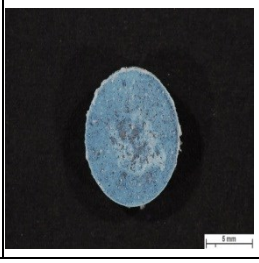	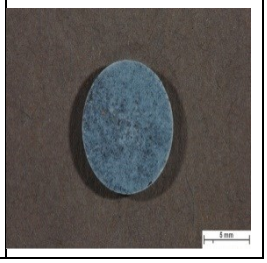

Fig 15. Overview picture of Mg10Gd specimens after 1, 2, 3 and 8 days of immersion in DMEM with 10% FBS (Left to right). **Scale bars:** 5mm

Mg10Gd_Day 1	
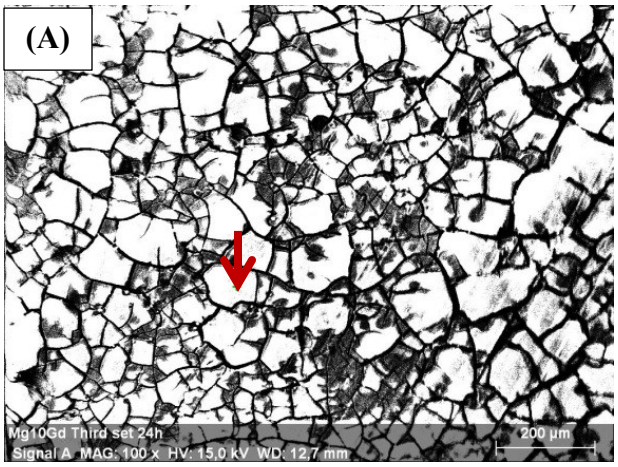	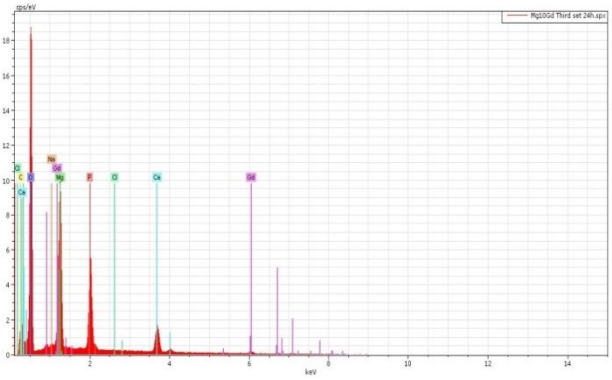
Mg10Gd_Day 2	
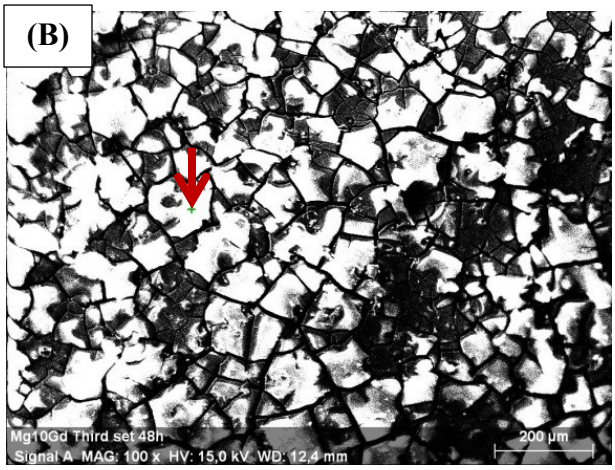	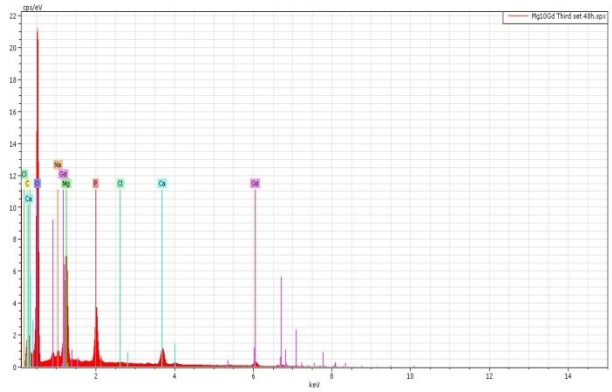

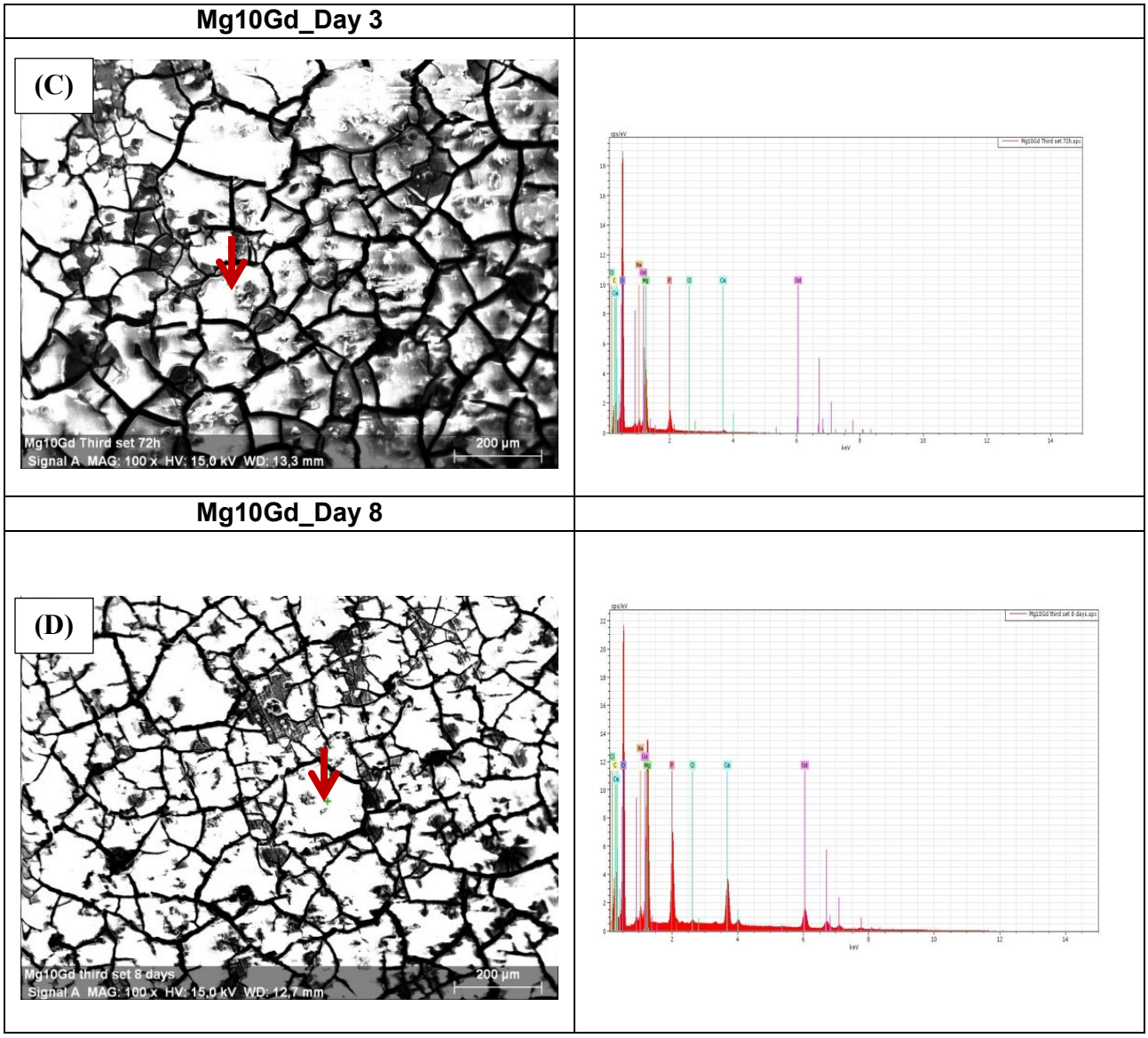

Fig 16. Scanning electron microscopy images with the corresponding Energy Dispersive X-ray Spectroscopy analyses for Mg10Gd immersed in DMEM with 10% FBS for 1, 2, 3 and 8 days (A-D) respectively. **Scale bars:** 200 µm, these results have been published in an original article (216).

Table 6. Elemental composition of Mg10Gd following 1, 2, 3 and 8 days of immersion in DMEM with 10% FBS determined by Energy-Dispersive X-ray Spectroscopy (EDS), these results have been published in an original article (216).

Elements	D1/Point1	D2/Point1	D3/Point1	D8/Point1
Oxygen	73.8	75.7	70.1	76.5
Magnesium	10.6	8.5	10.03	6.1
Calcium	2.3	1.9	1.9	1.5
Gadolinium	0.4	1.1	0.8	1.2
Phosphorus	5	3.2	3.8	3
Carbon	6.7	7.8	12.1	10
Sodium	0.7	1.4	0.7	0.6
Chlorine	0.05	0.1	0.2	0.1

3.2 Corrosion rate of Mg and Mg alloys

3.2.1 Magnesium ion release analysis

3.2.1.1 Analysis of Magnesium ion release without cells

Properties of pre-osteoblast (MC3T3-E1) cells cultured on the surface of Mg-based samples such as cell viability can be influenced by multiple factors including surface morphology, pH, chemical composition of the corroded surfaces and corrosion-associated Mg ion release. In this study Mg ion concentration was measured by inductively coupled plasma atomic emission spectroscopy (ICP-OES) in DMEM supplemented with 10% fetal bovine serum. Figure 17 shows Mg ion release from pure Mg, Mg2Ag and Mg10Gd. A significant increase in Mg^{2+} concentration derived from Mg2Ag and pure Mg occurred during 3 days of immersion but plateaued by day 8, demonstrating a reduced corrosion rate at this time point. Mg ion concentration initially increased in cell culture medium with all Mg-based samples due to surface deterioration (First 3 days). Subsequently the corrosion process, impeded on pure Mg due to the formation of massive levels of corrosion products, culminated in a consumption of Mg ions from the medium and reduced Mg ion concentrations (3-8 days).

With Mg2Ag, the Mg^{2+} ion concentration plateaued during days 3 to 8 of immersion as a result of a moderate corrosion process and slow precipitation of corrosion products on the surface. Since reduced Mg ion release coincided with crystal formation for both Mg2Ag and pure Mg samples, it can be concluded that crystals are stable corrosion deposits which can hinder further corrosion and ion release (Fig 17). Mg10Gd exhibited a different release pattern compared to Mg2Ag and pure Mg. Mg ion release, increased gradually during 8 days of immersion of Mg10Gd. No significant difference was detected in the surface morphology of Mg10Gd specimens at 3 and 8 days of immersion, which indicates that deposition of corrosion products cannot protect the surface completely from further corrosion (Fig 17). The reduction of Mg on the surface of different samples was accompanied by comparable time-dependent increases in the concentration of Mg ions in the supernatant. The highest time-dependent release of Mg ions into the supernatant was observed when Mg10Gd was immersed for 8 days in cell culture medium (1day: 0.4 ±0.01 mg/mL; 8 days: 1.8±0.01 mg/mL) (Fig 17), which was statistically significant ($F(4) = 37.444$ $p = 0.000$). These results have been published in an original article (216).

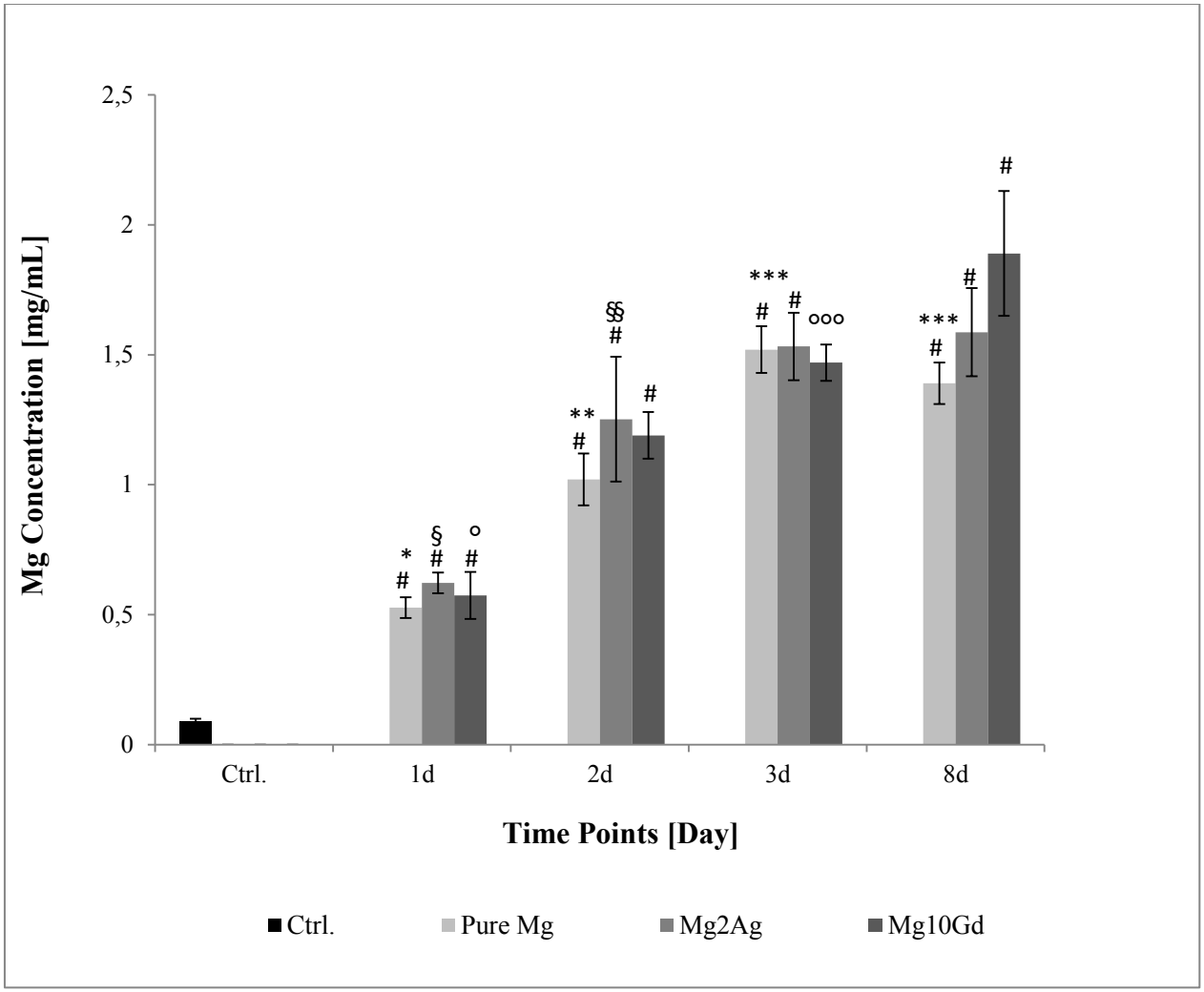

Fig 17. Changes in Mg^{2+} release into the supernatant during corrosion of pure Mg, Mg2Ag and Mg10Gd determined by ICP-OES analysis. Mg ion concentration in the supernatant (DMEM, 10%FBS) of Mg and Mg alloys was measured at 1, 2, 3 and 8 days by ICP-OES; n=5. Statistical significance was tested using a One-way ANOVA test. # $p<0.05$ as compared to the control (Magnesium level of the basal medium); * $p<0.05$ as compared to ion release from pure Mg at day 2, 3 and 8; ** $p<0.05$ as compared to ion release from pure Mg at day 1, 3 and 8; *** $p<0.05$ as compared to ion release from pure Mg at day 1 and 2; § $p<0.05$ as compared to ion release from Mg2Ag at day 2, 3 and 8; §§ $p<0.05$ as compared to ion release from Mg2Ag at day 1 and 8; ° $p<0.05$ as compared to ion release from Mg10Gd at day 2, 3 and 8; °° $p<0.05$ as compared to ion release from Mg10Gd at day 1, 3 and 8; °°° $p<0.05$ as compared to ion release from Mg10Gd at day 1, 2 and 8, these results have been published in an original article (216).

Release of Mg ions is normally associated with an increase in pH which can also affect the corrosion process. pH was monitored when samples were immersed in cell culture medium. With pure Mg pH increased promptly from day 0 to 2, declined slowly at day 3 and remained constant from days 3 to 8. The pH of the medium with Mg10Gd specimens showed a similar trend to the Mg^{2+} ion release results. A gradual increase in pH was observed during 8 days of immersion

showing that corrosion products cannot protect the surface from further corrosion. As observed for $Mg2^{+}$ release, Mg2Ag showed the highest pH value at the beginning (although the differences between the groups were not statistically significant) (Fig 18). These results have been published in an original article (216).

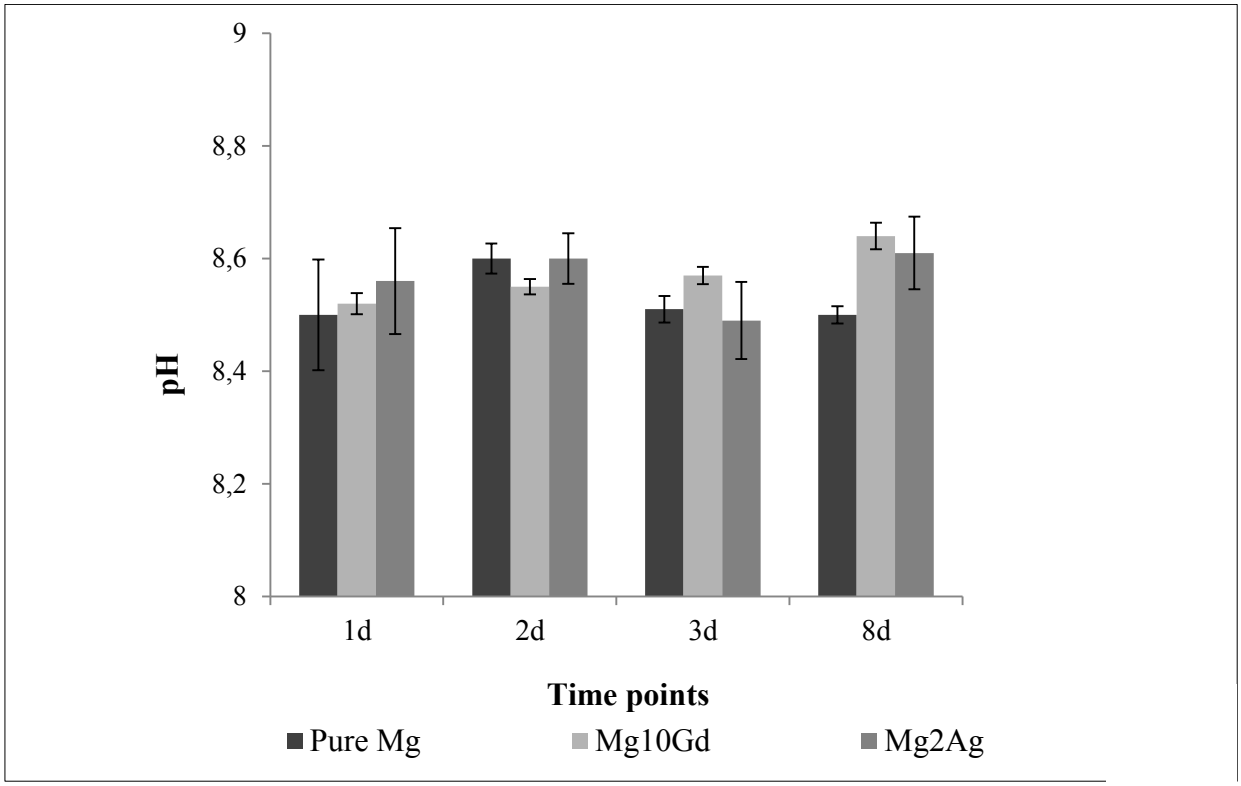

Fig 18. Changes in pH for pure Mg, Mg2Ag and Mg10Gd respectively at 1, 2, 3 and 8 days of immersion in DMEM with 10% FBS determined by pH meter, these results have been published in an original article (216).

3.2.1.2 Analysis of Magnesium ion release with cells

The presence of cells on the surface of Mg based implants is known to influence the corrosion rate of these samples. The release of Magnesium ions into cell culture medium was therefore measured for the specimens under cell culture conditions for 1, 2 and 3 days with and without attached cells. As explained above, a static immersion system was used in this study. The maximum immersion time for this set of experiments was therefore 3 days, since cells cannot survive longer immersion times without fresh medium. The results showed that Mg ion release was slower for specimens with cells compared to the samples without cells throughout the entire immersion period (24-72 hours) which indicates that cell material interaction resulted in slower a

corrosion rate evident from a slower ion release from, Mg2Ag, Mg10Gd and pure Mg. Whilst decreased Mg ion release was observed with all specimens, the differences were not statistically significant (Fig 19). These results have been published in an original article (216).

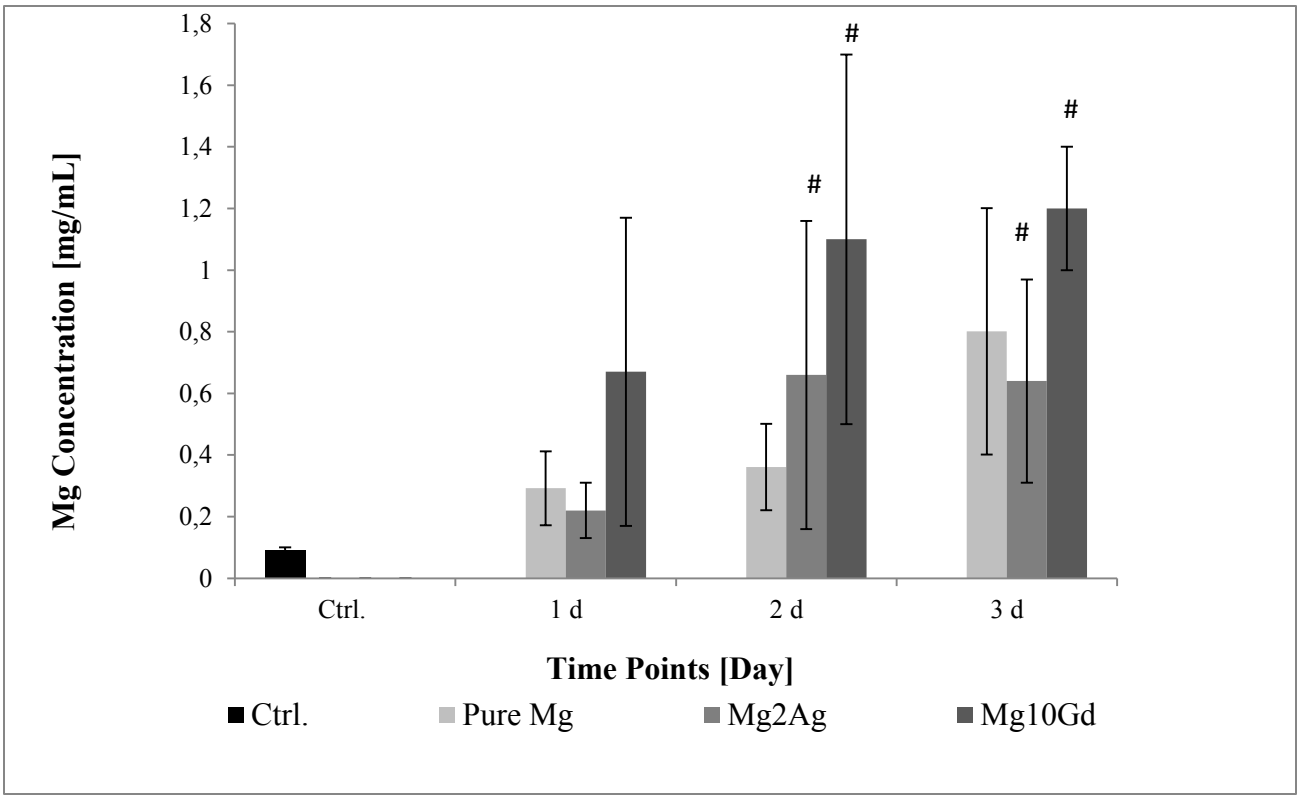

Fig 19. Changes in Mg^{2+} release from pure Mg, Mg2Ag and Mg10Gd when MC3T3-E1 cells were cultivated on the surface. Mg ion release was measured during culturing of MC3T3-E1 cells on the surface of the non-corroded Mg and Mg alloys for 1, 2 and 3 days by ICP-OES; n=5. Statistical significance was tested with a One-Way ANOVA test. #$p<0.05$ as compared to the control (Magnesium level of the basal medium), these results have been published in an original article (216).

3.3 Cytocompatibility assays

3.3.1 Analysis of the metabolic activity of cells treated with different Magnesium concentrations (pH adjusted)

In order to evaluate the effect of corrosion-associated Mg ion release on cell viability, pre-osteoblast (MC3T3-E1) cells were treated for 24h with different concentration of Mg ions derived by incubation of Mg specimens in cell culture medium for 3 days. The supernatants of immersed samples were diluted into four concentration ranges (0.3, 0.6, 0.9, 1.2 mg/mL) for this purpose (Fig 20). Metabolic activity of the cells was analyzed by MTT assay after 1 day of

incubation. The viability of MC3T3-E1 cells cultured in medium containing 0.3 mg/mL Mg^{2+} was significantly higher ($p<0.05$) than control cells (cultured in normal cell culture medium), showing a potential stimulatory effect of Mg^{2+} on the cells at a low Mg^{2+} concentration. In contrast, there were no significant differences between the control and cells treated with 0.6 and 0.9 mg/ml Mg^{2+}. At the highest concentration, cell viability dropped to approximately 80% of the control value. The relatively high cell viability observed (according to ISO standards viability greater than 75% is considered as a safety level) showed, however, that Mg^{2+} derived from pure Mg extracts did not have any toxic effect on the cells even at the highest concentration tested (1.2 mg/ml).

Cells exhibited similar viability when exposed to pure Mg extracts as when they were treated with 0.3 and 0.6 mg/mL Mg^{2+} derived from Mg2Ag. Conversely, at 0.9 mg/ml Mg^{2+} cell metabolic activity dropped to approximately 60% and the highest concentration of Mg^{2+} derived from Mg2Ag extracts (1.2 mg/ml Mg^{2+}) was completely toxic for the cells.

As observed with pure Mg and Mg2Ag, cell metabolic activity was reduced by exposure to increasing Mg^{2+} ion concentrations from Mg10Gd extracts. MC3T3-E1 cells exhibited higher viability at Mg^{2+} concentrations of 0.3 and 0.6 mg/ml compared to the control. Even at a Mg^{2+} concentration of 0.9 mg/ml cell metabolic activity exceeded 80%. No cells however survived exposure to the highest Mg^{2+} concentration tested (1.2 mg/ml). MC3T3-E1 cells better tolerated a 1.2 mg/ml Mg^{2+} concentration derived from pure Mg extracts than from Mg2Ag and Mg10Gd. In order to determine whether the release of other ions such as Ag^{+} or Gd^{3+} (which were used as alloying elements) can affect cell viability and cause cell death, these ions were also measured in the supernatants of the immersed specimens. Ag and Gd levels were however at the limit of quantification (LOQ) at all immersion times, indicating that Ag and Gd ions cannot cause cytotoxicity at these concentrations (Table 7).

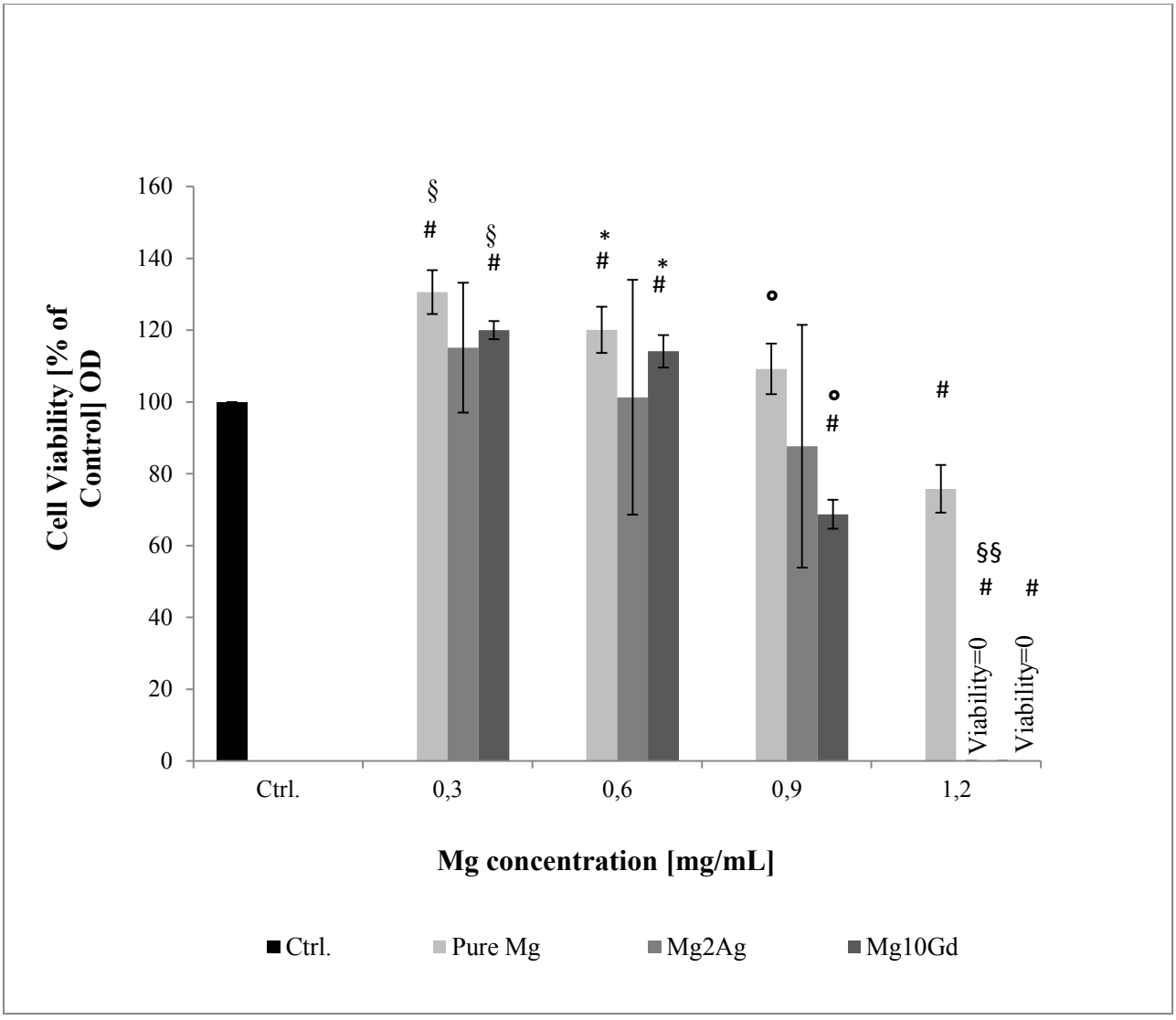

Fig 20. Viability of MC3T3-E1 cells treated with different concentration of Mg^{2+} (diluted to standard concentrations from the supernatants of pure Mg, Mg2Ag and Mg10Gd). Different concentrations of Mg^{2+} (0.3-0.6-0.9 and 1.2 mg/mL) were added to the cells and after 24hrs cell viability was determined by MTT assay. The pH of the extracts was adjusted to 7.4. Decreased viability of MC3T3-E1 cells was detected at concentrations of 0.9 to 1.2 mg/mL Mg^{2+}. Statistical significance was tested with a One-way ANOVA test. **# p<0.05** as compared to the cell viability of the control; **§p<0.05** as compared to cell viability at concentration of 0.6, 0.9 and 1.2 mg/mL Mg^{2+} resulted from pure Mg and Mg10Gd extracts; ***p<0.05** as compared to cell viability at concentration of 0.9 and 1.2 mg/mL Mg^{2+} concentration resulted from pure Mg and Mg10Gd extracts; **° p<0.05** as compared to cell viability at 1.2 mg/mL Mg^{2+} concentration resulted from pure Mg and Mg10Gd extracts; **§§ p<0.05** as compared to cell viability at concentration of 0.3, 0.6 and 0.9 mg/mL Mg^{2+} concentration resulted from Mg2Ag (Significance level was set at $p < 0.05$; n = 4 per group), these results have been published in an original article (216).

Table 7. Changes in Ag^{+} and Gd^{3+} release from Mg2Ag and Mg10Gd during 1, 2, 3 and 8 days of corrosion, these results have been published in an original article (216).

Mg2Ag	**Day 1**	**Day 2**	**Day 3**	**Day 8**
Ag^{+} (mg/mL)	LOQ	0.00145	0.002	0.002
Mg10Gd	**Day 1**	**Day 2**	**Day 3**	**Day 8**
Gd^{3+} (mg/mL)	LOQ	0.0007	0.0008	0.0012

3.3.2 Analysis of metabolic activity of cells treated with different concentrations of Magnesium (pH not adjusted)

Besides the important effect of Mg ions on cell viability, pH can also influence this process. Since corrosion of Mg implants is associated with increasing pH, it is of great importance to monitor cell viability without pH adjustment. In order to check the impact of pH on cell viability, cell metabolic was therefore examined without pH adjustment (Fig. 21). Figure 21 shows the metabolic activity of MC3T3-E1 cells after treatment with different concentrations of Mg derived from pure Mg and Mg10Gd extracts. MC3T3-E1 cells showed a high degree of tolerance at all Mg concentrations after 24h of incubation. Even at the highest concentration of Mg^{2+} tested (1.2 mg/ml), the cells were completely viable, showing that pH values of 8.4-8.6 might even have a stimulatory effect on the cells. MTT assay data however showed a different outcome for cells treated with the highest concentration of Mg2Ag supernatant. At 1.2 mg/ml Mg^{2+} no viable cells were detected. The cells showed high viability at lower concentrations of Mg derived from Mg2Ag extracts (0.3, 0.6 and 0.9 mg/ml Mg^{2+}). In general, cell metabolic activity was higher when pH was not adjusted, showing that increased pH can have positive effects on cell viability. These results have been published in an original article (216).

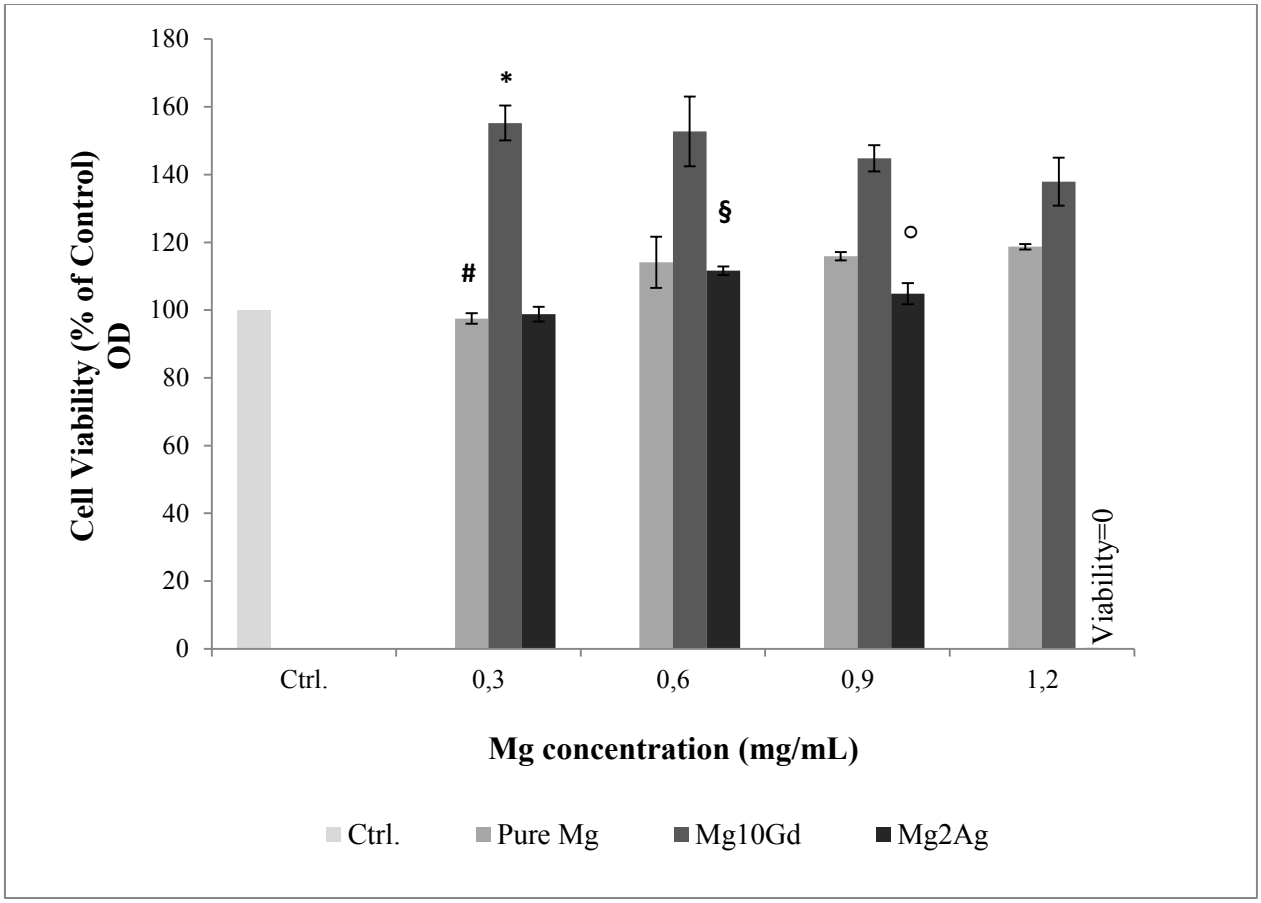

Fig 21. Viability of MC3T3-E1 cells treated with different concentrations of Mg^{2+} derived from pure Mg, Mg2Ag and Mg10Gd extracts determined by MTT assay.
Viability of MC3T3-E1 cells determined by MTT assay after incubation for 24hrs with 0.3, 0.6, 0.9 and 1.2 mg/ml Mg^{2+} resulted from pure Magnesium, Mg2Ag and Mg10Gd extracts. The pH of the extracts did not adjust to physiological level. At a pH of 8.6 cell viability was not affected. Statistical significance was tested with a One-way ANOVA test. *** $p<0.05$** as compared to cell viability of the control; **# $p<0.05$** as compared to cell viability at concentration of 1.2 mg/ml Mg^{2+} derived from Pure Mg extracts; **§ and °: $p<0.05$** as compared to cell viability at concentrations of 1.2 mg/ml Mg^{2+} derived from Mg2Ag extracts, these results have been published in an original article (216).

3.4 Biocompatibility testing of Magnesium-based implants pre-corroded in cell culture medium for 1, 2 and 3 days

3.4.1 Live-dead staining

Surface characteristics greatly influence cell viability and proliferation kinetics. In order to estimate whether pre-corroded Mg samples can decrease corrosion rates and influence cell viability, non-manipulated Mg and Mg alloys were immersed in cell culture medium for 1, 2 and 3 days. Non-corroded specimens were used as a control and the cells were cultured on these

samples using a similar procedure. Cell viability decreased markedly when the cells were cultured on pre-corroded samples (1, 2 days) and no viable cells were detected on 3 day pre-corroded pure Mg specimens (Fig 22). In contrast, cells grown on non-corroded and pre-corroded (1-2 days) Mg2Ag and Mg10Gd specimens were highly viable, showing that (1-2 days) pre-corrosion of the aforementioned samples did not have any negative impact on cell viability. Pronounced cells death was detected on Mg2Ag and Mg10Gd corroded for 3 days. In comparison to Mg2Ag corroded for 3 days, the cells showed higher viability on Mg10Gd for a similar immersion time (Fig 23 and 24). In general, cell viability was not negatively affected by cultivation on non-corroded specimens (Figs 22, 23 and 24). From live-dead results it can be concluded that cell death observed after 24h of cell cultivation on 2 or 3 day pre-corroded samples was not caused by high Mg^{2+} ion release into the supernatant. Since in this study the cells were only cultivated on pre-corroded samples for 24h, and, according to the results shown in Fig. 19, the amount of Mg^{2+} released into the medium in 24h was not higher than 0.5-0.6 mg/ml. These concentrations were not toxic for the cells, since according to the MTT results a notable decrease in metabolic activity of the cells only occurred at a Mg^{2+} concentration greater than 0.9 mg/ml for all Mg samples (Fig 20). These results have been published in an original article (216).

MC3T3-E1 cells cultivated on non-corroded pure Mg	MC3T3-E1 cells cultivated on 1 day corroded pure Mg
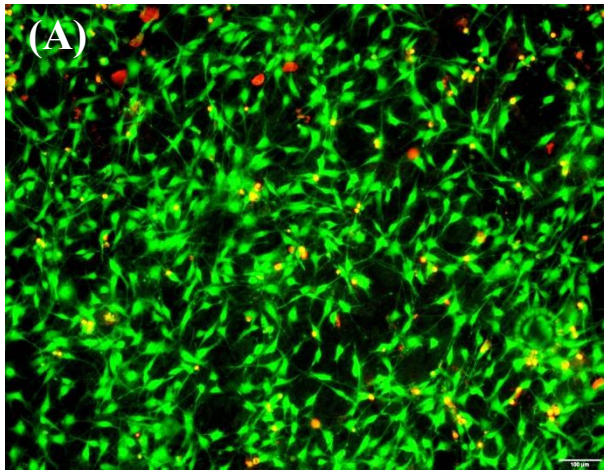	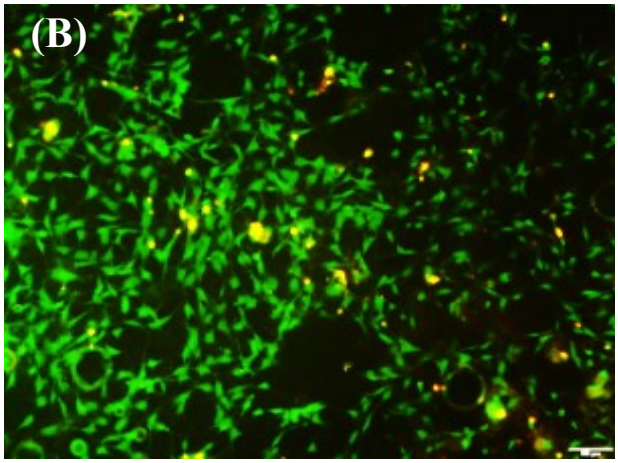
MC3T3-E1 cells cultivated on 2 day corroded pure Mg	**MC3T3-E1 cells cultivated on 3 day corroded pure Mg**
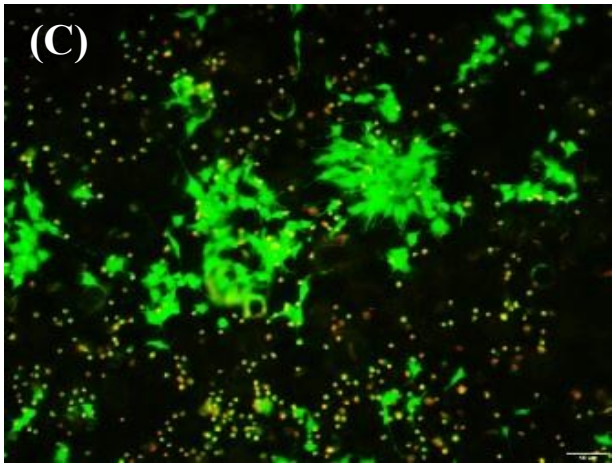	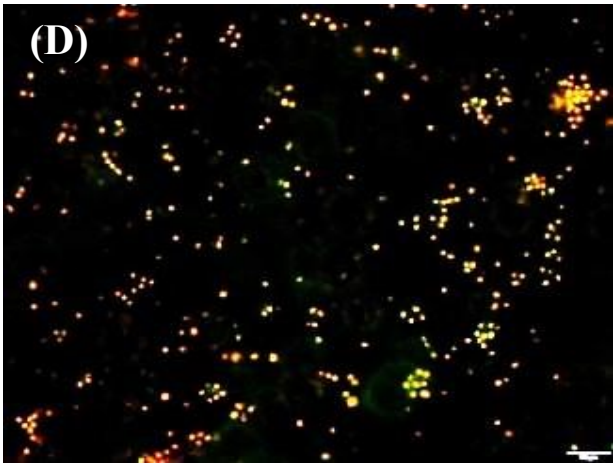

Fig 22. Viability of MC 3T3-E1 cultured on non-corroded pure Mg and specimens corroded for 1, 2, 3 days (A-D) respectively, determined by live-dead staining. **Scale bars:** 100 μm in all the pictures, these results have been published in an original article (216).

MC3T3-E1 cells cultivated on non-corroded Mg2Ag	MC3T3-E1 cells cultivated on 1 day corroded Mg2Ag
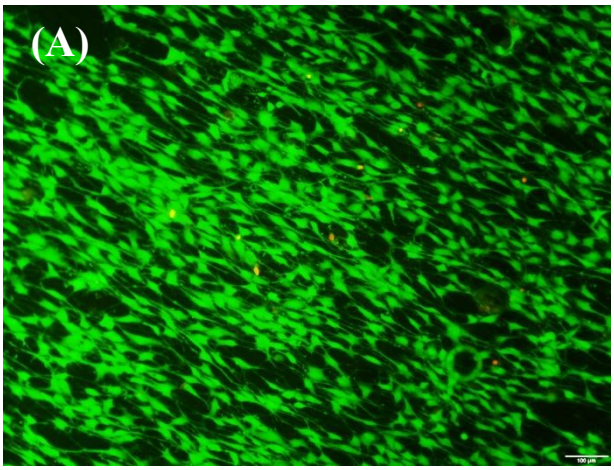	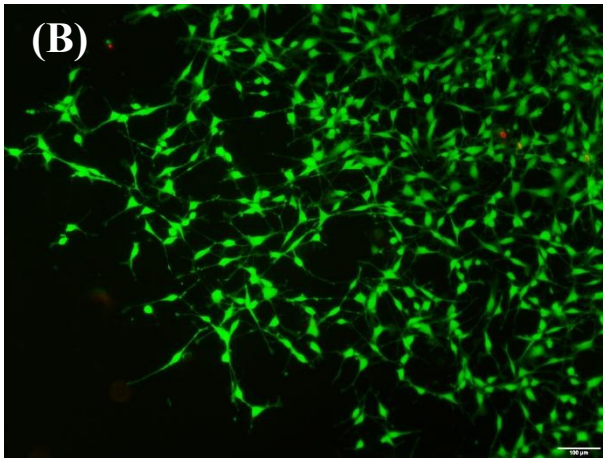
MC3T3-E1 cells cultivated on 2 days corroded Mg2Ag	**MC3T3-E1 cells cultivated on 3 days corroded Mg2Ag**
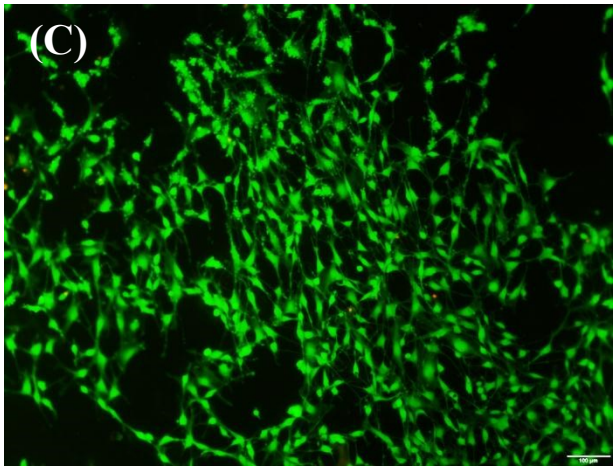	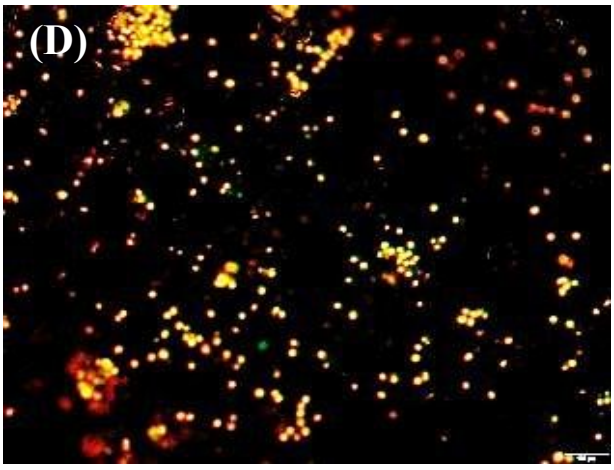

Fig 23. Viability of MC3T3-E1 cells cultured on non-corroded Mg2Ag and specimens corroded for 1, 2 and 3 days (A-D) respectively, determined by live-dead staining. **Scale bars:** 100 μm in all the pictures, these results have been published in an original article (216).

MC3T3-E1 cells cultivated on non-corroded Mg10Gd	MC3T3-E1 cells cultivated on 1 day corroded Mg210Gd
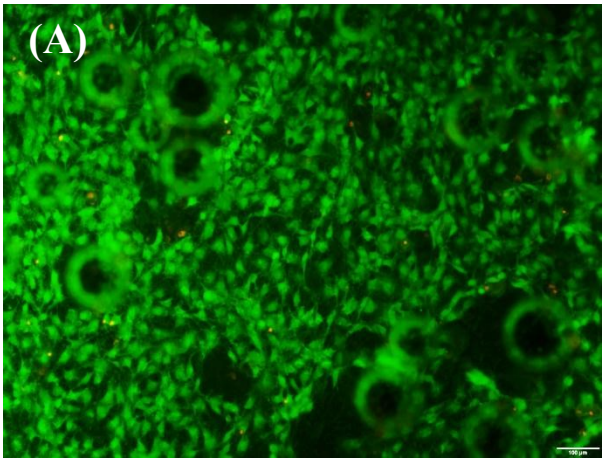	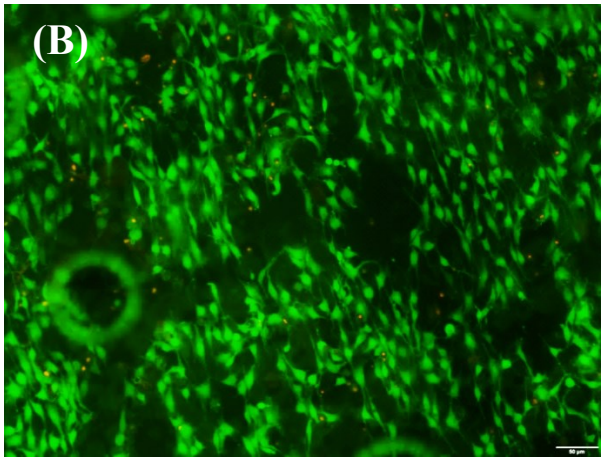
MC3T3-E1 cells cultivated on 2 day corroded Mg10Gd	**MC3T3-E1 cells cultivated on 3 day corroded Mg10Gd**
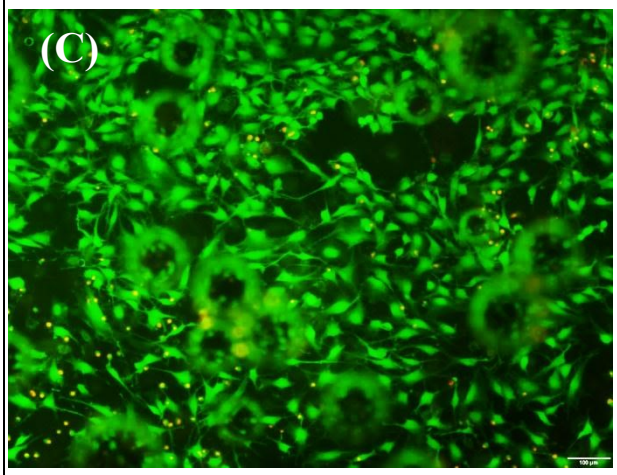	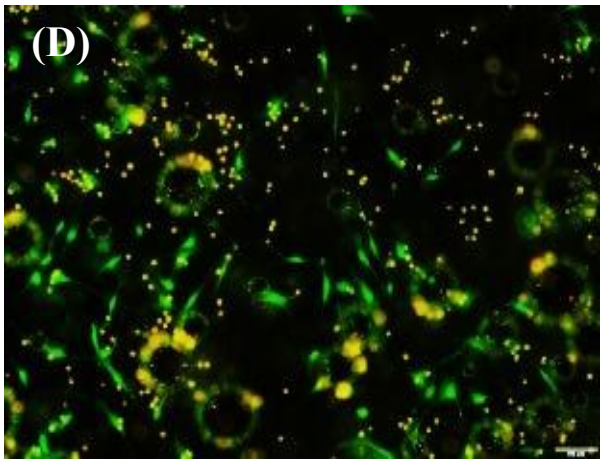

Fig 24. Viability of MC3T3-E1 cultured for 24hrs on non-corroded Mg10Gd and specimens corroded for 1, 2 and 3 days (A-D) respectively, determined by live-dead staining. **Scale bars:** 100 μm, these results have been published in an original article (216).

3.4.2 F-actin staining

Alterations in surface morphology during corrosion influence cell attachment and cell morphology. In order to evaluate the positive and/or negative influences of pre-corrosion of the Mg samples in cell culture medium on cell morphology, Mg-based implants were immersed in DMEM+10% FBS for 1, 2 and 3 days. The conclusions from live-dead staining were further substantiated by analysis of alterations in the morphology of cells cultivated on corroded and non-corroded specimens using F-actin staining and scanning electron microscopy. Actin filaments greatly influence cell adhesion and cell migration. The assessment of actin fibers and development of focal adhesions on the surface of materials with different surface structures is summarized in Figs 25, 26 and 27. Modification of the cytoskeletal system and evolution of focal adhesion networks during cell migration results in effective cell spreading, which is observable by florescent staining of actin filaments. A migrant cell displays various actin complexes in order to bind to the extracellular matrix. Actin filaments can be found in the form of Fillopodia or Lammelopodia. The flattened morphology of the MC3T3-E1 cells which were cultured on non-corroded pure Mg and Mg10Gd, and even multiple cell extensions which were recognized in cells cultured on non-corroded Mg2Ag specimens, illustrated the corrosion-independent effect of the sample surface on cell behavior. It can be concluded that the alloying system influenced cell morphology when pre-osteoblasts were cultured on non-corroded samples. Corroded Mg samples seemed to amplify cell structure based on actin filaments which can be defined by an increase in cell extensions. This phenomenon was especially prominent when cells were cultivated on pure Mg, Mg2Ag and Mg10Gd pre-corroded for 1 to 2 days (Figs 25, 26 and 27). For all Mg-based implants, increased corrosion time (up to 3 days) resulted in decreased cell viability. The number of cells declined significantly on Mg10Gd corroded for 3 days in cell culture medium compared to untreated specimens. In the overview picture (not shown here) relatively few cells were healthy and attached to the surface. Most of the cells exhibited a rounded morphology consistent with cell detachment apparently caused by cell death. Spherical cells were found on 3 day pre-corroded pure Mg and Mg2Ag, showing poor attachment of the cells to the surface of these specimens possibly due to cell death. These results demonstrate harmful influences of pre-corroded Mg samples on aspects of cell behavior such as cell morphology, cell viability and cell proliferation. These results have been published in an original article (216).

MC3T3-E1 cells cultivated on non-corroded pure Mg	MC3T3-E1 cells cultivated on 1 day corroded pure Mg
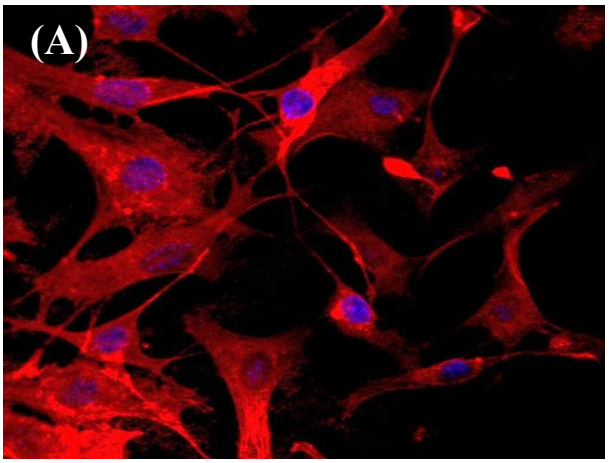	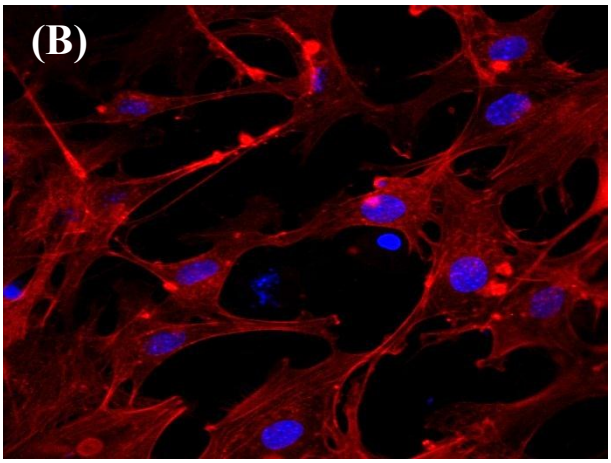
MC3T3-E1 cells cultivated on 2 day corroded pure Mg	**MC3T3-E1 cells cultivated on 3 day corroded pure Mg**
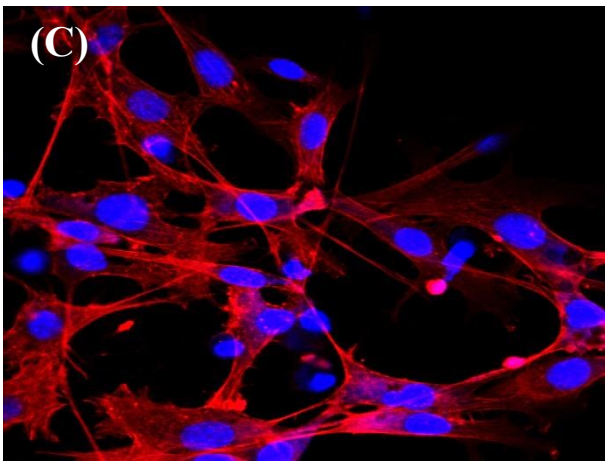	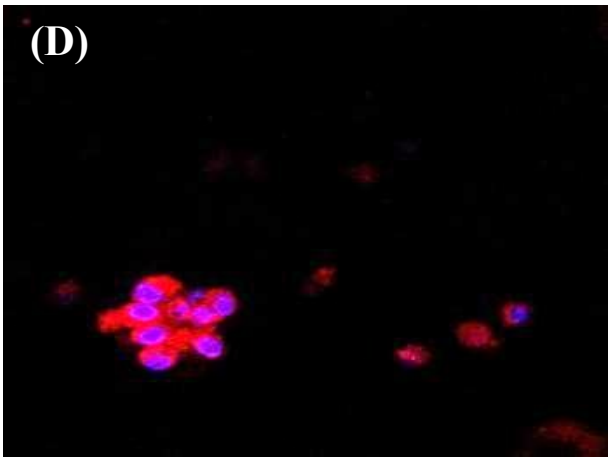

Fig 25. Changes in morphology of MC3T3-E1 cells cultured on non-corroded pure Mg, and specimens corroded for 1, 2 and 3 days (A-D) determined by phalloidin staining scanning. Cell nuclei were counterstained with DAPI. **Scale bars:** 20 μm, these results have been published in an original article (216).

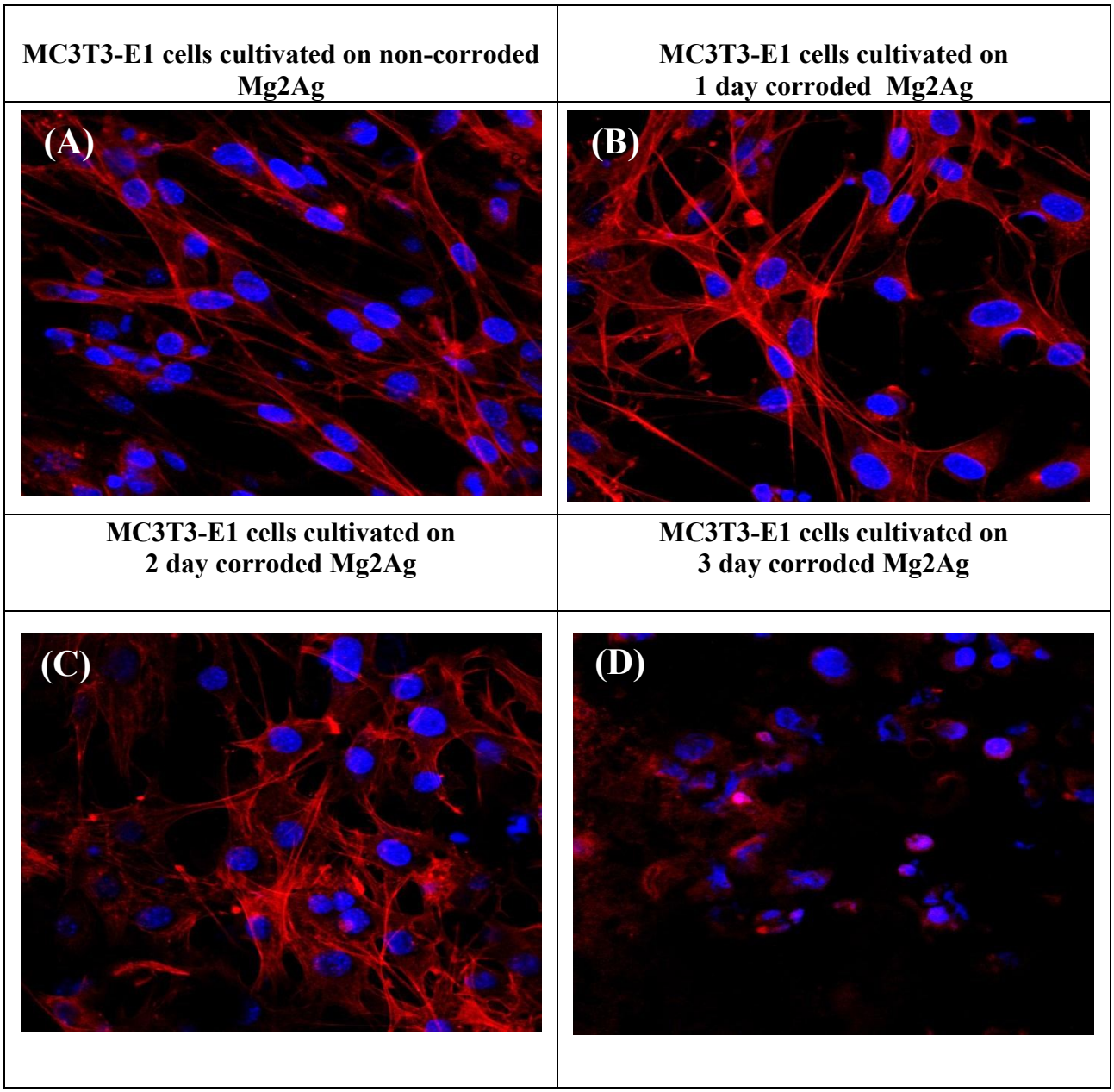

Fig 26. Changes in morphology of MC3T3-E1 cells cultured on non-corroded Mg2Ag, and specimens corroded for 1, 2 and 3 days (A-D) determined by phalloidin staining scanning. Cell nuclei were counterstained with DAPI. **Scale bars:** 20 μm, these results have been published in an original article (216).

MC3T3-E1 cells cultivated on non-corroded Mg10Gd	MC3T3-E1 cells cultivated on 1 day corroded Mg10Gd
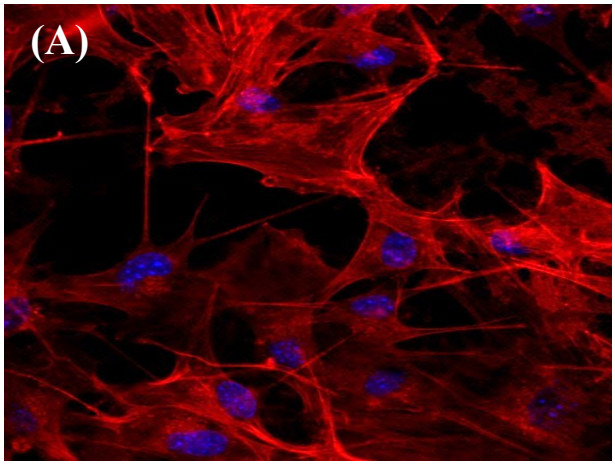	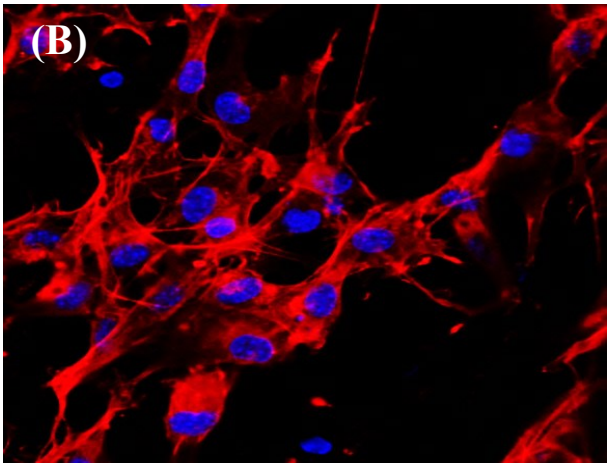
MC3T3-E1 cells cultivated on 2 day corroded Mg10Gd	**MC3T3-E1 cells cultivated on 3 day corroded Mg10Gd**
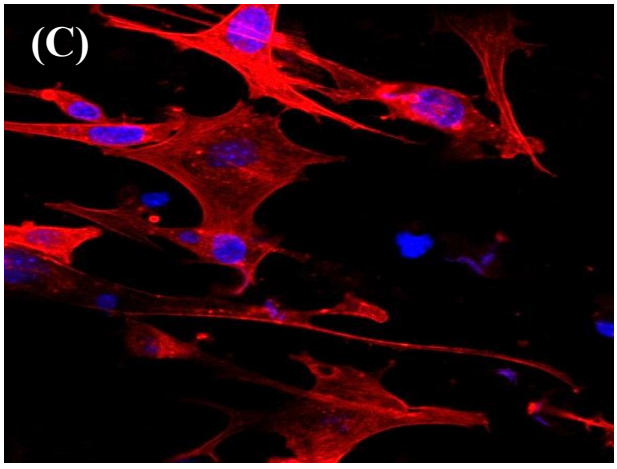	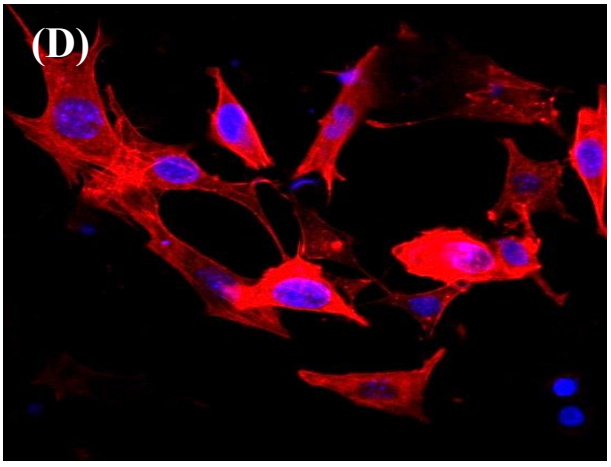

Fig 27. Changes in morphology of MC (3T3-E1) cells cultured on non-corroded Mg10Gd, and specimens corroded for 1, 2 and 3 days (A-D) determined by phalloidin staining scanning. Cell nuclei were counterstained with DAPI. **Scale bars:** 20 μm, these results have been published in an original article (216).

3.4.3 Scanning electron microscopy

The anchorage of cells to different Magnesium-based specimens as well as the morphology of cells attached to these surfaces were investigated by scanning electron microscopy (Figs 28, 29 and 30). Cell morphology can be better analysed in scanning electron microscopy pictures. As already shown by florescent staining of actin filaments, the alloying system used and alterations in the surface morphology of the specimens greatly influenced cell morphology. According to the SEM images, a variety of morphologies resulted from the passive deformation and active restructuring of the cytoskeleton during the adhesion procedure. The pictures captured by scanning electron microscopy were consistent with the results of F-actin staining. The cells exhibited a completely flattened morphology on non-corroded pure Mg and Mg10Gd specimens. Prolonged pre-corrosion times (up to 3 days) resulted in formation of more corrosion products which had a detrimental effect on cell morphology and caused cell death based on spherical cell morphology. Actin filaments seemed to develop with increased corrosion times, based on increased cell stretching. When cells were cultured on untreated Mg2Ag, actin filament extensions in different directions, comparable to controls (cells cultured on coverslips) were clearly observed. These results have been published in an original article (216).

MC3T3-E1 cells cultivated on non-corroded pure Mg	MC3T3-E1 cells cultivated on 1 day corroded pure Mg
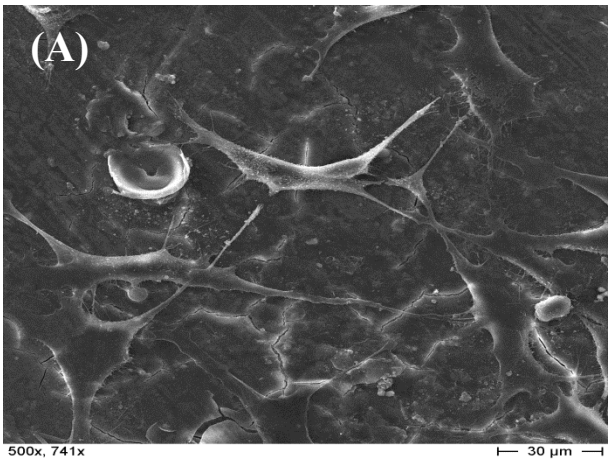	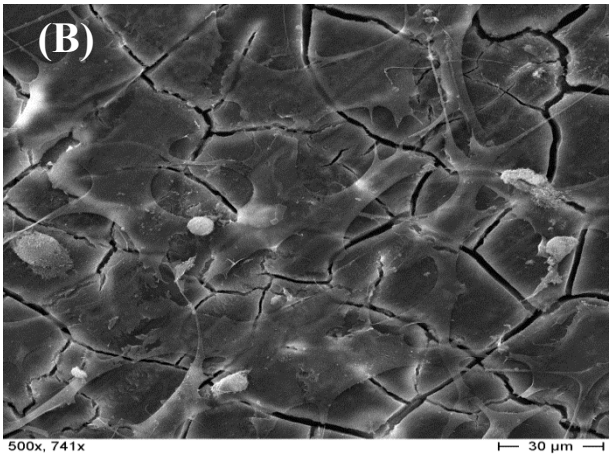
MC3T3-E1 cells cultivated on 2 day corroded pure Mg	**MC3T3-E1 cells cultivated on 3 day corroded pure Mg**
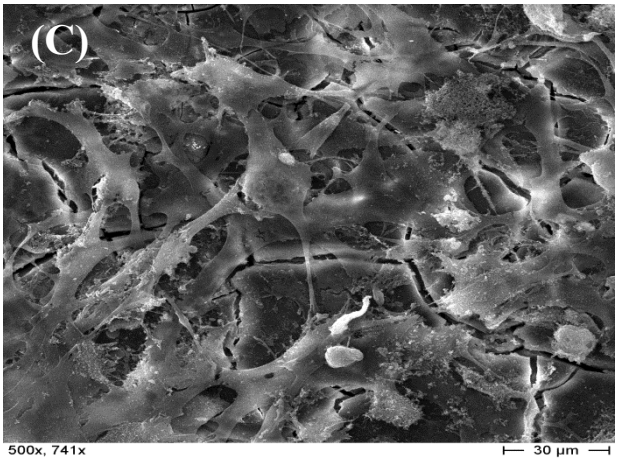	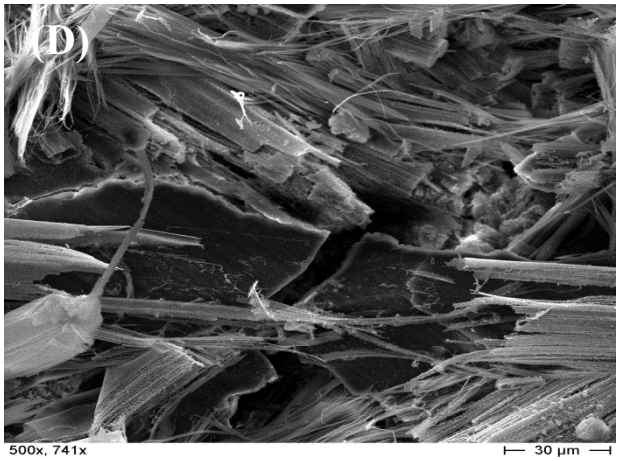

Fig 28. Changes in morphology of MC3T3-E1 cells cultured on non-corroded pure Mg and specimens corroded for 1, 2 and 3 days (A-D) determined by scanning electron microscopy. Images were obtained at 500x. **Scale bars:** 30 µm, these results have been published in an original article (216).

MC3T3-E1 cells cultivated on non-corroded Mg2Ag	MC3T3-E1 cells cultivated on 1 day corroded Mg2Ag
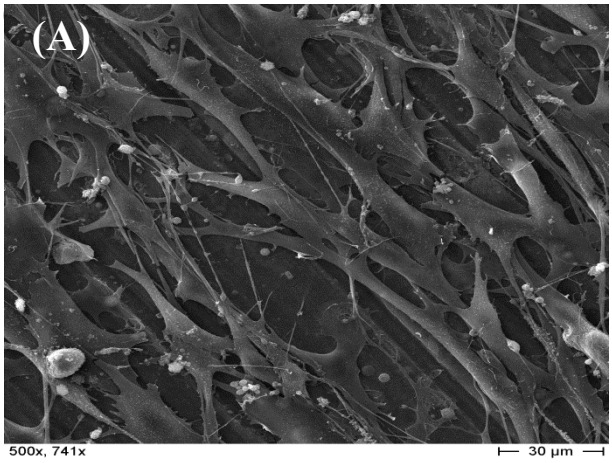	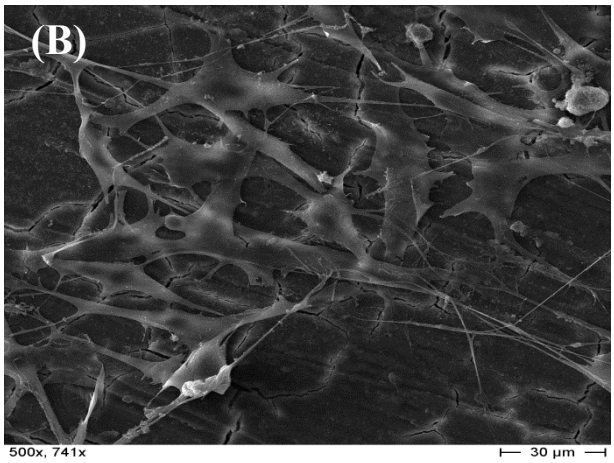
MC3T3-E1 cells cultivated on 2 day corroded Mg2Ag	**MC3T3-E1 cells cultivated on 3 day corroded Mg2Ag**
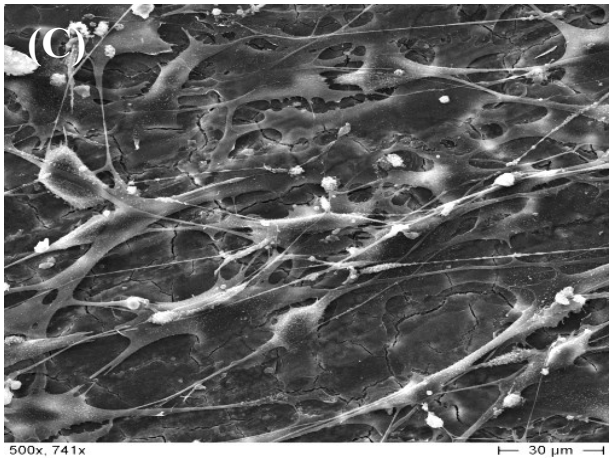	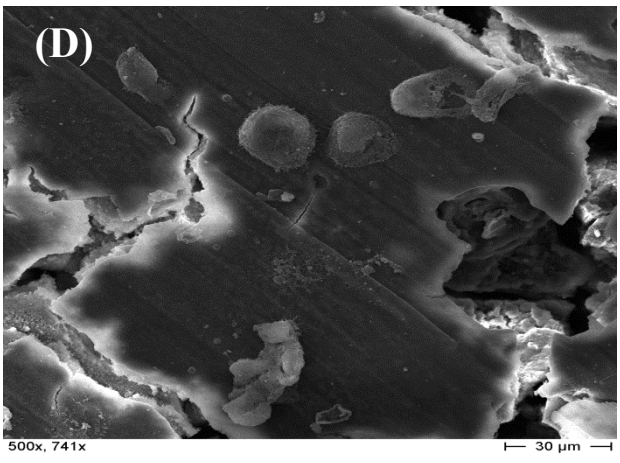

Fig 29. Changes in morphology of MC3T3-E1 cells cultured on non-corroded Mg2Ag and specimens corroded for 1, 2, and 3 days (A-D) determined by scanning electron microscopy. Images were obtained at 500x. **Scale bars:** 30 µm, these results have been published in an original article (216).

MC3T3-E1 cells cultivated on non-corroded Mg10Gd	MC3T3-E1 cells cultivated on 1 day corroded Mg10Gd
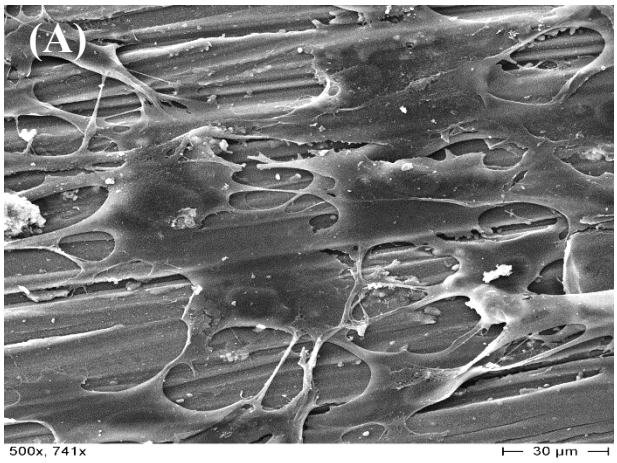	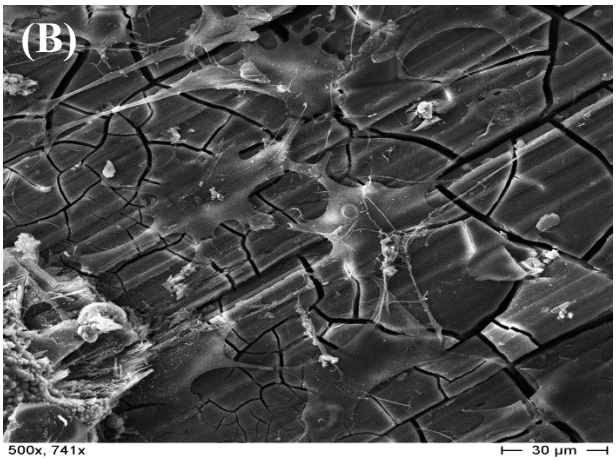
MC3T3-E1 cells cultivated on 2 day corroded Mg10Gd	**MC3T3-E1 cells cultivated on 3 day corroded Mg10Gd**
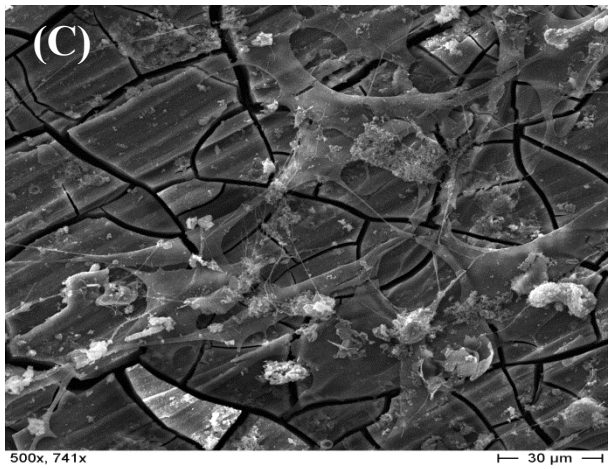	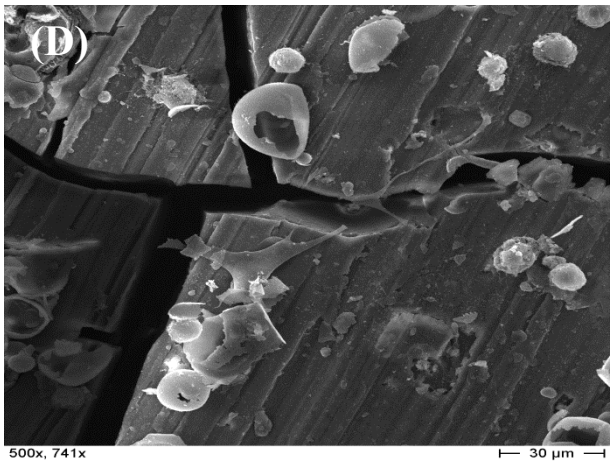

Fig 30. Changes in morphology of MC3T3-E1 cells cultured on non-corroded Mg10Gd, and specimens corroded for 1, 2 and 3 days (A-D) determined by scanning electron microscopy. Images were obtained at 500x. **Scale bars:** 30 µm, these results have been published in an original article (216).

3.5 Effect of Magnesium ions on cell morphology

Direct effects of corrosion and corrosion products on cell morphology were described in Parts 3.4.2 and 3.4.3. In these experiments, indirect effects of corrosion (Mg ions and pH) on cell morphology were assessed by cultivation of MC3T3-E1 cells for 24 hours in different concentration of Mg derived from pure Mg, Mg2Ag and Mg10Gd extracts. Fluorescent staining of F-actin filaments showed slight differences in the morphology of cells treated indirectly with Mg ions derived from Mg extracts compared to cells cultured directly on Mg-based specimens. Cells exhibited vigorous extensions in various directions when treated with a Mg^{2+} concentration of 0.3 mg/ml. The cells, moreover, exhibited a healthy appearance with many cell-cell interactions. Both Fillopodia and Lammelopodia like structures were observable in cells at this concentration. Similar morphologies were detected when the cells were treated with Mg ion concentrations of 0.6, 0.9 and 1.2 mg/ml. Cells produced minor extensions when cultured directly on untreated pure Mg specimens. In contrast, prominent extensions were observed when cells were treated indirectly with different concentrations of Pure Mg extracts (Fig 31 (A-D)).

Actin filaments were extended intensively in different directions when the cells were treated with 0.3 and 0.6 mg/ml Mg^{2+} derived from Mg2Ag extracts. When the cells were incubated in medium containing 0.9 mg/ml Mg^{2+}, no more extensions were observable. Cells with short Fillopodia appeared semi-healthy at this concentration. 1.2 mg/ml Mg^{2+} was completely toxic for the cells. The morphology of cells treated with Mg^{2+} concentrations of 0.3 and 0.6 mg/ml was similar to that of cells cultured directly on Mg2Ag specimens (Fig. 31 A-D). MC3T3-E1 cells exhibited pronounced Fillopodia as well as a flattened morphology after treatment with 0.3, 0.6 and 0.9 mg/ml Mg^{2+} derived from Mg10Gd extracts similar to that observed on the surface of untreated Mg10Gd specimens. Cells treated with a Mg^{2+} concentration 1.2 mg/ml, exhibited a spherical morphology probably indicative of cell death (Fig 31 (I-L)). This result was consistent with MTT assay results showing that the cells were completely healthy after treatment with different concentrations of Mg (pure Mg extracts) (Fig 20). At the highest concentration of Mg^{2+} tested (1.2 mg/ml) derived from Mg2Ag and Mg10Gd extracts, no viable cells were detected which was consistent with immunofluorescent staining results showing a cell morphology.

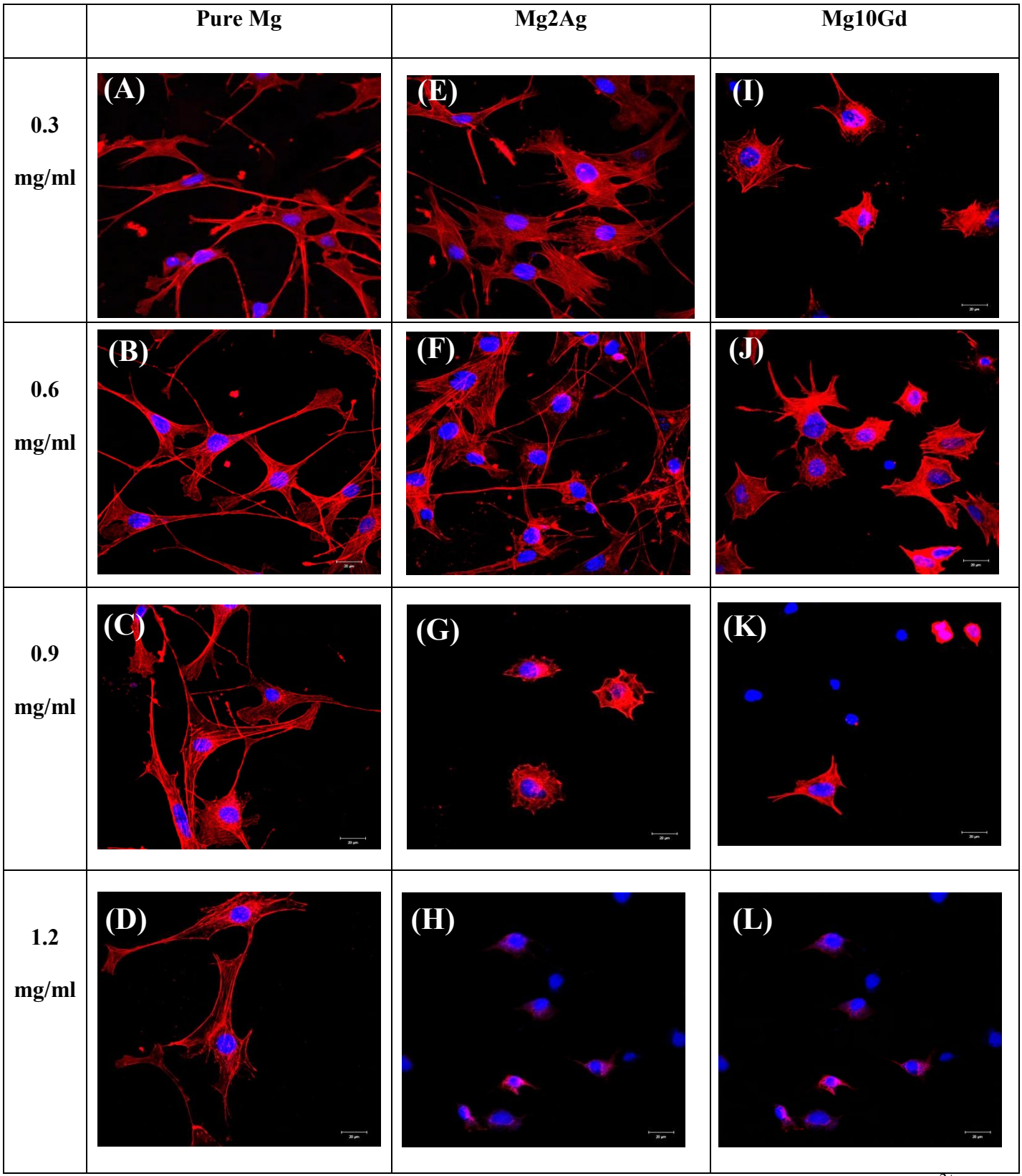

Fig 31. Changes in morphology of MC3T3-E1 cells treated with 0.3, 0.6, 0.9 and 1.2 mg/ml Mg^{2+} derived from pure Mg, Mg2Ag and Mg10Gd extracts after 24hrs, determined by phalloidin staining. Cell nuclei were counterstained with DAPI. **Scale bars:** 20 µm

3.6Real time PCR

Real time PCR was performed to track the expression profiles of osteogenic markers during direct culture of MC3T3-E1 cells on pure magnesium implants. Before analyzing the expression pattern of osteogenic markers, expression of five housekeeping genes (18sRNA, 28sRNA, 36b4, beta actin and GAPDH) was controlled to determine whether Mg, as a major component of the biodegradable implants, has any influence on the expression of these genes. The results showed strong regulation of housekeeping genes at different time points compared to controls (cells cultured on tissue culture plate) (Fig 32). Mg is known to be a cofactor for the Taq polymerase enzyme and to play an important role during the reaction process. Since Mg-based implants strongly regulated housekeeping genes, the experiments were performed at the protein level (western blot experiments).

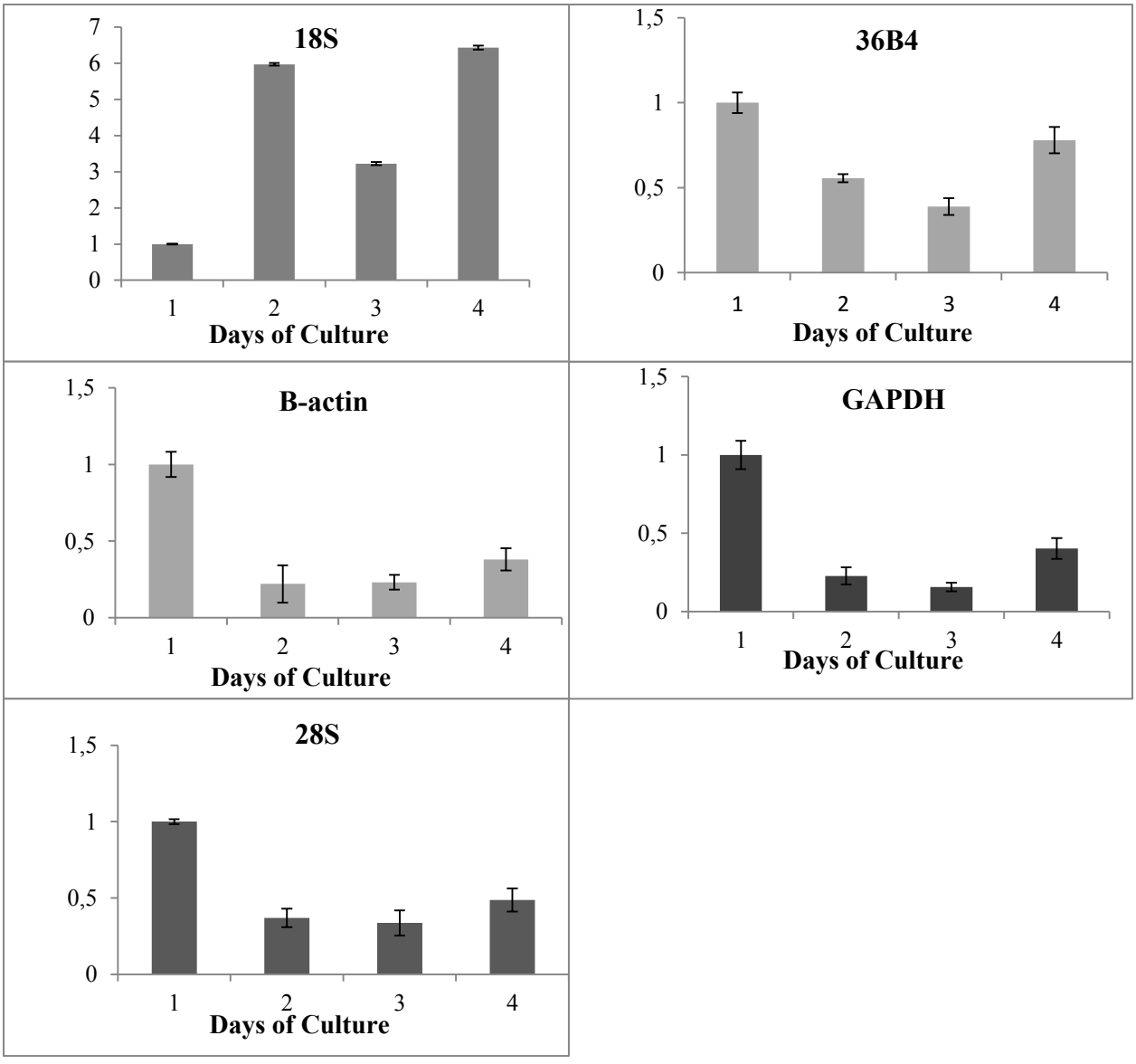

Fig 32. Quantitative real time PCR of MC3T3-E1 cultured on pure Magnesium for 2, 4 and 6 days. Cells cultured on cell culture plate were used as control. 18sRNA, 36B4, B-actin, GAPDH, 28sRNA were used as housekeeping genes.

3.7 Immunocytochemistry

Extracellular matrix proteins play an important role in endochondral bone ossification and bone development. Collagen I expression for example reaches a maximum during the ossification phase. Mutation of Collagen I in mice has been reported to result in a destructive form of osteogenesis imperfecta characterized by bones that are prone to cracking (230). In order to address the effect of different Magnesium alloys on the expression of bone osteogenic markers over time collagen expression was evaluated by immunocytochemistry.

An early down-regulation of Collagen I expression was recognized in cells cultured on Mg-based implants compared to control (cells cultured on cover slips without alloying system). No significant increase in the expression level of Collagen I was observed over time. At late time points, however, a significant rise in the expression of Collagen I comparable to the control level was only recognized for cells cultured on Mg10Gd. Collagen I expression was significantly down-regulated in cells cultured on pure Mg compared to the control, whilst no clear differences in collagen I expression were observed at different time points. A similar trend was observed when cells were cultured on Mg2Ag specimens, which exhibited no significant differences in collagen I expression level at different time points (Fig 33). These results have been published in an original article (216).

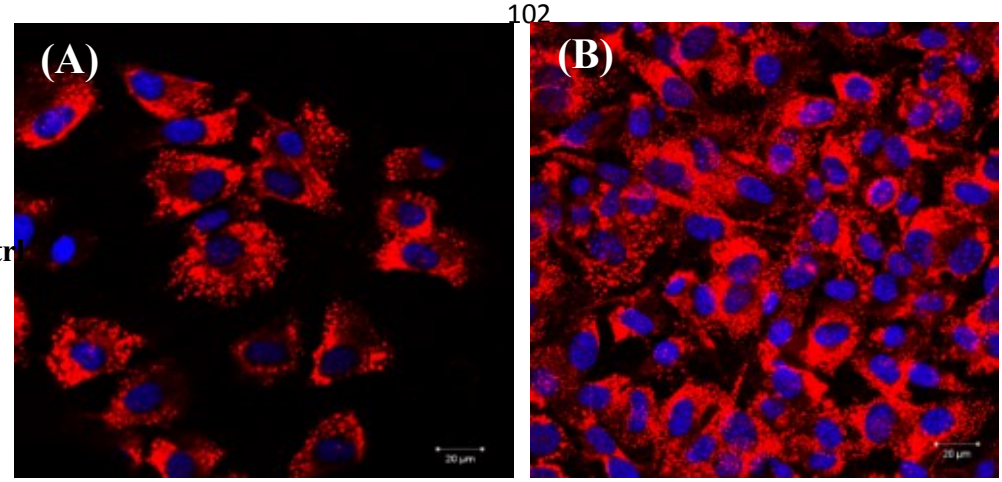

Positive Ctrl

Day 2 Day 4 Day 8 Day 12

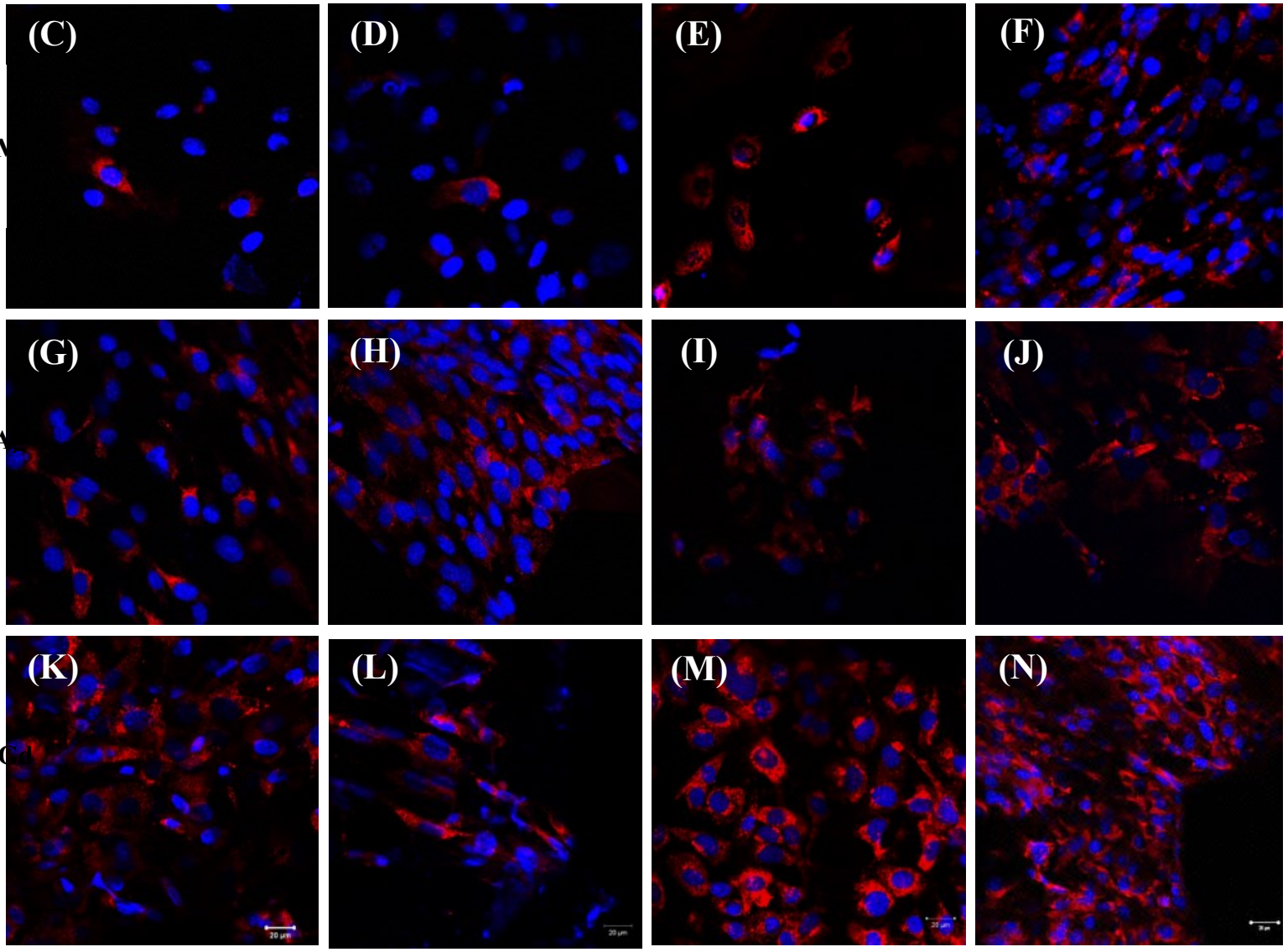

pure M

Mg2A

Mg10C

Fig 33. Immunostaining of MC3T3-E1 cells cultured on non-corroded pure Mg, Mg2Ag and Mg10Gd for Collagen I at days 2, 4, 8 and 12 (A-N). Cells on coverslips were used as a control. Cell nuclei were counterstained with DAPI. **Scale bars:** 20 μm, these results have been published in an original article (216).

3.8 Western blots and Live-dead staining

The expression patterns of two important osteogenic markers (Runx2 and Collagen I) were assessed on days 2, 4, 6, 8, 10 and 12. Runx2 is a key transcription factor which is correlated with osteoblast differentiation. Collagen I is one of the extracellular matrix proteins which build the organic matrix of the bone. Before performing western blots to track the differentiation process at the molecular level and determine the effect of different magnesium alloys on the expression of bone osteogenic markers, cells were cultured on non-corroded Mg based implants for 2, 4, 8 and 12 days. Cell viability following longer incubation times was determined by Live-dead staining. Evidence of cell proliferation when cells were cultured on all of the different Magnesium-based implants over time (2-12 days) was provided below (Figs 34, 35 and 36). Cultivation of MC3T3-E1 cells on Mg2Ag, Mg10Gd and pure Mg did not result in noticeable cell death. ICP-OES results showed a reduction in corrosion rate (demonstrated by moderate release of Mg ions), when cells were cultured on Magnesium-based implants. As shown by immunocytochemistry experiments, an early alloy system-independent down-regulation of Collagen I expression was detected in pre-osteoblasts compared to control cells cultured on cell culture plates. At late time points, however, a notable rise in expression of Collagen I was detected only when cells were cultured on Mg10Gd specimens. Expression of Collagen I in MC3T3-E1 cells declined during the whole cultivation period, when cells were cultured on Mg2Ag and pure Mg specimens (Figs 37, 38 and 39). Western blot results indicated a similar pattern of expression for Runx2 in MC3T3-E1 cells. Although an initial down-regulation of Runx2 expression was observed in MC3T3-E1 cells compared to control cells, the osteogenic potential of the cells recovered when cultured on Mg10Gd specimens. In contrast, expression of Runx2 in pre-osteoblasts cultured on Mg2Ag and pure Mg declined constantly, leading to undetectable levels of Runx2 after 12 days of cultivation. Although the differences between expression levels at different time points were not statistically significant, the results demonstrated a noticeable deterioration in the osteogenic potential of the cells to be caused by Mg2Ag and pure Mg (Figs 37, 38 and 39). These results have been published in an original article (216).

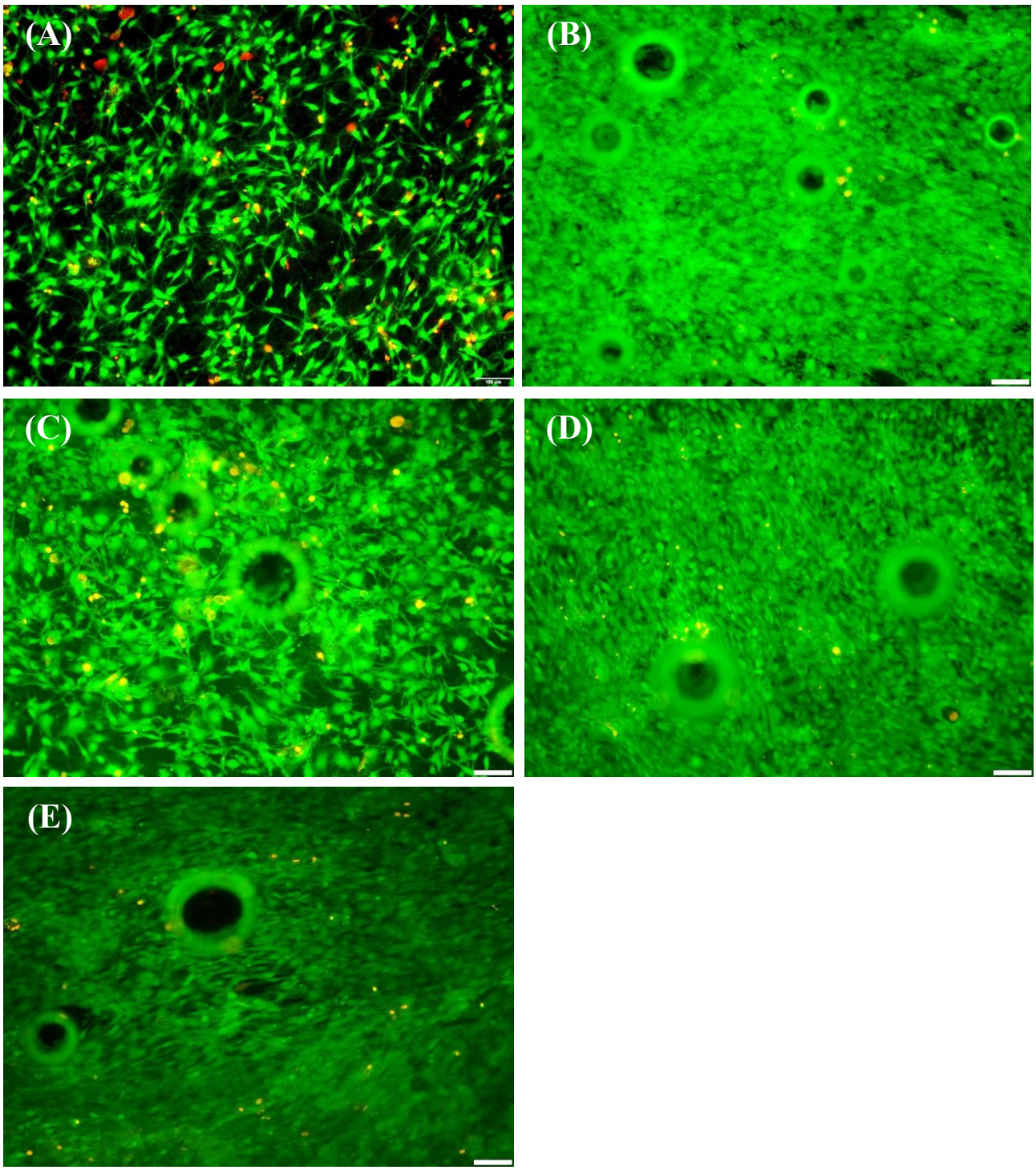

Fig 34. Viability of MC3T3-E1 cells cultured on pure Mg, without pre-incubation at days 2, 4, 6, 8 and 12 determined by live-dead staining (A-E respectively). **Scale bars:** 100 μm, these results have been published in an original article (216).

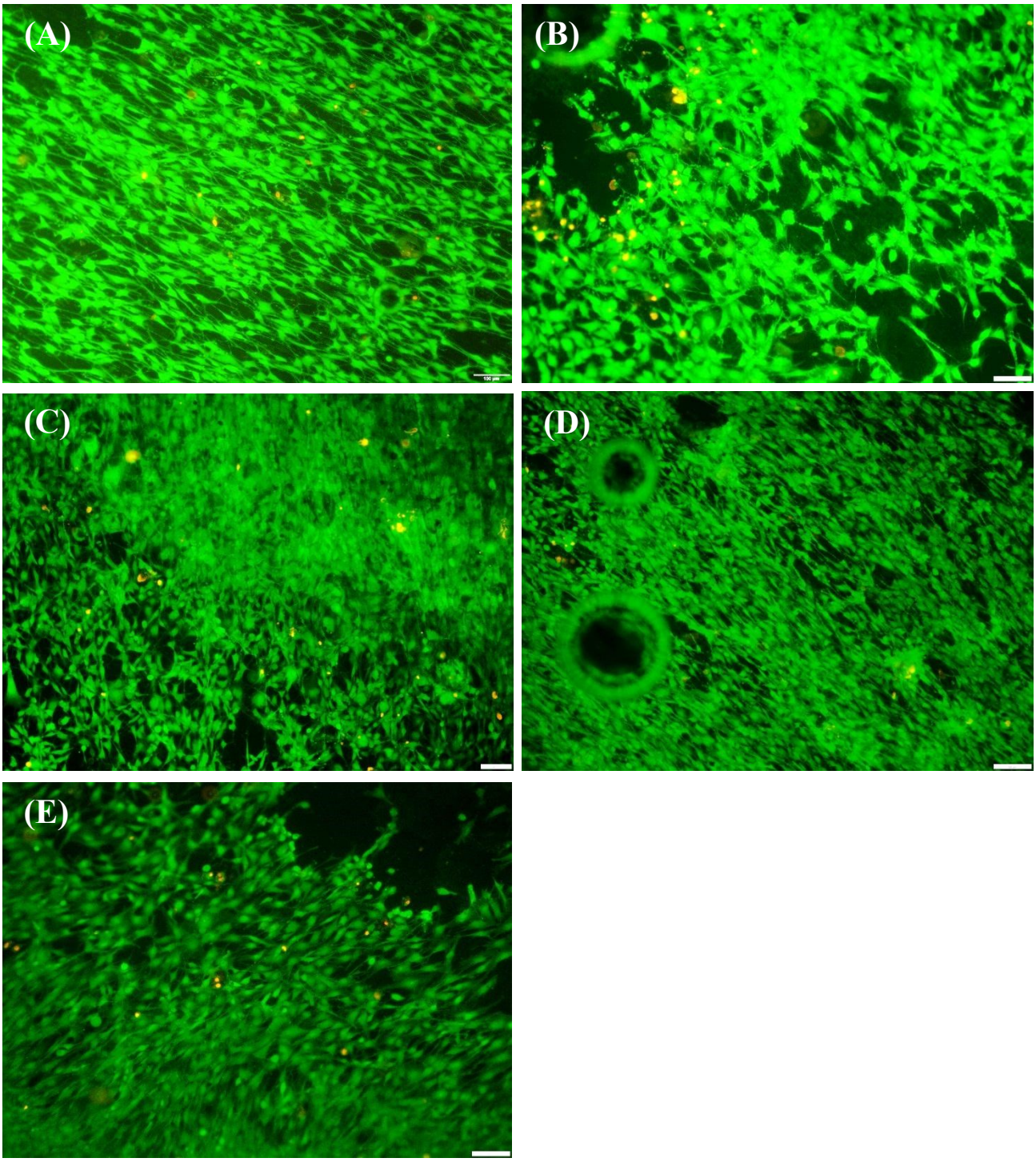

Fig 35. Viability of MC3T3-E1 cells cultured on Mg2Ag, without pre-incubation at days 2, 4, 6, 8 and 12, determined by live-dead staining (A-E respectively). **Scale bars:** 100 μm, these results have been published in an original article (216).

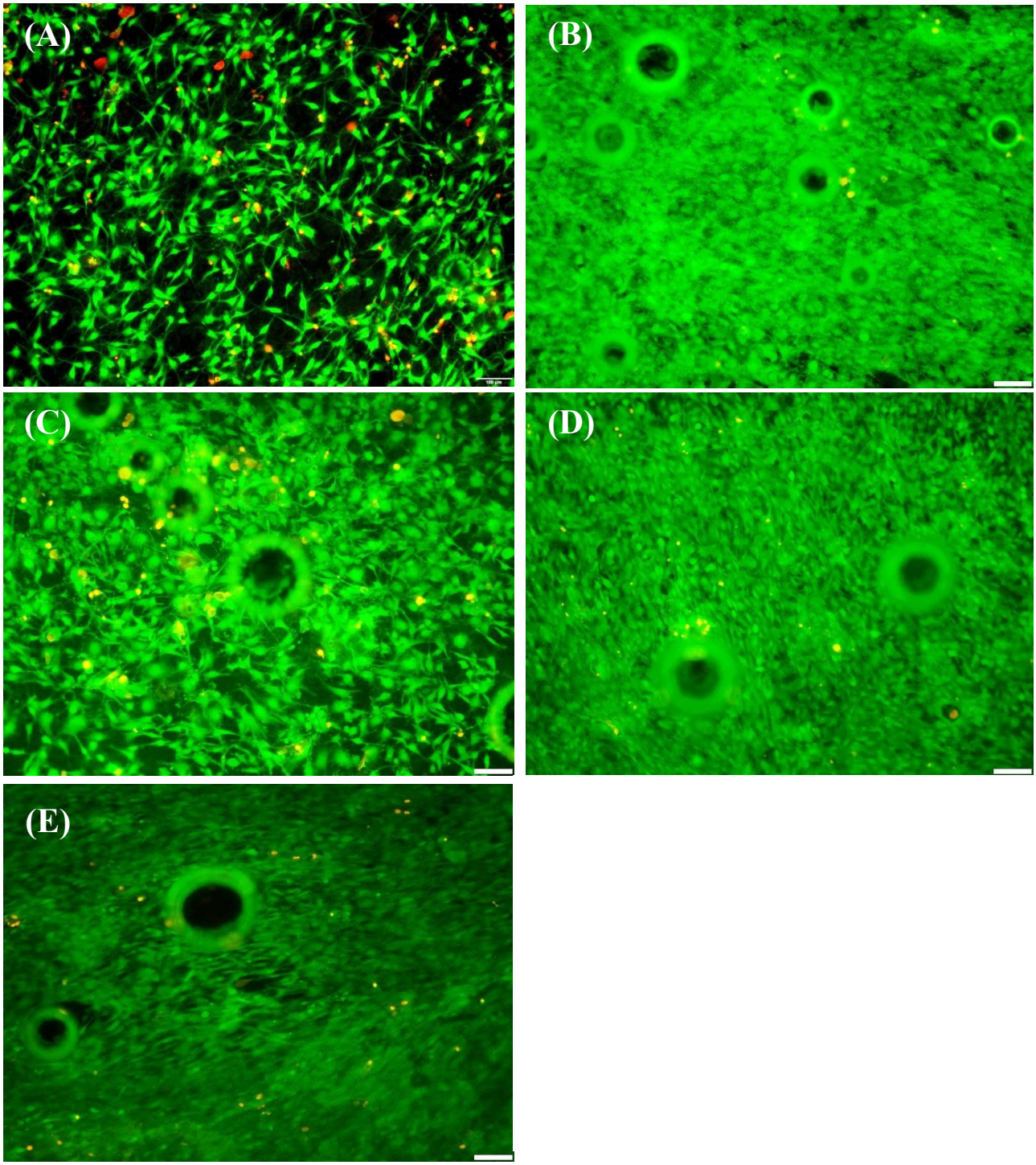

Fig 36. Viability of MC3T3-E1 cultured on Mg10Gd, without pre-incubation at day 2, 4, 6, 8 and 12 determined by live-dead staining (A-E respectively). **Scale bars:** 100 μm, these results have been published in an original article (216).

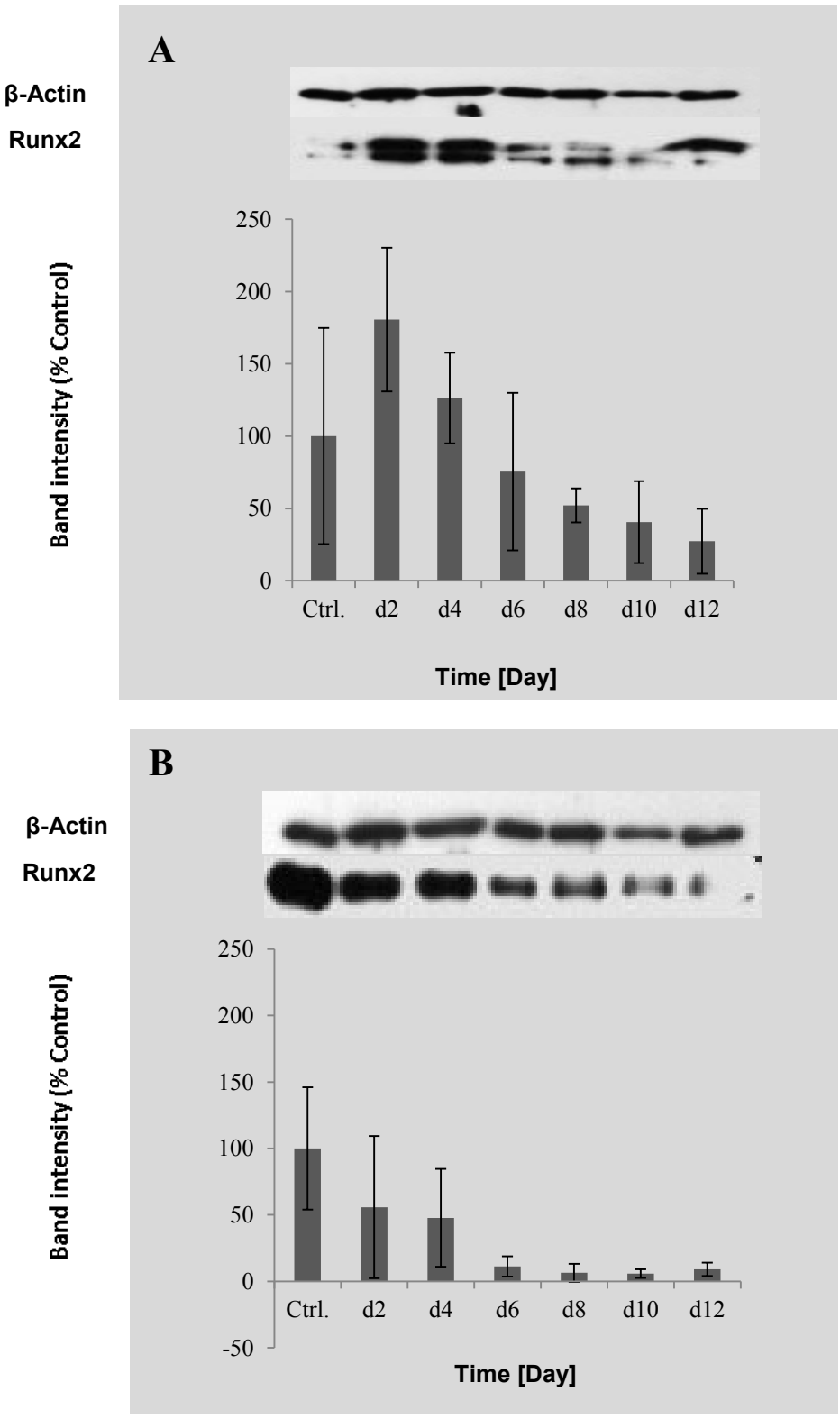

Fig 37. Protein expression levels of (A) Collagen I and (B) Runx2 in MC3T3-E1 cells cultured directly on pure Mg at days 2, 4, 6, 8, 10 and 12 determined by western blot, these results have been published in an original article (216).

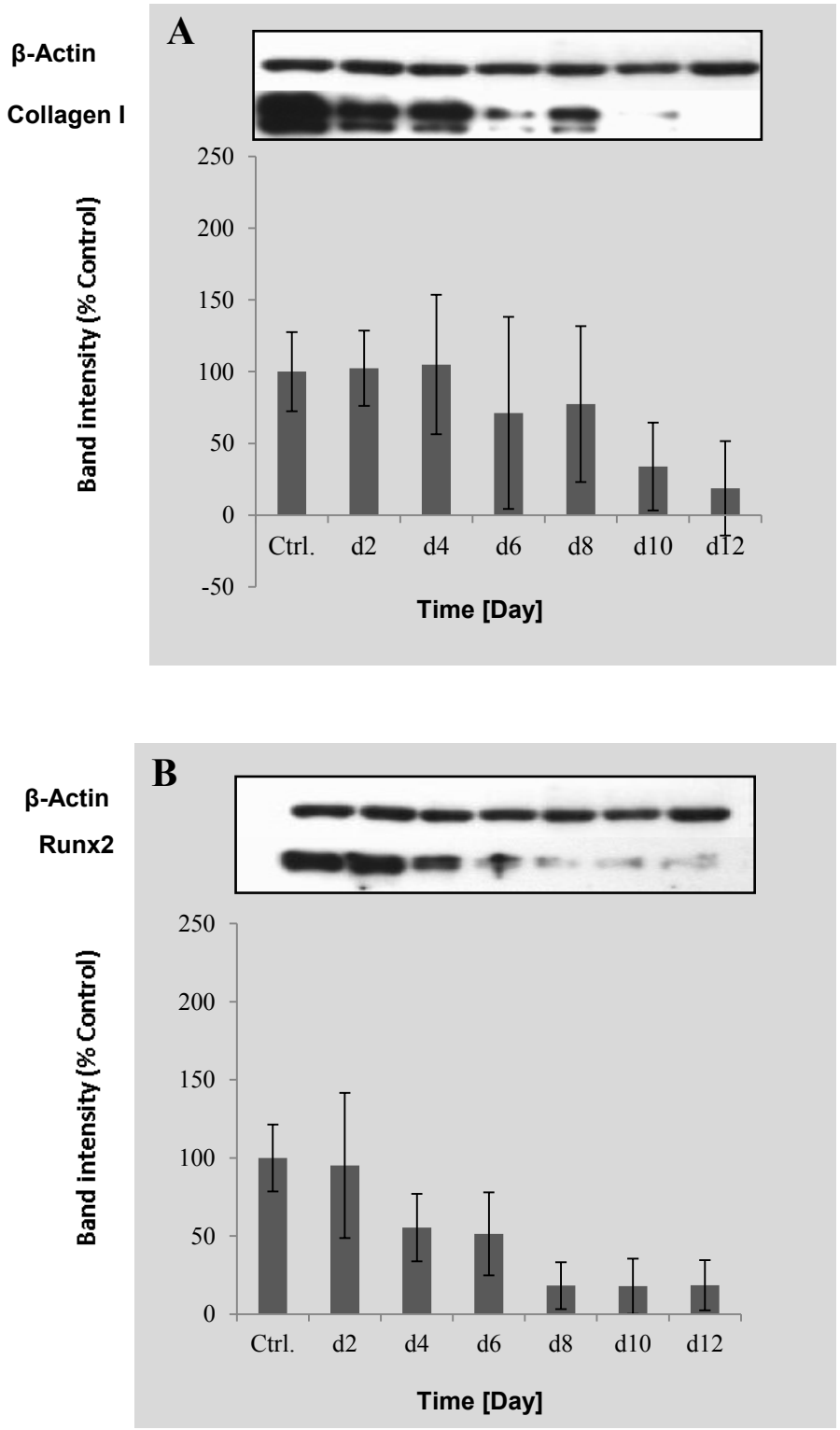

Fig 38. Protein expression levels of (A) Collagen I and (B) Runx2 in MC 3T3-E1 cells cultured directly on Mg2Ag at days 2, 4, 6, 8, 10 and 12 determined by western blot, these results have been published in an original article (216).

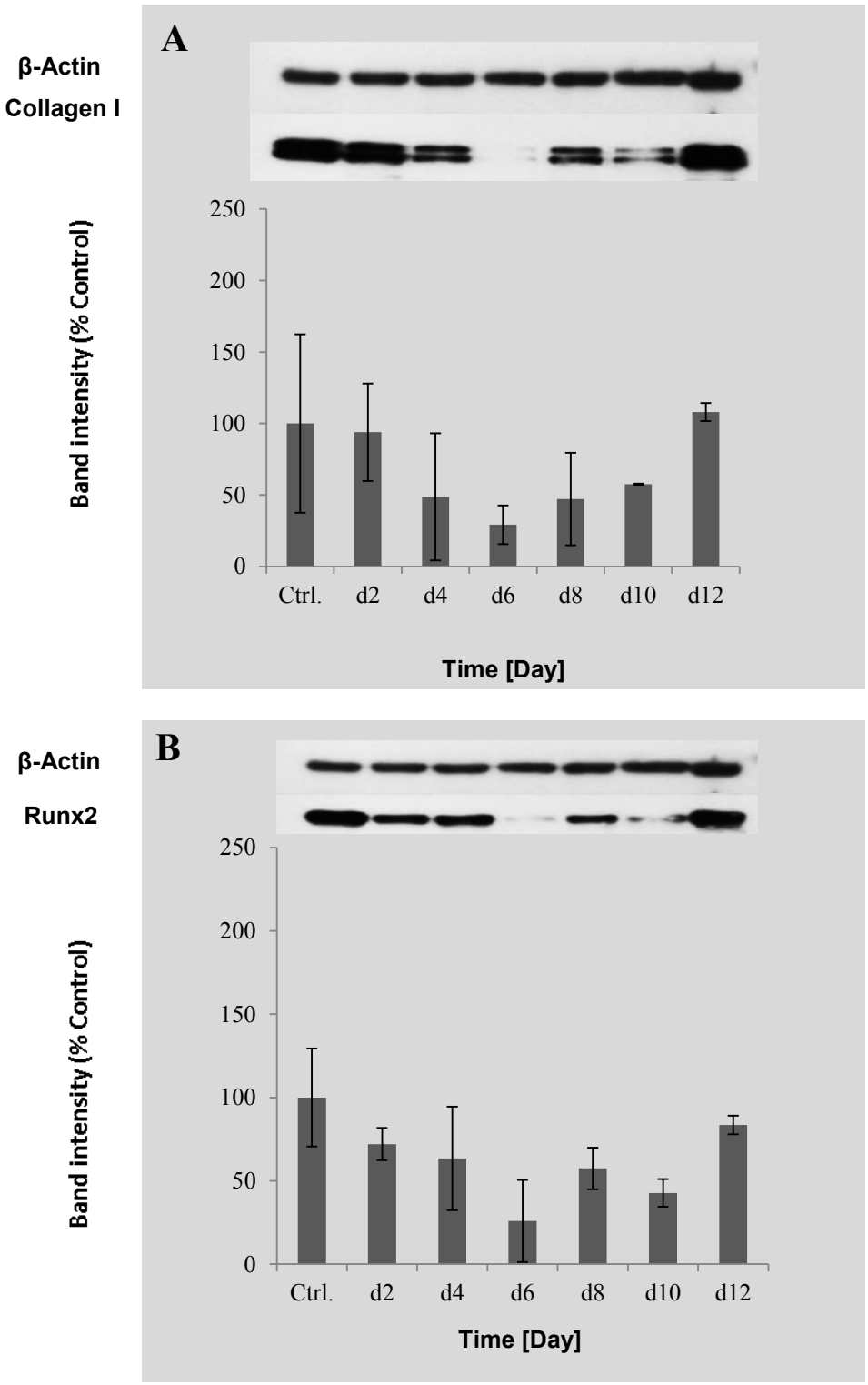

Fig 39. Protein expression levels of (A) Collagen I and (B) Runx2 in MC 3T3-E1 cells cultured directly on Mg10Gd at days 2, 4, 6, 8, 10 and 12 determined by western blot, these results have been published in an original article (216).

3.9 Antimicrobial activity of silver containing specimens

Silver has been reported to have antimicrobial properties. Some studies have furthermore reported an increased antibacterial activity of Mg-based implants with an increased silver content. In this study, survival of two bacterial strains (S.aureus and S. epidermidis) was analysed during treatment over a 72h period with different dilutions of extracts derived from Mg2Ag, Mg4Ag and Mg6Ag specimens.

S.aureus showed high viability in a low dilution of Mg2Ag, Mg4Ag and Mg6Ag (10% dilution). Initial growth restriction was detected in S.aureus only when treated with 25% diluted Mg2Ag extracts. In contrast, S.aureus showed high viability (comparable to the control) in 25% diluted extracts of Mg4Ag and Mg6Ag. No bacterial growth was detected in 50% diluted Mg2Ag extracts. Growth of S. aureus was only delayed after treatment with 50% diluted Mg4Ag and Mg6Ag extracts. Growth level returned to normal at later time points. No bacterial growth was detected in 75% and 100% dilutions of all silver-containing specimens, showing the antibacterial function of these specimens as bioresorbable implants (Fig 40).

S.epidermidis showed larger peaks after treatment with extracts of Ag-containing specimens in comparison to S. aureus, which exhibited evidence of biofilm formation. Like S.aureus, S.epidermidis showed high viability in 10% diluted Mg4Ag and Mg6Ag extracts. S.epidermidis showed lower viability at similar dilutions of Mg2Ag extracts. 25% diluted Mg4Ag and Mg6Ag extracts resulted in an initial growth restriction of S.epidermidis. Interestingly, the same dilution which was derived from Mg2Ag extracts was completely toxic for this bacterium. No viable bacteria were found in 50%, 75% and 100% diluted extracts. These results were consistent with antibacterial activity of silver-containing bioresorbable materials. Mg2Ag however possessed higher antibacterial activity against both bacterial strains, even at lower dilutions compared to Mg4Ag and Mg6Ag, showing that an increased silver content does not significantly influence bacterial survival (Fig 41).

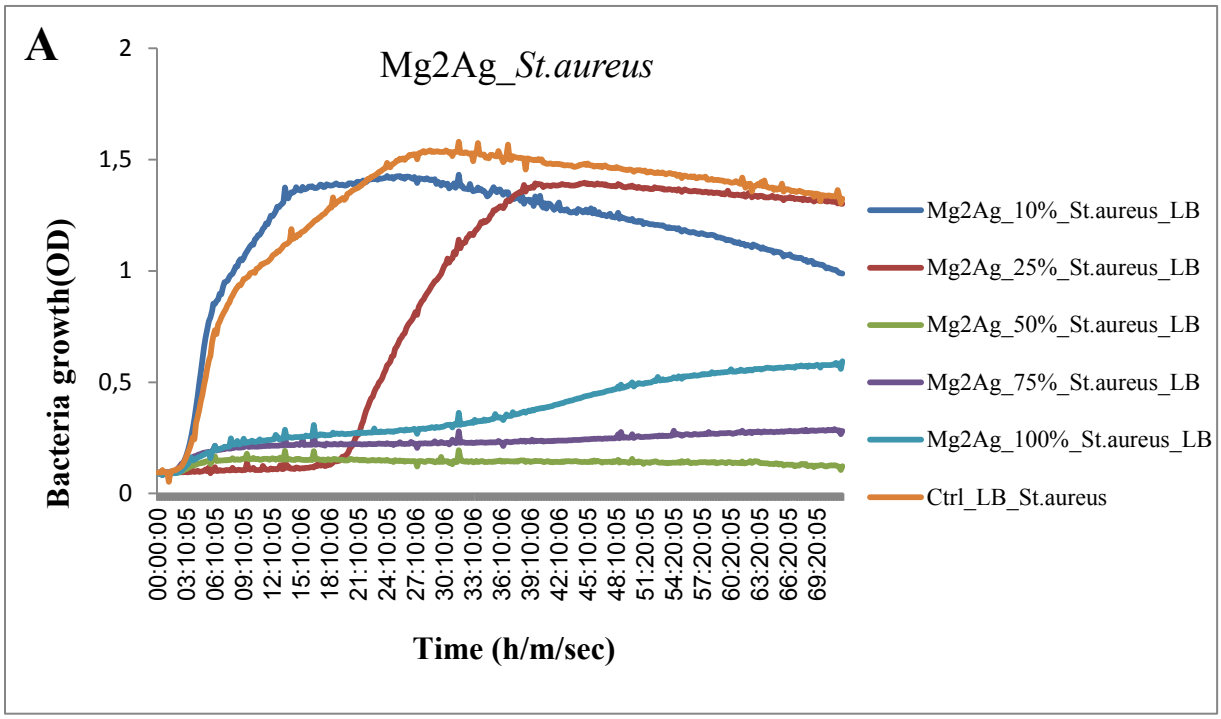
A
Mg2Ag_St.aureus
Bacteria growth(OD)
2
1,5
1
0,5
0
00:00:00
03:10:05
06:10:05
09:10:05
12:10:05
15:10:06
18:10:06
21:10:05
24:10:05
27:10:06
30:10:06
33:10:06
36:10:06
39:10:06
42:10:06
45:10:05
48:10:05
51:20:05
54:20:05
57:20:05
60:20:05
63:20:05
66:20:05
69:20:05
Time (h/m/sec)
Mg2Ag_10%_St.aureus_LB
Mg2Ag_25%_St.aureus_LB
Mg2Ag_50%_St.aureus_LB
Mg2Ag_75%_St.aureus_LB
Mg2Ag_100%_St.aureus_LB
Ctrl_LB_St.aureus

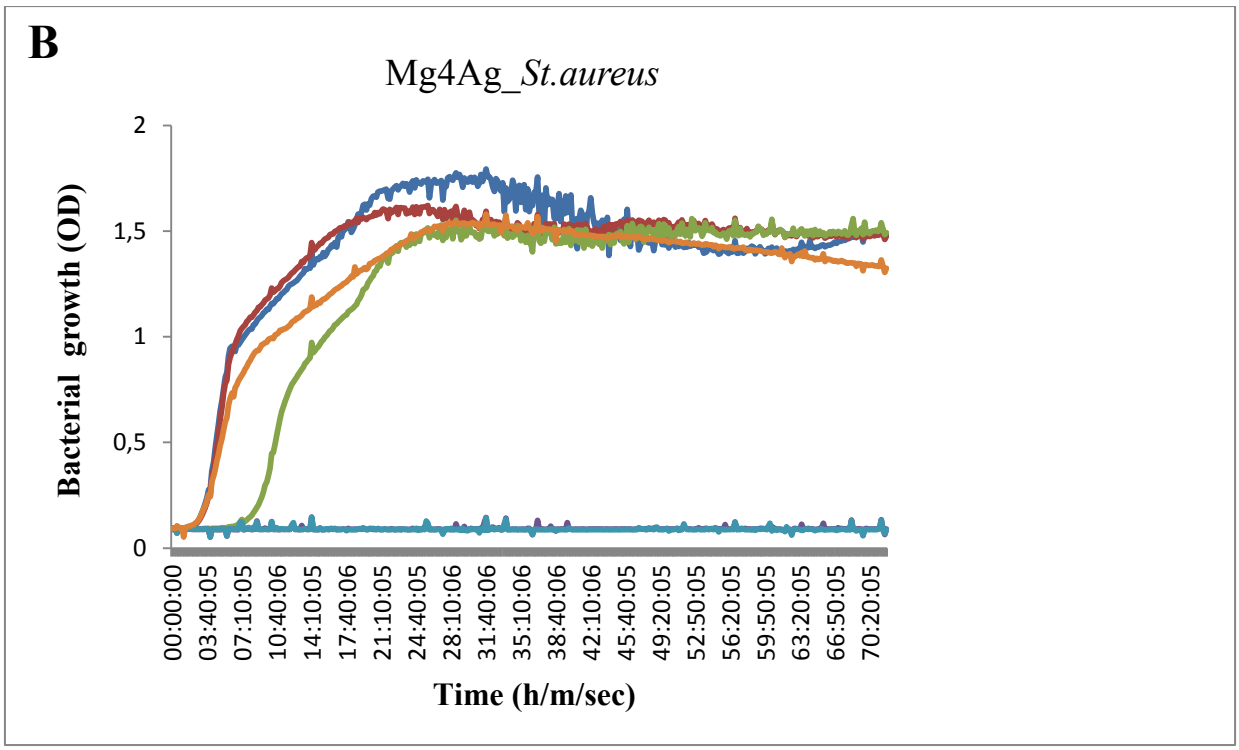
B
Mg4Ag_St.aureus
Bacterial growth (OD)
2
1,5
1
0,5
0
00:00:00
03:40:05
07:10:05
10:40:06
14:10:05
17:40:06
21:10:05
24:40:05
28:10:06
31:40:06
35:10:06
38:40:06
42:10:06
45:40:05
49:20:05
52:50:05
56:20:05
59:50:05
63:20:05
66:50:05
70:20:05
Time (h/m/sec)

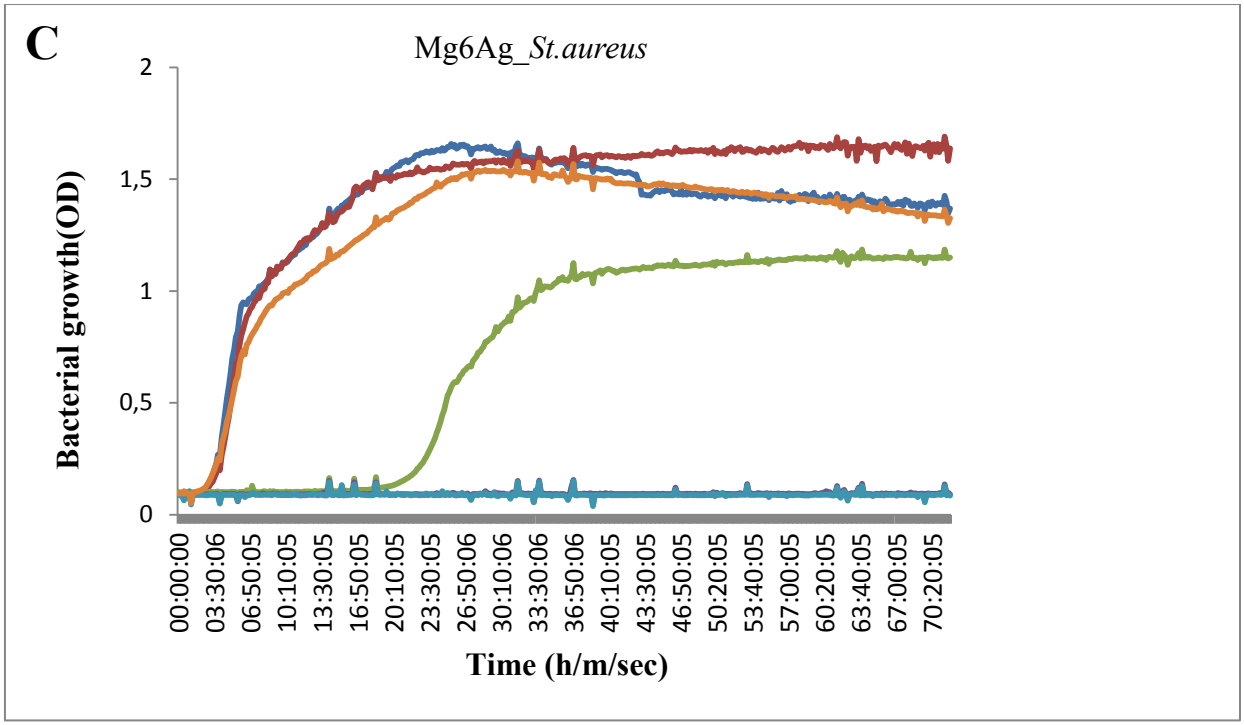

Fig 40. Antimicrobial activity of (A) Mg2Ag, (B) Mg4Ag, (C) Mg6Ag at 10%, 25%, 50%, 75%, 100% dilutions against S.aureus during 3 days of culture in LB broth, (with the permission from Plos one Journal) (216).

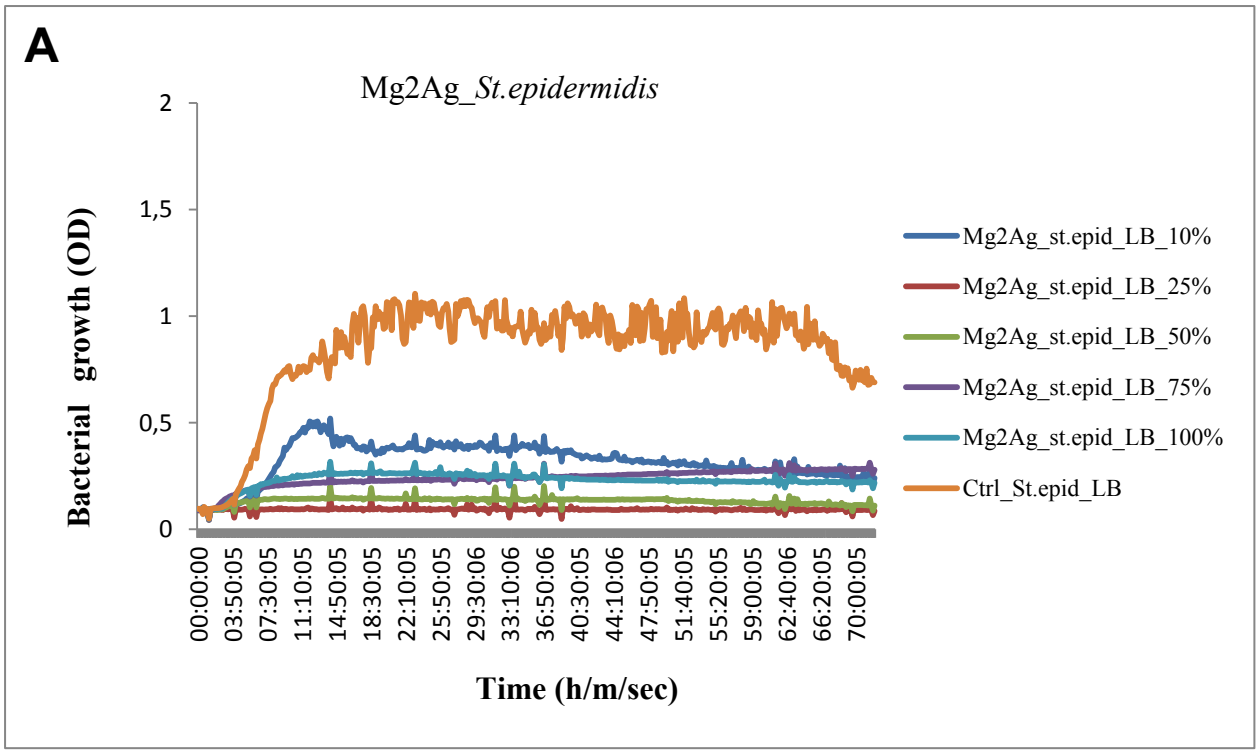

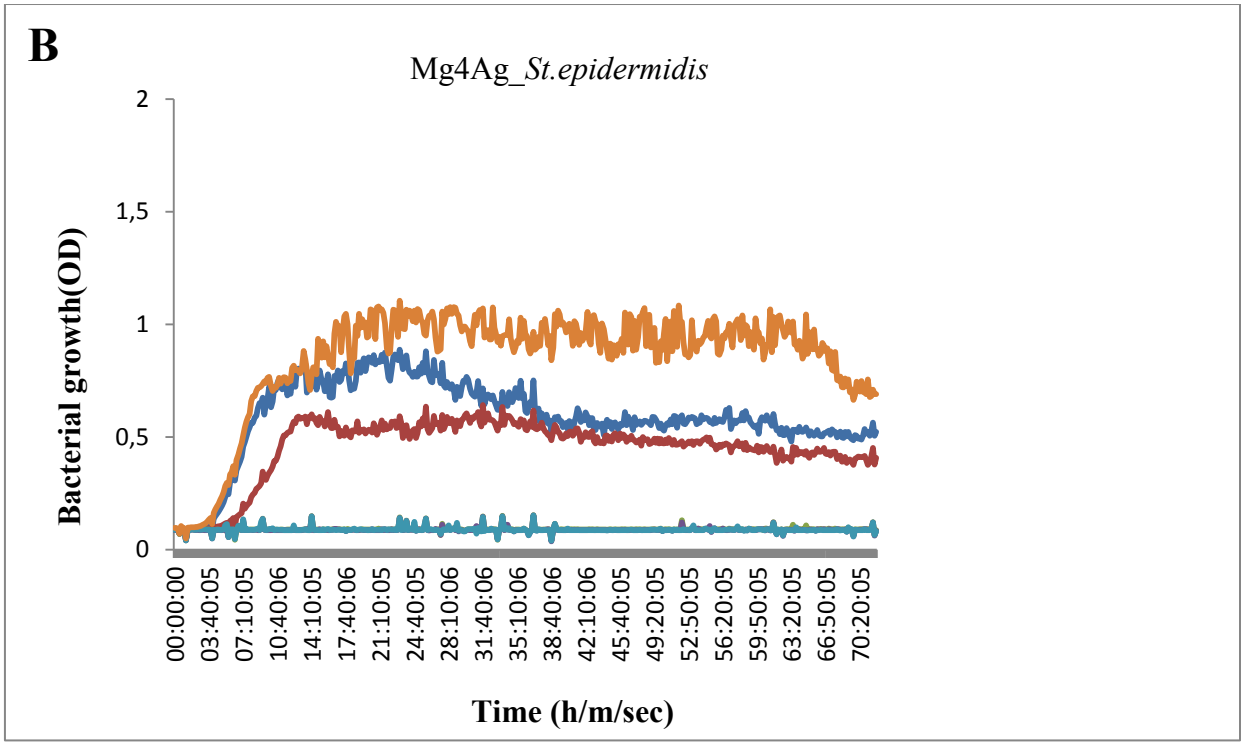

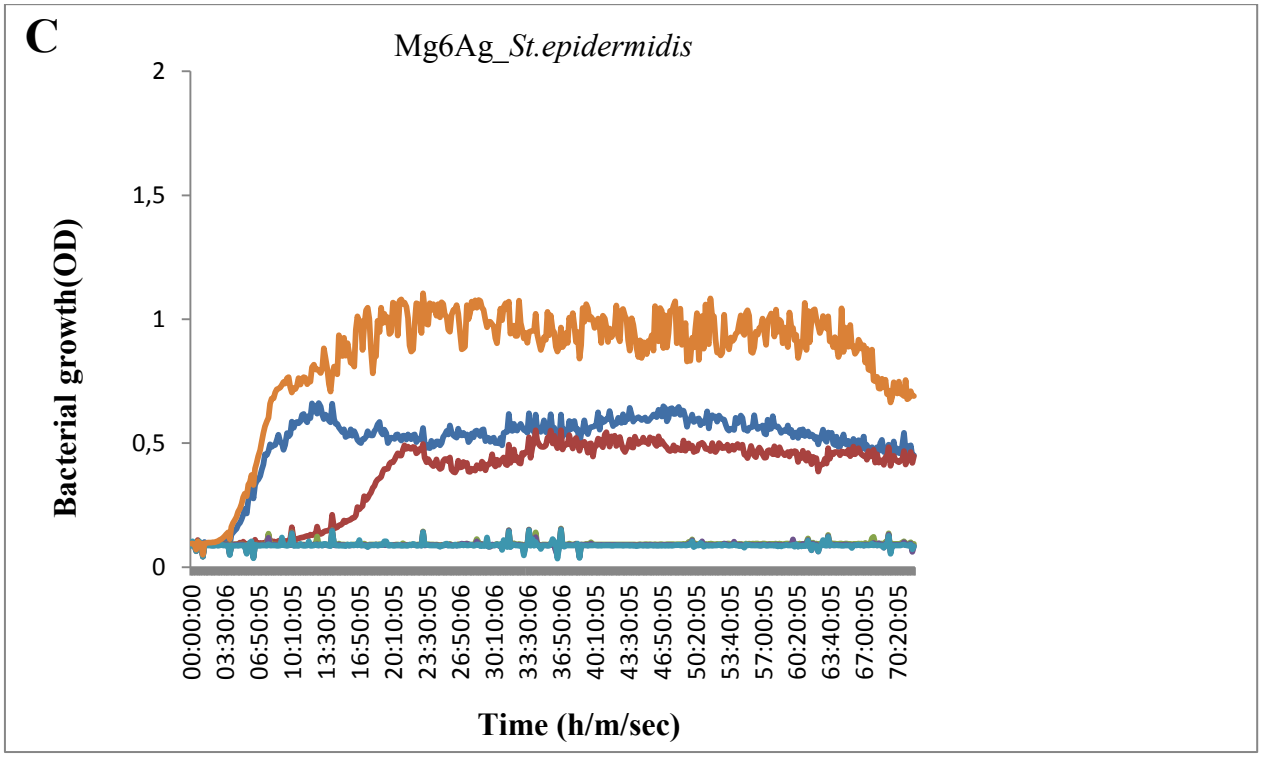

Fig 41. Antimicrobial activity of (A) Mg2Ag, (B) Mg4Ag, (C) Mg6Ag at 10%, 25%, 50%, 75%, 100% dilutions against S.epidermidis during 3 days of culture in LB broth, (with the permission from Plos one Journal) (216).

4. Discussion

Conventional biomaterials such as Titanium, Titanium alloys, cobalt chromium and stainless steel are commonly used as permanent biomaterials in orthopedic applications by virtue of their appropriate mechanical properties and high corrosion resistance. Beside their excellent clinical out-comes, they have several drawbacks such as release of toxic metallic ions during corrosion and their divergent elastic moduli compared to natural bone which highlights the need of removing these permanent implants when bone healing is completed (18). Bioresorbable polymers are, in contrast, able to degrade after accomplishment of the bone healing process, but their relatively weak mechanical properties compared to conventional metal implants limits their clinical application (18).

Besides an ability of biomaterials to corrode within the body, appropriate mechanical properties are other crucial factors which must be considered in the structure of bone implants. Since Mg and Mg alloys are able to fulfill most of the criteria needed for bone applications, these are receiving great attention as biodegradable implants in clinical bone studies (231).

Magnesium is one of the most abundant elements in the human body and necessary for most biological reactions (232). Research studies results have demonstrated that Magnesium is able to corrode harmlessly in the body and be eliminated in urine (64, 65). Furthermore, since Mg is a natural body constituent, corrosion products released from Mg-based implants during corrosion cannot be toxic. Mg has an elastic modulus close to cortical bone which avoids the risk of stress shielding and implant loosening (46, 233). It has furthermore been reported that Mg can induce bone formation and osteointegration alongside degradation (234, 235). It can thus be considered as a beneficial alternative to conventional materials for regenerative bone applications.

Whilst Mg-based implants have great advantages due to their suitable mechanical properties and biocompatibility, their high corrosion rate is recognized to be a major obstacle which must be controlled. Mg corrosion is accompanied by the formation of Hydrogen gas in bone cavities, which can prevent effective bone healing process, as well as initial cell/material attachment (95, 96). Different processing systems and alloying elements have been used in order to control the corrosion rate of Mg-based implants. These however suffer from major drawbacks due to the potential cytotoxic effects of alloying elements (46, 126, 236).

In the present study, the corrosion profiles (corrosion rate, surface chemistry and ion release) of three Mg-based implants (pure Mg, Mg2Ag and Mg10Gd) were analyzed under cell culture conditions. Initial interactions between the implant as a foreign material and cells and proteins play an important role in determining the subsequent cellular and molecular reactions which can generate proper cell attachment and tissue formation. It is thus important to study the modification of the surrounding environment of these implants in vitro, including ion release, corrosion rate, chemical composition of the surface, cytocompatibility and gene expression profile, before studying them under in vivo conditions.

4.1 Determination of surface morphology, elemental composition and ion release

As explained above, interactions between the surface of materials with the surrounding biological environment is an important issue in the field of applied biomaterials. The surface of a given material should fulfill special criteria with respect to chemical composition and surface morphology in order to provide a suitable platform for cell and tissue survival.

The type of corrosion medium used for corrosion experiments is known to greatly influence the degradation process, as well as surface morphology and the chemical composition of the corrosion deposits. Recently published biocompatibility and corrosion studies, investigated corrosion characteristics and cell material interaction using cell culture medium (104, 131, 237), since this can adequately model physiological conditions for in vitro corrosion testing of Mg implants (66, 173, 174). Components of the corrosion medium are known to be able to adsorb to the surface of the implant, act as redox mediators and chelate metal ions, which can subsequently affect the corrosion mechanism and film formation on Mg implants (238-240). $CaCl_2$, $MgSO_4$, KCl, $NAHCO_3$, NaCl and Na_2HPO_4 are known to be the most important inorganic salts in cell culture medium. Release of ions such as Chloride into the medium are known to have detrimental effect on the corrosion resistance of Mg implants and media with higher chloride ion content such as Hanks solution, SBF and NaCl are known to be more aggressive in terms of inducing corrosion compared to cell culture medium (175, 241). Reaction of phosphate and carbonate ions with Mg leads to the formation of a stable layer which can efficiently prevent the occurrence of corrosion (241). Sulfate ions are able to attack Mg ions and induce corrosion (241). Besides the important role of inorganic salts in the Mg implant corrosion process, other cell culture medium constituents such as amino acids, proteins and sugars can also play an important role in this process. Amino acids can accelerate the corrosion process by inhibiting the formation of

insoluble salts as a protective layer on the surface (242). Addition of proteins such as those in FBS, can facilitate the formation of a massive insoluble salt layer on the surface and so efficiently impede corrosion (175). Similar observations were made by ZENG et al (242). Yang et al, in contrast, reported that addition of proteins under physiological conditions to cell culture medium resulted in a decreased pH and a subsequent increase in osmolality. In this case, more ions were released from the samples and an increase in corrosion rate of the materials was observable (243). It has been reported that increased pH may result in the formation of a protective layer under physiological conditions (103). The results observed by Yang et al may be attributable to the buffering capacity of the proteins which decreased pH and thereby prevented the formation of a corrosive layer under physiologic condition (243). Whilst the outcome of the study performed by Willumeit et al was similar to that the Yang et al study, they described the influence of proteins on the formation of a corrosive layer from other perspectives. Interaction of pure Mg specimens with corrosion medium (HBSS and DMEM) containing different percentages of proteins was analyzed under cell culture condition by Willumeit et al. They observed higher osmolality for specimens immersed in HBSS compared to DMEM. They furthermore detected increased osmolality based on the percentage of proteins added to the corrosion medium. Addition of proteins partially affected the pH of the medium in their study. Thicker corrosion layers were detected on the surface of specimens immersed in HBSS+20% FBS and DMEM+10% FBS. However, since addition of proteins resulted in reduced weight gain, it can be concluded that addition of proteins to the corrosion medium can cause both formation of a less compact layer and a higher rate of corrosion of Mg specimens (244). Influence of proteins on corrosion correlates with several factors such as undefined protein charges, the existing protein concentration in the cell culture medium and the composition of the alloying system of Mg implants. These factors require further study (238).

An ability of biomaterials to integrate into bone tissue is one of the most important goals of orthopedic applications. It is hence necessary to optimize the surface of a given biomaterial in a way that facilitates cellular attachment as well as the tissue healing process (157). There are several methods for biomaterial surface modification. Alteration of surface topography (e.g. surface roughness,..), or coating the surface with biomolecules (e.g. with proteins, peptides, or enzymes) can facilitate interaction with cells at the tissue-material interface (107, 245, 246). However, maintenance of the coating on the surface and controlling the function of the coated biomolecules at the desired site is complicated. Cost efficiency is, moreover, another important

factor which should be taken into consideration, especially for clinical applications. therefore Other, simple changes to the surface of the implants were therefore employed in the present study.

Various studies have shown that surface modification of Mg specimens can delay initial corrosion and improve cell viability and cytocompatibility (246). One of the most optimal surface modifications is achieved by immersing samples in cell culture medium (247) which can result in the formation of a corrosion layer. To determine whether pre-corrosion of Mg specimens and alteration in surface morphology influences cell viability and cell morphology, an investigation of surface morphology changes over time was conducted. All Mg specimens exhibited cracks and degradation products on the surface as reported by other studies (72, 248, 249). SEM analysis revealed the formation of needle-shaped crystals on the surface of pure Mg and Mg2Ag after 72hrs and 8 days of immersion respectively. Willumeit et al observed similar crystals on the surface of pure Mg after immersion in DMEM+10% FBS (244). Although Tie et al used similar Mg alloys in their experiments, they did not detect any crystals in their study (139). The differences between these two studies may be attributable to the use of a static immersion system in our study which might have resulted in saturation of the medium by further release of ions into the low volume of medium used (volume calculated according to the surface ratio). Elevated pH can furthermore strongly influence crystal formation, as reported by Fischer et al (250).

Whilst the corrosion pattern of Mg10Gd was similar to Mg2Ag and pure Mg based on ICP-OES analysis, no crystal formation was observed on the surface of Mg10Gd even after 8 days of immersion, underlining a lack of corrosion protection. Furthermore, the corrosion layer was more even and compact on the surface of Mg10Gd compared to Mg2Ag and pure Mg, without extensive surface morphology. According to EDX analysis, crystal formation on Mg2Ag and pure Mg was associated with an increase in the atomic % of oxygen and decreases in Ca and P content, which was not detectable for 8 day corroded Mg10Gd. Gd is known to be able to adsorb Ca and P and chelate these elements on the surface. Hence, we hypothesize that Ca and P bound to the surface might inhibit oxidation and therefore block the formation of stable needle-shaped crystals (251).

It should be taken into consideration that it is not possible to identify the exact composition of corrosion deposits formed on the surface by EDX analysis. Compounds such as MgO, $Mg(OH)_2$,

and $MgCO_3$, $Ca_3(PO_4)_2$ and $Mg_3(PO_4)_2$ are presumably present on the surface during the corrosion process given the high Oxygen and Mg contents (139, 244, 252, 253).

In our study, corrosion rate was evaluated by measuring Mg content in medium exposed to the Mg specimens. Magnesium ion release initially increased during 72h of immersion for all specimens due to exposure to the corrosion medium. The rate of ion release subsequently slowed for Mg2Ag and pure Mg as a result of formation of stable, protective surface layers which actively hindered further ion release. Studies conducted by Razavi et al and Nguyen et al are in good agreement with our results (159, 162). Our results demonstrated a slight decrease in Mg concentration (3 to 8 days) which may be attributable to a consumption of Mg ions from the corrosion medium and deposition of these ions as corrosion products on the surface. Mg10Gd exhibited a different ion release pattern which indicated that in this case the protective layer could not fully block further ion release from the sample, even after a 72h immersion. This phenomenon has also been reported by other studies (162).

4.2 Effect of surface morphology on cell viability

In this study we observed that pre-corrosion of Mg specimens for 1 and 2 days did not significantly improve biocompatibility compared to controls (specimens without pre-corrosion), which contrasts with results reported in the literature (160). Keim et al reported that pre-corrosion of pure Mg in DMEM+10% FBS led to the formation of a fully protective layer able to slow down corrosion and improve biocompatibility (160). Although the Magnesium used in both studies was of a similar purity (99.9%), the discordances can probably be explained by differences in sample size, the volume of the immersion medium and the cell types used. Polishing, which can actively influence the cell responses to the surface, could also be another reason for the discrepancies between two studies. In another study, Willumeit et al reported that 6h pre-corrosion of pure Mg specimens in cell culture medium supplemented with 10% FBS is sufficient for formation of a protective layer able to improve cell viability and cell adhesion (247). Our results showing high cell viability on 1 and 2 day pre-corroded samples are in good agreement with their study.

In their study, cells exhibited better survival and morphology when cultured on 3 day corroded pure Mg specimens. It should be noted that they did not detect needle-shaped crystals on the surface of pure Mg after 3 days pre-corrosion of the specimens in their study. Crystal formation was, however, reported in their previous publication (244), so crystal formation might thus be

considered a factor which hampers cell survival. Willumeit et al cultivated cells on corroded surfaces for 3 days and did not change the medium during this immersion, which might have caused increased Mg ion concentrations and pH values that can stimulate cell growth. We have shown that low concentrations of Mg (0.2-0.8 mg/mL) derived from pure Mg can enhance cell survival. This concentration spectrum was detected when MC3T3-E1 cells were cultivated for up to three days on the surface of pure Mg, similar to the study performed by Willumeit et al (Fig 19).

Cultivation of cells on specimens without pre-corrosion resulted in an impairment of cell survival in their study. In our study, in contrast, the cells were highly viable and well adhered, even on specimens without pre-corrosion. The differences between the two studies could be due to differences in the cell types used and the corrosion patterns of the specimens.

In this study, MC3T3-E1 cells were only cultured for 24h on corroded and non-corroded specimens, and the release of Mg ions during this period should therefore not exceed the range of 0.5-0.6 mg/mL as shown in Fig. 19. According to MTT results, cell metabolic activity was increased at these concentrations and decreased cell viability was only detected at Mg ion concentrations of 0.9 mg/mL and above (Fig. 20). It can therefore be concluded that high concentrations of Mg do not mediate cell death when the cells were cultivated directly on the surface of the specimens (See Fig. 20).

Since effects of high Mg concentration on cells were excluded in this study, extensive cell death on 3 day pre-corroded Mg2Ag and pure Mg specimens may correlate with surface modification and surface formation of crystals. This was verified when MC3T3-E1 cells were cultivated for 12 days on non-corroded pure Mg, Mg2Ag and Mg10Gd. Cells exhibited high viability on these samples and often grew to confluence.

Although there was no evidence of crystal formation on the surface of Mg10Gd at any immersion time, the high number of rounded cells on the surface of 3 day pre-corroded Mg10Gd specimens established a detrimental effect of corrosion deposits on cell viability during the corrosion process. As in our study, Cecchinato et al have reported a reduction in the viability of cells cultured on 3 day pre-corroded specimens. Changes in pH, osmolality and formation of localized corrosion products on the surface were cited to explain their observation (156). Ngueyen et al concluded that pre-corrosion of Mg-based implants in cell culture medium cannot protect the

surface from degradation. In their study D-Mg (pre-corroded sample) induced a level of cell death similar to that induced by M-Mg (without pre-corrosion within first 30 hours of incubation) (162). Whilst we did not observe such rapid cell death during the first 30h of our experiments, the outcome of our study was similar to what they observed, indicating that pre-corrosion did not result in the formation of protective layer able to improve cell survival. The reason for fast cell death in their study might be a greater sensitivity of HMSC compared to the MC3T3-E1 cell line used in our study. In another study, Witte et al reported that pre-corrosion did not influence or reduce the viability of MG63 cells compared to direct assay (without pre-corrosion) which is in accordance with our results (163).

In our study, MC3T3-E1 cells exhibited high viability on the tested samples, even on materials without pre-corrosion. Non-corroded specimens were therefore used for long-term evaluation of cell viability. Live-dead staining revealed high cell viability on all samples at longer immersion times (up to 12 days). There was furthermore evidence of cell proliferation over time, as reported by Ostrowsky et al (158), indicative of a rate of corrosion of all three materials that was not too fast to prevent provision of a suitable surface for cell attachment and cell proliferation. It should be noted that cells cultured on Mg-based specimens were able to decrease the corrosion rate (as shown by slower Mg ion release in our results) (Fig. 19).

4.3 Effects of Mg ion concentration and pH on cell viability

MC3T3-E1 cells were treated for 24h with Mg ion concentrations ranging from 12.5 to 50mM. Cell viability was decreased by all samples as a result of increasing Mg concentrations. Recent studies have produced similar results (136, 188, 189, 237, 254-258). In our study, cells exhibited more than 70% viability when exposed to the highest Mg concentration (50mM) derived from pure Mg supernatants. In contrast, the highest Mg concentration derived from the other Mg alloys (Mg2Ag and Mg10Gd) was completely toxic for the cells and led to cell death. In the study conducted by Wang et al no negative effect on viability was observed for cells cultured with 10mM Mg (192). Yun et al reported a slight inhibition of the U2-OS cell growth at a Mg concentration greater than 5mM (259). Another study report showed significant reductions in the viability of MG63 and two primary osteoblasts when exposed to a Mg concentration of 59.5 derived from pure Mg, Mg1Ca and Mg0.6Ca extracts (188). MC3T3-E1 cells exhibited highest viability when exposed to Mg concentrations of 2-4mM (260). The loss of viability of various

cell lines at different Mg concentrations might mirror capacity of the cells to the corrosion deposits during cell material reaction.

Mg concentration aside, changes in the pH exert marked effects on cell metabolic activity. F.Seuss et al reported a dramatic reduction in HeLa cell viability at a pH above 10 (101). In another study conducted by Cipriano et al, a significant reduction in cell number was detected at a pH above 9.5 (261), and, in the study performed by Wang et al, cells exhibited low viability at a pH higher than 9 (257). Wang et al, in contrast, have reported that a pH higher than 8.5 stimulates the growth of MC3T3-E1 and BMSC (192). We can exclude an effect of pH on cell viability in our study since the pH never exceeded 8.6. Moreover, pH was adjusted to 7.4 (physiological level) to exclude an effect of pH on cell viability prior to viability experiments.

In summary, cell viability can be influenced, including elevated extract pH (101, 188, 189), high Mg concentration (136, 256, 258, 259), duration of cell cultivation with extraction medium (262, 263) and cell type (162, 188). The resultant scope for variability can explain the discrepancies between in vitro studies.

4.4 Effect of surface morphology on cell morphology

Actin is a key protein in all eukaryotic cells with multiple cellular functions including mobility and shrinkage of cells during cell division. The directional distribution of actin filaments is important since they can determine cellular shape, cellular junctions and cellular motility of cells cultured on the surface of the various specimens. Diverse actin binding proteins regulate the association and dissociation of actin filaments, formation of networks and association of these filaments with other cellular structures (264).

Many studies have shown that surface modification can improve cell attachment (159, 160, 249, 254, 260, 265-268). The results of the present study however show that Mg specimens without surface alteration (pre-corrosion) can provide a suitable surface for cell attachment and cell growth. The results of our study showed distinct alloy-associated alterations in the morphology of cells cultivated on non-corroded specimens. The cells appeared alive and well-spread on non-corroded specimens and were able to build connections through cell protrusions over surface cracks. There was no evidence of spherical morphology on non-corroded samples exhibiting the high biocompatibility of Mg2Ag, Mg10Gd and pure Mg in this condition. Despite the observed high cell viability and fine morphology of cells on non-corroded surfaces, longer pre-corrosion

times (3 days) seemed to be detrimental for the cells and resulted in decreased cell numbers. F-actin staining revealed a rounded morphology of cells on pure Mg and Mg2Ag corroded for 3 days. Progressive formation of aggressive corrosion products might explain the low cell density and rounded morphology observed after longer immersion times.

It seems that corrosion of Mg and Mg alloys can result in the development of actin filaments and stress fibers determined by an increase in cell extensions. Our results demonstrated that pre-corrosion of Mg specimens for 1 and 2 days had a remarkable effect on the morphology of pre-osteoblasts in terms of increased cell extensions compared to non-corroded specimens. The cells built clusters on 2 day pre-corroded pure Mg specimens which may correlate with the physical and chemical interactions of the cells with the corroded surface. Razavi et al, reported that, corrosion products may detach from the surface during immersion owing to a severe volume mismatch between the corrosion layer and the substrate. Formation of corrosion products followed by the detachment of these deposits was shown to antagonize cell attachment, in accordance with our results (159). Willumeit et al showed a spread morphology of SaO2 cells on specimens pre-corroded for 3 days, a finding which contrasts with our results (247). The material production process, the immersion system used (static, semi static or dynamic), corrosion medium, and the volume of corrosion medium used for immersion tests are key variables which can affect the corrosion process and subsequently cause such differences (122, 168, 169, 175, 243, 269-272). Cipriano et al showed surface chemical composition and elemental distribution not to affect BMSC adhesion and concluded that surface topography plays an important role in controlling cellular reactions (261). The result of their survey is in good agreement with our study. However, we also concluded that surface chemical composition and elemental distribution play an important role in corrosion deposit formation. The high atomic% of oxygen which was detected on 3 days pre-corroded Pure Mg and Mg2Ag specimens for example was associated with surface formation of needle-shaped crystals. The existence of elements such as Ca and P on the surface of 3 days pre-corroded Mg10Gd, in contrast, played an important role in suppressing crystal formation. It can be concluded that chemical composition might influence cell morphology indirectly by affecting surface topography.

4.5 Differentiation potential of 3T3-E1 cells cultivated on Mg-based implants

In most in vitro studies, the effect of Magnesium on the expression of bone osteogenic markers has been reported indirectly, meaning that cells were treated with different concentration of Mg

extracts prior to gene expression measurement. Since, however, other factors associated with the corrosion of biodegradable Mg and Mg alloys, such as corrosion rate, pH, surface roughness and osmolality have an important influence on gene expression, direct cell culture on the surface of the biomaterials will provide better information about the expression pattern of osteogenic markers. Accordingly, it is difficult to compare the results of the present study with those of other studies in the literature since in most cases the latter focused on indirect effects of Mg on the expression of osteogenic markers. Mg has, however, been reported to enhance the expression of bone markers during both direct and indirect cell culture. According to the study of Yoshizawa, increasing concentrations of Mg^{2+} (0.8 to 10mM) prepared with $MgSO_4$ extracts, can enhance the expression of bone osteogenic markers by hBMSc (273, 274). Another study conducted by Yang et al, reported no inhibitory effect of Mg on osteogenic differentiation of hBMSc at a Mg concentration of 10mM. They deemed the alkaline pH resulting from the high rate of corrosion of Mg specimens to be an undesirable factor that can negatively influence osteogenic differentiation of hBMSc (275). Dou et al reported reduced expression of ALP, Collagen type I, RUNX2 and OPN by MC3T3-E1 cells at day 3 after treatment with increasing concentration of Mg-1Ca. The differences were however not significant compared to the control (276). Differentiation potential of the cells based on the concentration of Mg was not detected in the present study. Besides Mg, several factors associated with biomaterial corrosion such as corrosion rate, corrosion deposits, surface elemental composition and pH can influence the expression potential of bone cells. In this study, the markers chosen to detect the potential of pre-osteoblast cells to differentiate to the mineralized phenotype, correspond to those of the early differentiation process during osteogenesis. Runt related transcription factor 2 (Runx2) and Collagen I were selected as early markers. Runx2 is known to play an important role in the differentiation of osteoblasts. Runx2 deficient mice have been shown to display a total lack of osteogenesis. Runx2 is furthermore able to increase the expression of other osteogenic markers such as Osteocalcin, Osteopontin and Collagen I (277, 278). Collagen I controls important cellular functions such as cell adhesion and osteoblastic differentiation (279). Runx2 and Collagen I were analyzed according to their expression profile on Mg alloys and corrosion environment on days 2, 4, 6, 8, 10 and 12. At day 2, early Mg allow-independent down-regulation of both markers was detected compared to the control. Both markers were continuously down-regulated when the cells were cultured on Mg2Ag and pure Mg, even with longer immersion times (up to 12 days), showing an inhibitory effect of corrosion products or corrosion associated modulations on expression of bone osteogenic

markers. In contrast, the differential potential of the cells recovered when cultured for longer periods on Mg10Gd specimens. In a study performed by Myginds et al, maximum expression of osteogenic markers was detected after 14 days of culture (280). Depprich et al similarly reported up-regulation of Collagen I on Titanium and Zirconia surfaces after 14 days (281). According to the above observations we postulate that cells regain their osteogenic potential after longer immersion times, and thus that extended culture times reveal more pronounced differences in the gene expression pattern of the cells. Medium used for cell culture studies has an important influence on the differentiation process. Addition of osteogenic medium has been reported to induce the differentiation process (282). The aim of the present study was to determine the effect of Mg and Mg alloys and their corrosion products on cell responses and the expression of osteogenic markers without exposure of cells to additional stimulators such as osteogenic medium.

4.6 Antibacterial activity of silver-containing implants

Bacterial contamination is one of the major problems which can occur during implantation in orthopedic surgeries. Infections associated with the implantation process can result in biofilm formation on the surface of the implant, with several potential consequences including chronic systemic infections. The bacteria which form biofilm are, furthermore, always resistant to different antimicrobial agents, and thus difficult to remove with traditional antimicrobial agents (283). Amongst biodegradable Mg implants, silver-containing specimens exhibit suitable antibacterial characteristics. The cytotoxicity of these implants must, however, be evaluated before usage of these implants in clinical applications (139).

In our study, the presence of silver did not cause additional toxicity for MC3T3-E1 cells compared to pure Mg. The cells, furthermore, exhibited adequate density and better extensions on silver containing implants. Antimicrobial testing was performed using a bio screen device to track the antibacterial activity of silver containing implants (Mg2Ag, Mg4Ag and Mg6Ag) for 72 h against two bacterial strains (*S.aureus* and *S.epidermidis*), which are responsible for most bacterial contaminations in bone surgeries. In our first experiment, in which extracts were prepared in cell culture medium (DMEM supplemented with 10% FBS), no bacterial growth was detected after 72h of immersion in both test and control samples, showing that cell culture medium with pH indicator (Phenol red) is not a suitable medium for analyzing the antibacterial activity of silver-containing implants. Similar results were obtained in our second experiment,

using two different cell culture media (DMEM without pH indicator and RPMI). Silver-containing implants were finally immersed in LBI broth and the activity of *S.aureus* and *S.epidermidis* analyzed in 5 different dilutions of these extracts. Our results were essentially in good agreement with those of the study performed by Die et al showing Ag-containing implants to possess sufficient antimicrobial activity. Our results demonstrated antimicrobial activity of Mg2Ag, Mg4Ag and Mg6Ag (at 75% and 100% dilutions) against *S. aureus* and (at 50%, 75% and 100% dilutions) against *S.epidermidis.* Unlike the Die et al study, an increased Silver content did not result in stronger antimicrobial activity in this study, since Mg2Ag implants exhibited greater antimicrobial activity even at lower dilutions (25% and 50%) compared to Mg4Ag and Mg6Ag. Since the materials used in the two studies were provided by the same source, the differences between the results can be attributed to the different experimental conditions used. Since Die et al evaluated the antibacterial activity of the materials by direct cell culture on the surface of the implants; many corrosion-associated factors could have influenced the results of their study. It is for instance known that culture medium has an important effect on ion release from a given material and the subsequent material corrosion rate (175). In our study, extracts were prepared using LB Broth. Process of ion release and corrosion has been not well studied in this medium. Differences between ion release in normal cell culture medium and LB medium, a medium especially formulated for bacterial growth can explain the discrepancies between two studies. Whilst in the present study we showed sufficient antimicrobial activity of Mg2Ag, Mg4Ag and Mg6Ag, further studies should determine the concentrations of silver released into other media and evaluate the antibacterial potential of other Mg-based implants

Conclusions

Degradation of Mg implants is a complex process which results in an increased concentration of soluble ions such as Mg, increased pH, surface layer modification and chemical surface element changes.

In corrosion experiments, prolonged immersion times (3 to 8 days) lead to the formation of needle-shaped crystals on the surface of pure Mg and Mg2Ag. A correlation was observed between high atomic % of Oxygen and Mg and crystal formation on the surface of these samples. Corrosion products in the form of crystals formed on the surface of Mg2Ag and pure Mg were considered stable corrosion deposits since they can cover the surface and actively inhibit further surface corrosion (as determined by Mg ion release).

High atomic% of elements such as Ca and P which were mostly detected on the surface of Mg10Gd after 8 days of immersion demonstrated the capacity of Gadolinium, a lanthanide element, to adsorb Ca and P and thereby suppress crystal formation on the surface of 8 day corroded Mg10Gd. In general, Mg10Gd specimens exhibited a more homogenous corrosion pattern when compared to two other materials. The layer formed on the surface of Mg10Gd was less stable than the corrosion products formed on the surface of Mg2Ag and pure Mg, which supported further ion release by Mg10Gd specimens (3-8 days).

Evaluation of cell metabolic activity showed that exposure of MC3T3-E1 cells to increasing concentrations of Mg^{2+} resulted in decreasing of cell viability. Low concentrations of Mg^{2+} (0.3-0.6 mg/mL) derived from all specimen extracts were shown to have a stimulatory effect on MC3T3-E1 cell viability. A high concentration of Mg^{2+} derived from Mg2Ag and Mg10Gd extracts (1.2 mg/mL) in contrast appeared to cause complete cell death. Mg^{2+} could not be deemed the reason of cell death, since the cells showed more than 75% viability when exposed to extracts derived from pure Mg specimens at a similar concentration (1.2 mg/mL). Furthermore, noticeable cell death in the supernatant of these two materials was not due to the toxic effect of other alloying elements such as Ag and Gd, since the amount of these ions were below the limits of detection. More detailed experiments are needed to figure out the reason for cell death caused by the supernatants of Mg2Ag and Mg10Gd.

pH values during the corrosion process ranged between 8.4-8.6 for all the specimens (Mg2Ag, Mg10Gd and pure Mg) at the stipulated immersion times. MTT results not only showed that the

pH changes observed in this study had no adverse effect on cells, but also that increased pH can stimulate cell viability within a defined pH range (8.4-8.6).

Pre-corrosion of Mg specimens in cell culture medium for 1, 2 and 3 days did not result in a decreased corrosion rate, as evidenced by increasing Mg ion concentration up to 3 days. Furthermore, formation of corrosion deposits on the surface of 1 and 2 day corroded pure Mg, Mg2Ag and Mg10Gd did not improve cell survival since the cells were provided with conditions allowing optimum viability and morphology by non-pre-corroded samples. The surfaces of 3 day pre-corroded samples were completely inhospitable for cells. Mg ion concentration and pH were not considered to underlie cell death in these experiments, since cells were only cultivated on corroded and non-corroded specimens for 1 day. At this time point, Mg ion concentration and pH were below cytotoxic levels. Formation of crystals and accumulation of corrosion deposits on the surface of 3 day corroded Mg specimens might therefore underlie the observed cell death.

Cultivation of cells on Mg-based implants resulted in a slower rate of corrosion of the material (evidenced by slower ion release compared to without cells). Cultivation of cells on non-corroded Mg and Mg alloy specimens furthermore prevented crystal formation, even after longer incubation times (up to 12 days).

Mg10Gd alloy appears to be the most promising material in this study in terms of degradation parameters, surface morphology, surface chemistry and biocompatibility.

Future Perspectives

The results of this thesis, together with previous findings, support the use of biodegradable Mg-based implants for clinical applications. Whilst the results of this study are promising, further investigations involving animal and human subjects with biodegradable Mg-based implants are needed.

Most of the in vitro investigations of materials performed in this study were based on static and semi-static sample immersion systems. These test systems are however not able to fully mimic conditions within body. Dynamic systems such as bioreactors can mimic the environment body within the body more closely and provide more accurate results.

Mg and the Mg alloys used in this study exhibited adequate biocompatibility. All biocompatibility experiments were however performed using the MC3T3-E1 cell line. Since

these materials are intended for use in clinical applications, evaluation of biocompatibility using cells isolated from the human body rather than modified cell lines is desirable. The use of primary cells might however be complicated by differences between cells isolated from different patients.

Mg10Gd stimulated the highest level of expression of osteogenic markers (Runx2 and Collagen I) at day 12 (comparable to the control level). Some studies have, however, demonstrated maximum expression of these markers at day 14 of culture. Longer incubation times (up to day 28) allowing a more detailed analysis of the osteogenic potential of these cells are therefore recommended. Longer incubation times, moreover, enable analysis of late osteogenic markers, which can provide more information about the expression pattern of cells cultivated on the surface of different Mg-based implants.

Whilst Mg2Ag alloys were found to exhibit adequate antibacterial properties in vitro, this antibacterial activity was only analyzed indirectly (by addition of diluted sample extracts). Direct evaluation of the antibacterial properties of these implants is therefore recommended since many factors can affect this process during corrosion. Biofilm formation by these bacteria on the surface of these implants should, furthermore, also be further investigated.

Bibliography

1. Sinikumpu JJ, Lautamo A, Pokka T, Serlo W. The increasing incidence of paediatric diaphyseal both-bone forearm fractures and their internal fixation during the last decade. Injury. 2012;43(3):362-6.
2. Quinn A, Hill ADK, Humphreys H. Evolving Issues in the Prevention of Surgical Site Infections. Surg-J R Coll Surg E. 2009;7(3):170-2.
3. Hakim DN, Pelly T, Kulendran M, Caris JA. Benign tumours of the bone: A review. J Bone Oncol. 2015;4(2):37-41.
4. Hannouche D, Petite H, Sedel L. Current trends in the enhancement of fracture healing. J Bone Joint Surg Br. 2001;83(2):157-64.
5. Johansen R, Nielsen OS, Keller J. Functional outcome in sarcomas treated with limb-salvage surgery or amputation. Sarcoma. 1998;2(1):19-23.
6. Chakarun CJ, Forrester DM, Gottsegen CJ, Patel DB, White EA, Matcuk GR, Jr. Giant cell tumor of bone: review, mimics, and new developments in treatment. Radiographics. 2013;33(1):197-211.
7. Pipitone PS, Rehman S. Management of traumatic bone loss in the lower extremity. Orthop Clin North Am. 2014;45(4):469-82.
8. Smrke D, Arnez ZM. Treatment of extensive bone and soft tissue defects of the lower limb by traction and free-flap transfer. Injury. 2000;31(3):153-62.
9. Halloran JP, Petrella AJ, Rullkoetter PJ. Explicit finite element modeling of total knee replacement mechanics. Journal of Biomechanics. 2005;38(2):323-31.
10. Brydone AS, Meek D, Maclaine S. Bone grafting, orthopaedic biomaterials, and the clinical need for bone engineering. Proc Inst Mech Eng H. 2010;224(12):1329-43.
11. Sidky A, Buckley RE. Hardware removal after tibial fracture has healed. Can J Surg. 2008;51(4):263-8.
12. Teoh SH. Fatigue of biomaterials: a review. Int J Fatigue. 2000;22(10):825-37.
13. Niinomi M. Fatigue characteristics of metallic biomaterials. Int J Fatigue. 2007;29(6):992-1000.
14. Hoffmeister BK, Smith SR, Handley SM, Rho JY. Anisotropy of Young's modulus of human tibial cortical bone. Med Biol Eng Comput. 2000;38(3):333-8.
15. Au AG, Raso VJ, Liggins AB, Amirfazli A. Contribution of loading conditions and material properties to stress shielding near the tibial component of total knee replacements. Journal of Biomechanics. 2007;40(6):1410-6.
16. Singh R, Dahotre NB. Corrosion degradation and prevention by surface modification of biometallic materials. J Mater Sci-Mater M. 2007;18(5):725-51.
17. Geetha M, Singh AK, Asokamani R, Gogia AK. Ti based biomaterials, the ultimate choice for orthopaedic implants - A review. Prog Mater Sci. 2009;54(3):397-425.
18. Navarro M, Michiardi A, Castano O, Planell JA. Biomaterials in orthopaedics. J R Soc Interface. 2008;5(27):1137-58.
19. Claffey N, Bashara H, O'Reilly P, Polyzois I. Evaluation of New Bone Formation and Osseointegration Around Subperiosteal Titanium Implants with Histometry and Nanoindentation. Int J Oral Max Impl. 2015;30(5):1004-10.
20. Agarwal R, Garcia AJ. Biomaterial strategies for engineering implants for enhanced osseointegration and bone repair. Adv Drug Deliv Rev. 2015;94:53-62.
21. Bazaka K, Ketheesan N, Jacob MV. Polymer Encapsulation of Magnesium to Control Biodegradability and Biocompatibility. Journal of nanoscience and nanotechnology. 2014;14(10):8087-93.
22. Engelberg I, Kohn J. Physicomechanical Properties of Degradable Polymers Used in Medical Applications - a Comparative-Study. Biomaterials. 1991;12(3):292-304.
23. Saini M, Singh Y, Arora P, Arora V, Jain K. Implant biomaterials: A comprehensive review. World J Clin Cases. 2015;3(1):52-7.
24. Moravej M, Mantovani D. Biodegradable Metals for Cardiovascular Stent Application: Interests and New Opportunities. International journal of molecular sciences. 2011;12(7):4250-70.
25. Park J, Lakes RS. Biomaterials. 3rd ed. New York: Springer SpringerLink; 2007.

26. Huiskes R, Weinans H, Vanrietbergen B. The Relationship between Stress Shielding and Bone-Resorption around Total Hip Stems and the Effects of Flexible Materials. Clin Orthop Relat R. 1992(274):124-34.
27. Puleo DA, Huh WW. Acute Toxicity of Metal-Ions in Cultures of Osteogenic Cells Derived from Bone-Marrow Stromal Cells. J Appl Biomater. 1995;6(2):109-16.
28. Lhotka C, Szekeres T, Steffan I, Zhuber K, Zweymuller K. Four-year study of cobalt and chromium blood levels in patients managed with two different metal-on-metal total hip replacements. J Orthopaed Res. 2003;21(2):189-95.
29. Jacobs JJ, Hallab NJ, Skipor AK, Urban RM. Metal degradation products - A cause for concern in metal-metal bearings? Clin Orthop Relat R. 2003(417):139-47.
30. Jacobs JJ, Skipor AK, Patteson LM, Hallab NJ, Paprosky WG, Black J, et al. Metal release in patients who have has a primary total hip arthroplasty - A prospective, controlled, longitudinal study. J Bone Joint Surg Am. 1998;80a(10):1447-58.
31. Orringer JS, Barcelona V, Buchman SR. Reasons for removal of rigid internal fixation devices in craniofacial surgery. J Craniofac Surg. 1998;9(1):40-4.
32. Okazaki Y, Gotoh E. Comparison of metal release from various metallic biomaterials in vitro. Biomaterials. 2005;26(1):11-21.
33. Ozturk O, Turkan U, Eroglu AE. Metal ion release from nitrogen ion implanted CoCrMo orthopedic implant material. Surf Coat Tech. 2006;200(20-21):5687-97.
34. Caicedo MS, Desai R, McAllister K, Reddy A, Jacobs JJ, Hallab NJ. Soluble and Particulate Co-Cr-Mo Alloy Implant Metals Activate the Inflammasome Danger Signaling Pathway in Human Macrophages: A Novel Mechanism for Implant Debris Reactivity. J Orthopaed Res. 2009;27(7):847-54.
35. Lin CW, Ju CP, Lin JHC. A comparison of the fatigue behavior of cast Ti-7.5Mo with c.p. titanium, Ti-6Al-4V and Ti-13Nb-13Zr alloys. Biomaterials. 2005;26(16):2899-907.
36. Okazaki Y, Gotoh E, Manabe T, Kobayashi K. Comparison of metal concentrations in rat tibia tissues with various metallic implants. Biomaterials. 2004;25(28):5913-20.
37. Wang ML, Tuli R, Manner PA, Sharkey PF, Hall DJ, Tuan RS. Direct and indirect induction of apoptosis in human mesenchymal stem cells in response to titanium particles. J Orthopaed Res. 2003;21(4):697-707.
38. Norholt SE, Pedersen TK, Jensen J. Le Fort I miniplate osteosynthesis: a randomized, prospective study comparing resorbable PLLA/PGA with titanium. Int J Oral Max Surg. 2004;33(3):245-52.
39. Staiger MP, Pietak AM, Huadmai J, Dias G. Magnesium and its alloys as orthopedic biomaterials: a review. Biomaterials. 2006;27(9):1728-34.
40. Williams DF. On the mechanisms of biocompatibility. Biomaterials. 2008;29(20):2941-53.
41. Sul YT, Johansson C, Albrektsson T. Which surface properties enhance bone response to implants? Comparison of oxidized magnesium, TiUnite, and osseotite implant surfaces. Int J Prosthodont. 2006;19(4):319-28.
42. Manivasagam G, Suwas S. Biodegradable Mg and Mg based alloys for biomedical implants. Mater Sci Tech-Lond. 2014;30(5):515-20.
43. Witte F. The history of biodegradable magnesium implants: A review. Acta biomaterialia. 2010;6(5):1680-92.
44. McBride ED. Absorbable metal in bone surgery - A further report on the use of magnesium alloys. J Amer Med Assoc. 1938;111:2464-6.
45. Troitskii VV. The resorbing metallic alloy ‘Osteosinthezit’ as material for fastening broken bone. 1944.
46. Witte F, Kaese V, Haferkamp H, Switzer E, Meyer-Lindenberg A, Wirth CJ, et al. In vivo corrosion of four magnesium alloys and the associated bone response. Biomaterials. 2005;26(17):3557-63.
47. Luthringer BJC, Feyerabend F, Willumeit-Romer R. Magnesium-based implants: a mini-review. Magnesium Res. 2014;27(4):142-54.
48. Altura BM. Basic biochemistry and physiology of magnesium: a brief review. Magnes Trace Elem. 1991;10(2-4):167-71.
49. Fox C, Ramsoomair D, Carter C. Magnesium: its proven and potential clinical significance. South Med J. 2001;94(12):1195-201.

50. Rubin H. Central role for magnesium in coordinate control of metabolism and growth in animal cells. Proc Natl Acad Sci U S A. 1975;72(9):3551-5.
51. Nadler MJ, Hermosura MC, Inabe K, Perraud AL, Zhu Q, Stokes AJ, et al. LTRPC7 is a Mg.ATP-regulated divalent cation channel required for cell viability. Nature. 2001;411(6837):590-5.
52. Garfinkel L, Garfinkel D. Magnesium regulation of the glycolytic pathway and the enzymes involved. Magnesium. 1985;4(2-3):60-72.
53. Swaminathan R. Magnesium metabolism and its disorders. Clin Biochem Rev. 2003;24(2):47-66.
54. Hartwig A. Role of magnesium in genomic stability. Mutat Res. 2001;475(1-2):113-21.
55. Watson JD, Crick FH. The structure of DNA. Cold Spring Harb Symp Quant Biol. 1953;18:123-31.
56. MacManus J, Heaton FW. The effect of magnesium deficiency on calcium homeostasis in the rat. Clin Sci. 1969;36(2):297-306.
57. Lote CJ, Thewles A, Wood JA, Zafar T. The hypomagnesaemic action of FK506: urinary excretion of magnesium and calcium and the role of parathyroid hormone. Clin Sci (Lond). 2000;99(4):285-92.
58. Huang CL, Kuo E. Mechanism of hypokalemia in magnesium deficiency. J Am Soc Nephrol. 2007;18(10):2649-52.
59. Fatemi S, Ryzen E, Flores J, Endres DB, Rude RK. Effect of Experimental Human Magnesium Depletion on Parathyroid-Hormone Secretion and 1,25-Dihydroxyvitamin-D Metabolism. J Clin Endocr Metab. 1991;73(5):1067-72.
60. Wallach S. Effects of Magnesium on Skeletal Metabolism. Magnesium Trace Elem. 1990;9(1):1-14.
61. Whang R. Magnesium deficiency. Causes and clinical implications. Drugs. 1984;28 Suppl 1:143-50.
62. Rude RK, Gruber HE, Wei LY, Frausto A, Mills BG. Magnesium deficiency: effect on bone and mineral metabolism in the mouse. Calcif Tissue Int. 2003;72(1):32-41.
63. Belluci MM, Giro G, del Barrio RA, Pereira RM, Marcantonio E, Jr., Orrico SR. Effects of magnesium intake deficiency on bone metabolism and bone tissue around osseointegrated implants. Clinical oral implants research. 2011;22(7):716-21.
64. Staiger MP, Pietak AM, Huadmai J, Dias G. Magnesium and its alloys as orthopedic biomaterials: A review. Biomaterials. 2006;27(9):1728-34.
65. Witte F, Hort N, Vogt C, Cohen S, Kainer KU, Willumeit R, et al. Degradable biomaterials based on magnesium corrosion. Curr Opin Solid St M. 2008;12(5-6):63-72.
66. Gu XN, Zheng YF, Cheng Y, Zhong SP, Xi TF. In vitro corrosion and biocompatibility of binary magnesium alloys. Biomaterials. 2009;30(4):484-98.
67. Xu LP, Yu GN, Zhang E, Pan F, Yang K. In vivo corrosion behavior of Mg-Mn-Zn alloy for bone implant application. Journal of Biomedical Materials Research Part A. 2007;83a(3):703-11.
68. Liu JG, Xu XX. [Stress shielding and fracture healing]. Zhonghua Yi Xue Za Zhi. 1994;74(8):483-5, 519.
69. Anderson JM. Biological responses to materials. Ann Rev Mater Res. 2001;31:81-110.
70. Chen DY, He YH, Tao HR, Zhang Y, Jiang Y, Zhang XN, et al. Biocompatibility of magnesium-zinc alloy in biodegradable orthopedic implants. International Journal of Molecular Medicine. 2011;28(3):343-8.
71. Charyeva O, Dakischew O, Sommer U, Heiss C, Schnettler R, Lips KS. Biocompatibility of magnesium implants in primary human reaming debris-derived cells stem cells in vitro. J Orthop Traumatol. 2016;17(1):63-73.
72. Li Z, Gu X, Lou S, Zheng Y. The development of binary Mg-Ca alloys for use as biodegradable materials within bone. Biomaterials. 2008;29(10):1329-44.
73. Xu L, Yu G, Zhang E, Pan F, Yang K. In vivo corrosion behavior of Mg-Mn-Zn alloy for bone implant application. Journal of biomedical materials research Part A. 2007;83(3):703-11.
74. Gu X, Zheng Y, Cheng Y, Zhong S, Xi T. In vitro corrosion and biocompatibility of binary magnesium alloys. Biomaterials. 2009;30(4):484-98.

75. Castellani C, Lindtner RA, Hausbrandt P, Tschegg E, Stanzl-Tschegg SE, Zanoni G, et al. Bone-implant interface strength and osseointegration: Biodegradable magnesium alloy versus standard titanium control. Acta biomaterialia. 2011;7(1):432-40.
76. Zhang SX, Zhang XN, Zhao CL, Li JA, Song Y, Xie CY, et al. Research on an Mg-Zn alloy as a degradable biomaterial. Acta biomaterialia. 2010;6(2):626-40.
77. Li ZJ, Gu XN, Lou SQ, Zheng YF. The development of binary Mg-Ca alloys for use as biodegradable materials within bone. Biomaterials. 2008;29(10):1329-44.
78. Kraus T, Fischerauer SF, Hanzi AC, Uggowitzer PJ, Loffler JF, Weinberg AM. Magnesium alloys for temporary implants in osteosynthesis: in vivo studies of their degradation and interaction with bone. Acta biomaterialia. 2012;8(3):1230-8.
79. Wilkins KE. Principles of fracture remodeling in children. Injury. 2005;36 Suppl 1:A3-11.
80. Clarke B. Normal bone anatomy and physiology. Clin J Am Soc Nephrol. 2008;3 Suppl 3:S131-9.
81. Doblare M, Garcia JM. On the modelling bone tissue fracture and healing of the bone tissue. Acta Cient Venez. 2003;54(1):58-75.
82. Cho TJ, Gerstenfeld LC, Einhorn TA. Differential temporal expression of members of the transforming growth factor beta superfamily during murine fracture healing. J Bone Miner Res. 2002;17(3):513-20.
83. LaStayo PC, Winters KM, Hardy M. Fracture healing: bone healing, fracture management, and current concepts related to the hand. J Hand Ther. 2003;16(2):81-93.
84. Oryan A, Moshiri A. A long term study on the role of exogenous human recombinant basic fibroblast growth factor on the superficial digital flexor tendon healing in rabbits. J Musculoskelet Neuronal Interact. 2011;11(2):185-95.
85. Oryan A, Moshiri A. Recombinant fibroblast growth protein enhances healing ability of experimentally induced tendon injury in vivo. J Tissue Eng Regen Med. 2014;8(6):421-31.
86. Schindeler A, McDonald MM, Bokko P, Little DG. Bone remodeling during fracture repair: The cellular picture. Semin Cell Dev Biol. 2008;19(5):459-66.
87. Alsousou J, Ali A, Willett K, Harrison P. The role of platelet-rich plasma in tissue regeneration. Platelets. 2013;24(3):173-82.
88. Carano RAD, Filvaroff EH. Angiogenesis and bone repair. Drug Discov Today. 2003;8(21):980-9.
89. Alsousou J, Ali A, Willett K, Harrison P. The role of platelet-rich plasma in tissue regeneration. Platelets. 2013;24(3):173-82.
90. Webb JCJ, Tricker J. A review of fracture healing. Curr Orthopaed. 2000;14(6):457-63.
91. Marsell R, Einhorn TA. The biology of fracture healing. Injury. 2011;42(6):551-5.
92. Tsiridis E, Upadhyay N, Giannoudis P. Molecular aspects of fracture healing: which are the important molecules? Injury. 2007;38 Suppl 1:S11-25.
93. Einhorn TA, Gerstenfeld LC. Fracture healing: mechanisms and interventions. Nat Rev Rheumatol. 2015;11(1):45-54.
94. Farraro KF, Kim KE, Woo SL, Flowers JR, McCullough MB. Revolutionizing orthopaedic biomaterials: The potential of biodegradable and bioresorbable magnesium-based materials for functional tissue engineering. J Biomech. 2014;47(9):1979-86.
95. Wang JB, Jiang HF, Bi YZ, Sun JE, Chen MF, Liu DB. Effects of gas produced by degradation of Mg-Zn-Zr Alloy on cancellous bone tissue. Mat Sci Eng C-Mater. 2015;55:556-61.
96. Noviana D, Paramitha D, Ulum MF, Hermawan H. The effect of hydrogen gas evolution of magnesium implant on the postimplantation mortality of rats. J Orthop Transl. 2016;5:9-15.
97. Wang J, Jiang H, Bi Y, Sun J, Chen M, Liu D. Effects of gas produced by degradation of Mg-Zn-Zr Alloy on cancellous bone tissue. Materials science & engineering C, Materials for biological applications. 2015;55:556-61.
98. Myrissa A, Agha NA, Lu YY, Martinelli E, Eichler J, Szakacs G, et al. In vitro and in vivo comparison of binary Mg alloys and pure Mg. Mat Sci Eng C-Mater. 2016;61:865-74.
99. Atrens A, Liu M, Abidin NIZ. Corrosion mechanism applicable to biodegradable magnesium implants. Mater Sci Eng B-Adv. 2011;176(20):1609-36.

100. Atrens A, Song GL, Liu M, Shi ZM, Cao FY, Dargusch MS. Review of Recent Developments in the Field of Magnesium Corrosion. Adv Eng Mater. 2015;17(4):400-53.
101. Seuss F, Seuss S, Turhan MC, Fabry B, Virtanen S. Corrosion of Mg alloy AZ91D in the presence of living cells. J Biomed Mater Res B. 2011;99b(2):276-81.
102. Song GL, Atrens A. Understanding magnesium corrosion - A framework for improved alloy performance. Adv Eng Mater. 2003;5(12):837-58.
103. Song GL, Atrens A. Corrosion mechanisms of magnesium alloys. Adv Eng Mater. 1999;1(1):11-33.
104. Huan ZG, Leeflang S, Zhou J, Zhai WY, Chang J, Duszczyk J. In vitro degradation behavior and bioactivity of magnesium-Bioglass (R) composites for orthopedic applications. J Biomed Mater Res B. 2012;100b(2):437-46.
105. Li LC, Gao JC, Wang Y. Evaluation of cyto-toxicity and corrosion behavior of alkali-heat-treated magnesium in simulated body fluid. Surf Coat Tech. 2004;185(1):92-8.
106. Gray JE, Luan B. Protective coatings on magnesium and its alloys - a critical review. J Alloy Compd. 2002;336(1-2):88-113.
107. Iskandar ME, Aslani A, Liu HN. The effects of nanostructured hydroxyapatite coating on the biodegradation and cytocompatibility of magnesium implants. Journal of Biomedical Materials Research Part A. 2013;101(8):2340-54.
108. Kuwahara H, Al-Abdullat Y, Mazaki N, Tsutsumi S, Aizawa T. Precipitation of magnesium apatite on pure magnesium surface during immersing in Hank's solution. Mater Trans. 2001;42(7):1317-21.
109. Tian P, Liu XY, Ding CX. In vitro degradation behavior and cytocompatibility of biodegradable AZ31 alloy with PEO/HT composite coating. Colloid Surface B. 2015;128:44-54.
110. Zhang YJ, Wei M. Controlling the Biodegradation Rate of Magnesium Using Sol-Gel and Apatite Coatings. Int J Mod Phys B. 2009;23(6-7):1897-903.
111. Ye XY, Chen MF, Yang M, Wei J, Liu DB. In vitro corrosion resistance and cytocompatibility of nano-hydroxyapatite reinforced Mg-Zn-Zr composites. J Mater Sci-Mater M. 2010;21(4):1321-8.
112. Ostrowski N, Lee B, Enick N, Carlson B, Kunjukunju S, Roy A, et al. Corrosion protection and improved cytocompatibility of biodegradable polymeric layer-by-layer coatings on AZ31 magnesium alloys. Acta biomaterialia. 2013;9(10):8704-13.
113. Xu LP, Yamamoto A. Characteristics and cytocompatibility of biodegradable polymer film on magnesium by spin coating. Colloid Surface B. 2012;93:67-74.
114. Jo JH, Kang BG, Shin KS, Kim HE, Hahn BD, Park DS, et al. Hydroxyapatite coating on magnesium with MgF2 interlayer for enhanced corrosion resistance and biocompatibility. J Mater Sci-Mater M. 2011;22(11):2437-47.
115. Li HL, Pan HB, Ning CY, Tan GX, Liao JW, Ni GX. Magnesium with micro-arc oxidation coating and polymeric membrane: an in vitro study on microenvironment. J Mater Sci-Mater M. 2015;26(3).
116. Razavi M, Fathi M, Savabi O, Beni BH, Vashaee D, Tayebi L. Surface microstructure and in vitro analysis of nanostructured akermanite (Ca2MgSi2O7) coating on biodegradable magnesium alloy for biomedical applications. Colloid Surface B. 2014;117:432-40.
117. Razavi M, Fathi M, Savabi O, Vashaee D, Tayebi L. In vitro study of nanostructured diopside coating on Mg alloy orthopedic implants. Mat Sci Eng C-Mater. 2014;41:168-77.
118. Willumeit R, Mohring A, Feyerabend F. Optimization of Cell Adhesion on Mg Based Implant Materials by Pre-Incubation under Cell Culture Conditions. International journal of molecular sciences. 2014;15(5):7639-50.
119. Wong HM, Yeung KWK, Lam KO, Tam V, Chu PK, Luk KDK, et al. A biodegradable polymer-based coating to control the performance of magnesium alloy orthopaedic implants. Biomaterials. 2010;31(8):2084-96.
120. Keim S, Brunner JG, Fabry B, Virtanen S. Control of magnesium corrosion and biocompatibility with biomimetic coatings. J Biomed Mater Res B. 2011;96b(1):84-90.
121. Lorenz C, Brunner JG, Kollmannsberger P, Jaafar L, Fabry B, Virtanen S. Effect of surface pre-treatments on biocompatibility of magnesium. Acta biomaterialia. 2009;5(7):2783-9.

122. Wang JL, Qin L, Wang K, Wang J, Yue Y, Li YD, et al. Cytotoxicity studies of AZ31D alloy and the effects of carbon dioxide on its biodegradation behavior in vitro. Mat Sci Eng C-Mater. 2013;33(7):4416-26.
123. Shaw B. Corrosion Resistance of Magnesium Alloys. ASM Handbook: Corrosion: Fundamentals, Testing, and Protection. 2003;13A:692-6.
124. Seong JW, Kim WJ. Development of biodegradable Mg-Ca alloy sheets with enhanced strength and corrosion properties through the refinement and uniform dispersion of the Mg(2)Ca phase by high-ratio differential speed rolling. Acta biomaterialia. 2015;11:531-42.
125. Zhang E, Yang L, Xu J, Chen H. Microstructure, mechanical properties and bio-corrosion properties of Mg-Si(-Ca, Zn) alloy for biomedical application. Acta biomaterialia. 2010;6(5):1756-62.
126. Zhang LN, Hou ZT, Ye X, Xu ZB, Bai XL, Shang P. The effect of selected alloying element additions on properties of Mg-based alloy as bioimplants: A literature review. Front Mater Sci. 2013;7(3):227-36.
127. Bakhsheshi-Rad HR, Abdul-Kadir MR, Idris MH, Farahany S. Relationship between the corrosion behavior and the thermal characteristics and microstructure of Mg-0.5Ca-xZn alloys. Corros Sci. 2012;64:184-97.
128. Brar HS, Wong J, Manuel MV. Investigation of the mechanical and degradation properties of Mg-Sr and Mg-Zn-Sr alloys for use as potential biodegradable implant materials. Journal of the mechanical behavior of biomedical materials. 2012;7:87-95.
129. Zhang EL, Yin DS, Xu LP, Yang L, Yang K. Microstructure, mechanical and corrosion properties and biocompatibility of Mg-Zn-Mn alloys for biomedical application. Mat Sci Eng C-Bio S. 2009;29(3):987-93.
130. Du H, Wei ZJ, Liu XW, Zhang EL. Effects of Zn on the microstructure, mechanical property and bio-corrosion property of Mg-3Ca alloys for biomedical application. Mater Chem Phys. 2011;125(3):568-75.
131. Pompa L, Rahman ZU, Munoz E, Haider W. Surface characterization and cytotoxicity response of biodegradable magnesium alloys. Mat Sci Eng C-Mater. 2015;49:761-8.
132. StJohn DH, Qian M, Easton MA, Cao P, Hildebrand Z. Grain refinement of magnesium alloys. Metall Mater Trans A. 2005;36a(7):1669-79.
133. Li YC, Wen C, Mushahary D, Sravanthi R, Harishankar N, Pande G, et al. Mg-Zr-Sr alloys as biodegradable implant materials. Acta biomaterialia. 2012;8(8):3177-88.
134. Berglund IS, Brar HS, Dolgova N, Acharya AP, Keselowsky BG, Sarntinoranont M, et al. Synthesis and characterization of Mg-Ca-Sr alloys for biodegradable orthopedic implant applications. J Biomed Mater Res B. 2012;100b(6):1524-34.
135. Khan SA, Miyashita Y, Mutoh Y, Bin Sajuri Z. Influence of Mn content on mechanical properties and fatigue behavior of extruded Mg alloys. Mat Sci Eng a-Struct. 2006;420(1-2):315-21.
136. Willbold E, Gu X, Albert D, Kalla K, Bobe K, Brauneis M, et al. Effect of the addition of low rare earth elements (lanthanum, neodymium, cerium) on the biodegradation and biocompatibility of magnesium. Acta biomaterialia. 2015;11:554-62.
137. Feyerabend F, Fischer J, Holtz J, Witte F, Willumeit R, Drucker H, et al. Evaluation of short-term effects of rare earth and other elements used in magnesium alloys on primary cells and cell lines. Acta biomaterialia. 2010;6(5):1834-42.
138. Tie D, Feyerabend F, Muller WD, Schade R, Liefeith K, Kainer KU, et al. ANTIBACTERIAL BIODEGRADABLE Mg-Ag ALLOYS. European cells & materials. 2013;25:284-98.
139. Tie D, Feyerabend F, Muller WD, Schade R, Liefeith K, Kainer KU, et al. Antibacterial biodegradable Mg-Ag alloys. European cells & materials. 2013;25:284-98; discussion 98.
140. Rosenman KD, Moss A, Kon S. Argyria: clinical implications of exposure to silver nitrate and silver oxide. J Occup Med. 1979;21(6):430-5.
141. Rosenman KD, Seixas N, Jacobs I. Potential nephrotoxic effects of exposure to silver. Br J Ind Med. 1987;44(4):267-72.
142. Weir FW. Health hazard from occupational exposure to metallic copper and silver dust. Am Ind Hyg Assoc J. 1979;40(3):245-7.
143. G N, L G. Handbook on toxicity of inorganic compounds1988.

144. Fung MC, Bowen DL. Silver products for medical indications: risk-benefit assessment. J Toxicol Clin Toxicol. 1996;34(1):119-26.
145. Gulbranson SH, Hud JA, Hansen RC. Argyria following the use of dietary supplements containing colloidal silver protein. Cutis. 2000;66(5):373-+.
146. A F. Inactivity of two noble metals as carcinogens. 1978.
147. Drake PL, Hazelwood KJ. Exposure-related health effects of silver and silver compounds: A review. Ann Occup Hyg. 2005;49(7):575-85.
148. Charyeva O, Dakischew O, Sommer U, Heiss C, Schnettler R, Lips KS. Biocompatibility of magnesium implants in primary human reaming debris-derived cells stem cells in vitro. J Orthop Traumatol. 2015.
149. Hort N, Huang Y, Fechner D, Stormer M, Blawert C, Witte F, et al. Magnesium alloys as implant materials - Principles of property design for Mg-RE alloys. Acta biomaterialia. 2010;6(5):1714-25.
150. Macdonald NS, Nusbaum RE, Alexander GV, Ezmirlian F, Spain P, Rounds DE. The Skeletal Deposition of Yttrium. Journal of Biological Chemistry. 1952;195(2):837-41.
151. Johannss.O, Perrault G, Savoie L, Tuchwebe.B. Action of Various Metallic Chlorides on Calcaemia and Phosphataemia. British journal of pharmacology. 1968;33(1):91-&.
152. Sherry AD, Caravan P, Lenkinski RE. Primer on Gadolinium Chemistry. Journal of Magnetic Resonance Imaging. 2009;30(6):1240-8.
153. Haley TJ, Upham HC, Raymond K, Komesu N. Toxicological and Pharmacological Effects of Gadolinium and Samarium Chlorides. Brit J Pharm Chemoth. 1961;17(3):526-&.
154. Spencer AJ, Wilson SA, Batchelor J, Reid A, Rees J, Harpur E. Gadolinium chloride toxicity in the rat. Toxicologic Pathology. 1997;25(3):245-55.
155. Feyerabend F, Fischer J, Holtz J, Witte F, Willumeit R, Drucker H, et al. Evaluation of short-term effects of rare earth and other elements used in magnesium alloys on primary cells and cell lines. Acta biomaterialia. 2010;6(5):1834-42.
156. Cecchinato F, Agha NA, Martinez-Sanchez AH, Luthringer BJ, Feyerabend F, Jimbo R, et al. Influence of Magnesium Alloy Degradation on Undifferentiated Human Cells. PloS one. 2015;10(11):e0142117.
157. Uddin MS, Hall C, Murphy P. Surface treatments for controlling corrosion rate of biodegradable Mg and Mg-based alloy implants. Sci Technol Adv Mat. 2015;16(5).
158. Ostrowski NJ, Lee B, Roy A, Ramanathan M, Kumta PN. Biodegradable poly(lactide-co-glycolide) coatings on magnesium alloys for orthopedic applications. Journal of materials science Materials in medicine. 2013;24(1):85-96.
159. Razavi M, Fathi M, Savabi O, Vashaee D, Tayebi L. In vitro study of nanostructured diopside coating on Mg alloy orthopedic implants. Materials science & engineering C, Materials for biological applications. 2014;41:168-77.
160. Keim S, Brunner JG, Fabry B, Virtanen S. Control of magnesium corrosion and biocompatibility with biomimetic coatings. Journal of biomedical materials research Part B, Applied biomaterials. 2011;96(1):84-90.
161. Lorenz C, Brunner JG, Kollmannsberger P, Jaafar L, Fabry B, Virtanen S. Effect of surface pre-treatments on biocompatibility of magnesium. Acta biomaterialia. 2009;5(7):2783-9.
162. Nguyen TY, Liew CG, Liu H. An in vitro mechanism study on the proliferation and pluripotency of human embryonic stems cells in response to magnesium degradation. PloS one. 2013;8(10):e76547.
163. Witte F, Feyerabend F, Maier P, Fischer J, Stormer M, Blawert C, et al. Biodegradable magnesium-hydroxyapatite metal matrix composites. Biomaterials. 2007;28(13):2163-74.
164. Gu XN, Zheng W, Cheng Y, Zheng YF. A study on alkaline heat treated Mg-Ca alloy for the control of the biocorrosion rate. Acta biomaterialia. 2009;5(7):2790-9.
165. Mani G, Feldman MD, Patel D, Agrawal CM. Coronary stents: A materials perspective. Biomaterials. 2007;28(9):1689-710.
166. Erne P, Schier M, Resink TJ. The road to bioabsorbable stents: Reaching clinical reality? Cardiovasc Inter Rad. 2006;29(1):11-6.
167. Ng WF, Chiu KY, Cheng FT. Effect of pH on the in vitro corrosion rate of magnesium degradable implant material. Mat Sci Eng C-Mater. 2010;30(6):898-903.

168. Yang L, Zhang EL. Biocorrosion behavior of magnesium alloy in different simulated fluids for biomedical application. Mat Sci Eng C-Bio S. 2009;29(5):1691-6.
169. Hermawan H, Purnama A, Dube D, Couet J, Mantovani D. Fe-Mn alloys for metallic biodegradable stents: Degradation and cell viability studies. Acta biomaterialia. 2010;6(5):1852-60.
170. Feyerabend F, Drucker H, Laipple D, Vogt C, Stekker M, Hort N, et al. Ion release from magnesium materials in physiological solutions under different oxygen tensions. J Mater Sci-Mater M. 2012;23(1):9-24.
171. Agha NA, Feyerabend F, Mihailova B, Heidrich S, Bismayer U, Willumeit-Romer R. Magnesium degradation influenced by buffering salts in concentrations typical of in vitro and in vivo models. Mat Sci Eng C-Mater. 2016;58:817-25.
172. Zhen Z, Xi TF, Zheng YF, Li L, Li LG. In Vitro Study on Mg-Sn-Mn Alloy as Biodegradable Metals. J Mater Sci Technol. 2014;30(7):675-85.
173. Zheng YF, Gu XN, Xi YL, Chai DL. In vitro degradation and cytotoxicity of Mg/Ca composites produced by powder metallurgy. Acta biomaterialia. 2010;6(5):1783-91.
174. Bowen PK, Drelich J, Goldman J. A new in vitro-in vivo correlation for bioabsorbable magnesium stents from mechanical behavior. Mat Sci Eng C-Mater. 2013;33(8):5064-70.
175. Yamamoto A, Hiromoto S. Effect of inorganic salts, amino acids and proteins on the degradation of pure magnesium in vitro. Mat Sci Eng C-Bio S. 2009;29(5):1559-68.
176. Song YW, Shan DY, Han EH. Electrodeposition of hydroxyapatite coating on AZ91D magnesium alloy for biomaterial application. Mater Lett. 2008;62(17-18):3276-9.
177. Yao ZP, Li LL, Jiang ZH. Adjustment of the ratio of Ca/P in the ceramic coating on Mg alloy by plasma electrolytic oxidation. Appl Surf Sci. 2009;255(13-14):6724-8.
178. Xin YC, Jiang J, Huo KF, Tang GY, Tian XB, Chu PK. Corrosion resistance and cytocompatibility of biodegradable surgical magnesium alloy coated with hydrogenated amorphous silicon. Journal of Biomedical Materials Research Part A. 2009;89a(3):717-26.
179. Kannan MB, Raman RKS. In vitro degradation and mechanical integrity of calcium-containing magnesium alloys in modified-simulated body fluid. Biomaterials. 2008;29(15):2306-14.
180. Gong HB, Anasori B, Dennison CR, Wang K, Kumbur EC, Strich R, et al. Fabrication, biodegradation behavior and cytotoxicity of Mg-nanodiamond composites for implant application. J Mater Sci-Mater M. 2015;26(2).
181. Seitz JM, Collier K, Wulf E, Bormann D, Angrisani N, Meyer-Lindenberg A, et al. The Effect of Different Sterilization Methods on the Mechanical Strength of Magnesium Based Implant Materials. Adv Eng Mater. 2011;13(12):1146-51.
182. Huan Z, Leeflang S, Zhou J, Zhai W, Chang J, Duszczyk J. In vitro degradation behavior and bioactivity of magnesium-Bioglass((R)) composites for orthopedic applications. Journal of biomedical materials research Part B, Applied biomaterials. 2012;100(2):437-46.
183. Hermawan H, Purnama A, Dube D, Couet J, Mantovani D. Fe-Mn alloys for metallic biodegradable stents: degradation and cell viability studies. Acta biomaterialia. 2010;6(5):1852-60.
184. Razavi M, Fathi M, Savabi O, Vashaee D, Tayebi L. In vivo biocompatibility of Mg implants surface modified by nanostructured merwinite/PEO. J Mater Sci-Mater M. 2015;26(5).
185. Cipriano AF, Sallee A, Guan RG, Zhao ZY, Tayoba M, Sanchez J, et al. Investigation of magnesium-zinc-calcium alloys and bone marrow derived mesenchymal stem cell response in direct culture. Acta biomaterialia. 2015;12:298-321.
186. Cecchinato F, Agha NA, Martinez-Sanchez AH, Luthringer BJC, Feyerabend F, Jimbo R, et al. Influence of Magnesium Alloy Degradation on Undifferentiated Human Cells. PloS one. 2015;10(11).
187. Yun YH, Dong ZY, Tan ZQ, Schulz MJ. Development of an electrode cell impedance method to measure osteoblast cell activity in magnesium-conditioned media. Analytical and bioanalytical chemistry. 2010;396(8):3009-15.
188. Fischer J, Profrock D, Hort N, Willumeit R, Feyerabend F. Improved cytotoxicity testing of magnesium materials. Mater Sci Eng B-Adv. 2011;176(11):830-4.
189. Hanzi AC, Gerber I, Schinhammer M, Loffler JF, Uggowitzer PJ. On the in vitro and in vivo degradation performance and biological response of new biodegradable Mg-Y-Zn alloys. Acta biomaterialia. 2010;6(5):1824-33.

190. Witte F, Feyerabend F, Maier P, Fischer J, Stormer M, Blawert C, et al. Biodegradable magnesium-hydroxyapatite metal matrix composites. Biomaterials. 2007;28(13):2163-74.
191. Wang YB, Xie XH, Li HF, Wang XL, Zhao MZ, Zhang EW, et al. Biodegradable CaMgZn bulk metallic glass for potential skeletal application. Acta biomaterialia. 2011;7(8):3196-208.
192. Wang J, Witte F, Xi T, Zheng Y, Yang K, Yang Y, et al. Recommendation for modifying current cytotoxicity testing standards for biodegradable magnesium-based materials. Acta biomaterialia. 2015;21:237-49.
193. Wu LL, Luthringer BJC, Feyerabend F, Schilling AF, Willumeit R. Effects of extracellular magnesium on the differentiation and function of human osteoclasts. Acta biomaterialia. 2014;10(6):2843-54.
194. Burmester A, Luthringer B, Willumeit R, Feyerabend F. Comparison of the reaction of bone-derived cells to enhanced MgCl2-salt concentrations. Biomatter. 2014;4:e967616.
195. Huan ZG, Leeflang MA, Zhou J, Fratila-Apachitei LE, Duszczyk J. In vitro degradation behavior and cytocompatibility of Mg-Zn-Zr alloys. Journal of materials science Materials in medicine. 2010;21(9):2623-35.
196. Gu XN, Xie XH, Li N, Zheng YF, Qin L. In vitro and in vivo studies on a Mg-Sr binary alloy system developed as a new kind of biodegradable metal. Acta biomaterialia. 2012;8(6):2360-74.
197. Wang JL, Witte F, Xi TF, Zheng YF, Yang K, Yang YS, et al. Recommendation for modifying current cytotoxicity testing standards for biodegradable magnesium-based materials. Acta biomaterialia. 2015;21:237-49.
198. Barry FP, Murphy JM. Mesenchymal stem cells: clinical applications and biological characterization. Int J Biochem Cell B. 2004;36(4):568-84.
199. Caplan AI, Bruder SP. Mesenchymal stem cells: building blocks for molecular medicine in the 21st century. Trends Mol Med. 2001;7(6):259-64.
200. Dominici M, Le Blanc K, Mueller I, Slaper-Cortenbach I, Marini FC, Krause DS, et al. Minimal criteria for defining multipotent mesenchymal stromal cells. The International Society for Cellular Therapy position statement. Cytotherapy. 2006;8(4):315-7.
201. Kulterer B, Friedl G, Jandrositz A, Sanchez-Cabo F, Prokesch A, Paar C, et al. Gene expression profiling of human mesenchymal stem cells derived from bone marrow during expansion and osteoblast differentiation. Bmc Genomics. 2007;8.
202. Strauss PG, Closs EI, Schmidt J, Erfle V. Gene-Expression during Osteogenic Differentiation in Mandibular Condyles Invitro. Journal of Cell Biology. 1990;110(4):1369-78.
203. Marom R, Shur I, Solomon R, Benayahu D. Characterization of adhesion and differentiation markers of osteogenic marrow stromal cells. J Cell Physiol. 2005;202(1):41-8.
204. Sudo H, Kodama HA, Amagai Y, Yamamoto S, Kasai S. In vitro differentiation and calcification in a new clonal osteogenic cell line derived from newborn mouse calvaria. The Journal of cell biology. 1983;96(1):191-8.
205. Hu Y, Cai KY, Luo Z, Zhang Y, Li LQ, Lai M, et al. Regulation of the differentiation of mesenchymal stem cells in vitro and osteogenesis in vivo by microenvironmental modification of titanium alloy surfaces. Biomaterials. 2012;33(13):3515-28.
206. Zhao ZR, Zhao M, Xiao GZ, Franceschi RT. Gene transfer of the Runx2 transcription factor enhances osteogenic activity of bone marrow stromal cells in vitro and in vivo. Mol Ther. 2005;12(2):247-53.
207. Banerjee C, McCabe LR, Choi JY, Hiebert SW, Stein JL, Stein GS, et al. Runt homology domain proteins in osteoblast differentiation: AML3/CBFA1 is a major component of a bone-specific complex. Journal of Cellular Biochemistry. 1997;66(1):1-8.
208. Ducy P, Zhang R, Geoffroy V, Ridall AL, Karsenty G. Osf2/Cbfa1: A transcriptional activator of osteoblast differentiation. J Bone Miner Res. 1997;12:P202-P.
209. Pavlin D, Zadro R, Gluhak-Heinrich J. Temporal pattern of stimulation of osteoblast-associated genes during mechanically-induced osteogenesis in vivo: Early responses of osteocalcin and type I collagen. Connective tissue research. 2001;42(2):135-+.
210. Lebaron RG, Athanasiou KA. Extracellular matrix cell adhesion peptides: Functional applications in orthopedic materials. Tissue Eng. 2000;6(2):85-103.

211. Mizuno M, Fujisawa R, Kuboki Y. Type I collagen-induced osteoblastic differentiation of bone-marrow cells mediated by collagen-alpha 2 beta 1 integrin interaction. J Cell Physiol. 2000;184(2):207-13.
212. Jikko A, Harris SE, Chen D, Mendrick DL, Damsky CH. Collagen integrin receptors regulate early osteoblast differentiation induced by BMP-2. J Bone Miner Res. 1999;14(7):1075-83.
213. Merry K, Dodds R, Littlewood A, Gowen M. Expression of Osteopontin Messenger-Rna by Osteoclasts and Osteoblasts in Modeling Adult Human Bone. J Cell Sci. 1993;104:1013-20.
214. Chen Q, Shou PS, Zhang LY, Xu CL, Zheng CX, Han YY, et al. An Osteopontin-Integrin Interaction Plays a Critical Role in Directing Adipogenesis and Osteogenesis by Mesenchymal Stem Cells. Stem Cells. 2014;32(2):327-37.
215. Simonet WS, Lacey DL, Dunstan CR, Kelley M, Chang MS, Luthy R, et al. Osteoprotegerin: A novel secreted protein involved in the regulation of bone density. Cell. 1997;89(2):309-19.
216. Mostofi S, Bonyadi Rad E, Wiltsche H, Fasching U, Szakacs G, Ramskogler C, et al. Effects of Corroded and Non-Corroded Biodegradable Mg and Mg Alloys on Viability, Morphology and Differentiation of MC3T3-E1 Cells Elicited by Direct Cell/Material Interaction. PloS one. 2016;11(7):e0159879.
217. Duan K, Wang RZ. Surface modifications of bone implants through wet chemistry. J Mater Chem. 2006;16(24):2309-21.
218. Ercan B, Kummer KM, Tarquinio KM, Webster TJ. Decreased Staphylococcus aureus biofilm growth on anodized nanotubular titanium and the effect of electrical stimulation. Acta biomaterialia. 2011;7(7):3003-12.
219. Campoccia D, Montanaro L, Arciola CR. The significance of infection related to orthopedic devices and issues of antibiotic resistance. Biomaterials. 2006;27(11):2331-9.
220. Fey PD, Olson ME. Current concepts in biofilm formation of Staphylococcus epidermidis. Future Microbiol. 2010;5(6):917-33.
221. Lister JL, Horswill AR. Staphylococcus aureus biofilms: recent developments in biofilm dispersal. Front Cell Infect Mi. 2014;4.
222. Chevalier J, Gremillard L. Ceramics for medical applications: A picture for the next 20 years. J Eur Ceram Soc. 2009;29(7):1245-55.
223. Zilberman M, Elsner JJ. Antibiotic-eluting medical devices for various applications. Journal of Controlled Release. 2008;130(3):202-15.
224. Trampuz A, Osmon DR, Hanssen AD, Steckelberg JM, Patel R. Molecular and antibiofilm approaches to prosthetic joint infection. Clin Orthop Relat Res. 2003(414):69-88.
225. Davies D. Understanding biofilm resistance to antibacterial agents. Nat Rev Drug Discov. 2003;2(2):114-22.
226. Gristina AG, Naylor P, Myrvik Q. Infections from biomaterials and implants: a race for the surface. Med Prog Technol. 1988;14(3-4):205-24.
227. Bostman O, Pihlajamaki H. Clinical biocompatibility of biodegradable orthopaedic implants for internal fixation: a review. Biomaterials. 2000;21(24):2615-21.
228. Olesik JW. Elemental Analysis Using Icp-Oes and Icp Ms - an Evaluation and Assessment of Remaining Problems. Analytical chemistry. 1991;63(1):A12-A21.
229. Laskin A, Cowin JP. Automated single particle SEM/EDX analysis of submicrometer particles down to 0.1 mu m. Analytical chemistry. 2001;73(5):1023-9.
230. Kalajzic I, Terzic J, Rumboldt Z, Mack K, Naprta A, Ledgard F, et al. Osteoblastic response to the defective matrix in the osteogenesis imperfecta murine (oim) mouse. Endocrinology. 2002;143(5):1594-601.
231. Sheikh Z, Najeeb S, Khurshid Z, Verma V, Rashid H, Glogauer M. Biodegradable Materials for Bone Repair and Tissue Engineering Applications. Materials. 2015;8(9):5744-94.
232. Toba Y, Kajita Y, Masuyama R, Takada Y, Suzuki K, Aoe S. Dietary magnesium supplementation affects bone metabolism and dynamic strength of bone in ovariectomized rats. Journal of Nutrition. 2000;130(2):216-20.
233. Witte F, Fischer J, Nellesen J, Crostack HA, Kaese V, Pisch A, et al. In vitro and in vivo corrosion measurements of magnesium alloys. Biomaterials. 2006;27(7):1013-8.

234. Agha NA, Willumeit-Romer R, Laipple D, Luthringer B, Feyerabend F. The Degradation Interface of Magnesium Based Alloys in Direct Contact with Human Primary Osteoblast Cells. PloS one. 2016;11(6).
235. Liu C, Fu XK, Pan HB, Wan P, Wang L, Tan LL, et al. Biodegradable Mg-Cu alloys with enhanced osteogenesis, angiogenesis, and long-lasting antibacterial effects. Sci Rep-Uk. 2016;6.
236. Salahshoor M, Guo YB. Biodegradable Orthopedic Magnesium-Calcium (MgCa) Alloys, Processing, and Corrosion Performance. Materials. 2012;5(1):135-55.
237. Chou DT, Hong D, Saha P, Ferrero J, Lee B, Tan ZQ, et al. In vitro and in vivo corrosion, cytocompatibility and mechanical properties of biodegradable Mg-Y-Ca-Zr alloys as implant materials. Acta biomaterialia. 2013;9(10):8518-33.
238. Gu XN, Zheng YF, Chen LJ. Influence of artificial biological fluid composition on the biocorrosion of potential orthopedic Mg-Ca, AZ31, AZ91 alloys. Biomedical Materials. 2009;4(6).
239. Xu RZ, Yang XB, Li PH, Suen KW, Wu S, Chu PK. Eelectrochemical properties and corrosion resistance of carbon-ion-implanted magnesium. Corros Sci. 2014;82:173-9.
240. Zhen Z, Xi TF, Zheng YF. A review on in vitro corrosion performance test of biodegradable metallic materials. T Nonferr Metal Soc. 2013;23(8):2283-93.
241. Xin YC, Huo KF, Tao H, Tang GY, Chu PK. Influence of aggressive ions on the degradation behavior of biomedical magnesium alloy in physiological environment. Acta biomaterialia. 2008;4(6):2008-15.
242. Zeng RC, Dietzel W, Witte F, Hort N, Blawert C. Progress and challenge for magnesium alloys as biomaterials. Adv Eng Mater. 2008;10(8):B3-B14.
243. Yang L, Hort N, Willumeit R, Feyerabend F. Effects of corrosion environment and proteins on magnesium corrosion. Corros Eng Sci Techn. 2012;47(5):335-9.
244. Willumeit R, Fischer J, Feyerabend F, Hort N, Bismayer U, Heidrich S, et al. Chemical surface alteration of biodegradable magnesium exposed to corrosion media. Acta biomaterialia. 2011;7(6):2704-15.
245. Chen ZT, Mao XL, Tan LL, Friis T, Wu CT, Crawford R, et al. Osteoimmunomodulatory properties of magnesium scaffolds coated with beta-tricalcium phosphate. Biomaterials. 2014;35(30):8553-65.
246. Wang JL, Tang J, Zhang P, Li YD, Wang J, Lai YX, et al. Surface modification of magnesium alloys developed for bioabsorbable orthopedic implants: A general review. J Biomed Mater Res B. 2012;100b(6):1691-701.
247. Willumeit R, Mohring A, Feyerabend F. Optimization of cell adhesion on mg based implant materials by pre-incubation under cell culture conditions. International journal of molecular sciences. 2014;15(5):7639-50.
248. Ye X, Chen M, Yang M, Wei J, Liu D. In vitro corrosion resistance and cytocompatibility of nano-hydroxyapatite reinforced Mg-Zn-Zr composites. Journal of materials science Materials in medicine. 2010;21(4):1321-8.
249. Ostrowski N, Lee B, Enick N, Carlson B, Kunjukunju S, Roy A, et al. Corrosion protection and improved cytocompatibility of biodegradable polymeric layer-by-layer coatings on AZ31 magnesium alloys. Acta biomaterialia. 2013;9(10):8704-13.
250. Fischer J, Prosenc MH, Wolff M, Hort N, Willumeit R, Feyerabend F. Interference of magnesium corrosion with tetrazolium-based cytotoxicity assays. Acta biomaterialia. 2010;6(5):1813-23.
251. Wang XH, Huang J, Wang K, Neufurth M, Schroder HC, Wang SF, et al. The morphogenetically active polymer, inorganic polyphosphate complexed with GdCl3, as an inducer of hydroxyapatite formation in vitro. Biochem Pharmacol. 2016;102:97-106.
252. Song Y, Zhang S, Li J, Zhao C, Zhang X. Electrodeposition of Ca-P coatings on biodegradable Mg alloy: in vitro biomineralization behavior. Acta biomaterialia. 2010;6(5):1736-42.
253. Hagihara K, Fujii K, Matsugaki A, Nakano T. Possibility of Mg- and Ca-based intermetallic compounds as new biodegradable implant materials. Materials science & engineering C, Materials for biological applications. 2013;33(7):4101-11.

254. Wong HM, Yeung KW, Lam KO, Tam V, Chu PK, Luk KD, et al. A biodegradable polymer-based coating to control the performance of magnesium alloy orthopaedic implants. Biomaterials. 2010;31(8):2084-96.
255. Pichler K, Kraus T, Martinelli E, Sadoghi P, Musumeci G, Uggowitzer PJ, et al. Cellular reactions to biodegradable magnesium alloys on human growth plate chondrocytes and osteoblasts. International orthopaedics. 2014;38(4):881-9.
256. Hong D, Saha P, Chou DT, Lee B, Collins BE, Tan Z, et al. In vitro degradation and cytotoxicity response of Mg-4% Zn-0.5% Zr (ZK40) alloy as a potential biodegradable material. Acta biomaterialia. 2013;9(10):8534-47.
257. Wang YB, Xie XH, Li HF, Wang XL, Zhao MZ, Zhang EW, et al. Biodegradable CaMgZn bulk metallic glass for potential skeletal application. Acta biomaterialia. 2011;7(8):3196-208.
258. Burmester A, Luthringer B, Willumeit R, Feyerabend F. Comparison of the reaction of bone-derived cells to enhanced MgCl2-salt concentrations. Biomatter. 2014;4(1):e967616.
259. Yun Y, Dong Z, Tan Z, Schulz MJ. Development of an electrode cell impedance method to measure osteoblast cell activity in magnesium-conditioned media. Analytical and bioanalytical chemistry. 2010;396(8):3009-15.
260. Li H, Pan H, Ning C, Tan G, Liao J, Ni G. Magnesium with micro-arc oxidation coating and polymeric membrane: an in vitro study on microenvironment. Journal of materials science Materials in medicine. 2015;26(3):147.
261. Cipriano AF, Sallee A, Guan RG, Zhao ZY, Tayoba M, Sanchez J, et al. Investigation of magnesium-zinc-calcium alloys and bone marrow derived mesenchymal stem cell response in direct culture. Acta biomaterialia. 2015;12:298-321.
262. Wu L, Luthringer BJ, Feyerabend F, Schilling AF, Willumeit R. Effects of extracellular magnesium on the differentiation and function of human osteoclasts. Acta biomaterialia. 2014;10(6):2843-54.
263. Niederlaender J, Walter M, Krajewski S, Schweizer E, Post M, Schille C, et al. Cytocompatibility evaluation of different biodegradable magnesium alloys with human mesenchymal stem cells. Journal of materials science Materials in medicine. 2014;25(3):835-43.
264. Ciobanasu C, Faivre B, Le Clainche C. Actin dynamics associated with focal adhesions. Int J Cell Biol. 2012;2012:941292.
265. Zhao Y, Jamesh MI, Li WK, Wu G, Wang C, Zheng Y, et al. Enhanced antimicrobial properties, cytocompatibility, and corrosion resistance of plasma-modified biodegradable magnesium alloys. Acta biomaterialia. 2014;10(1):544-56.
266. Razavi M, Fathi M, Savabi O, Hashemi Beni B, Vashaee D, Tayebi L. Surface microstructure and in vitro analysis of nanostructured akermanite (Ca2MgSi2O7) coating on biodegradable magnesium alloy for biomedical applications. Colloids and surfaces B, Biointerfaces. 2014;117:432-40.
267. Jo JH, Kang BG, Shin KS, Kim HE, Hahn BD, Park DS, et al. Hydroxyapatite coating on magnesium with MgF(2) interlayer for enhanced corrosion resistance and biocompatibility. Journal of materials science Materials in medicine. 2011;22(11):2437-47.
268. Tian P, Liu X, Ding C. In vitro degradation behavior and cytocompatibility of biodegradable AZ31 alloy with PEO/HT composite coating. Colloids and surfaces B, Biointerfaces. 2015;128:44-54.
269. Walker J, Shadanbaz S, Woodfield TB, Staiger MP, Dias GJ. The in vitro and in vivo evaluation of the biocompatibility of Mg alloys. Biomed Mater. 2014;9(1):015006.
270. Mueller WD, de Mele MFL, Nascimento ML, Zeddies M. Degradation of magnesium and its alloys: Dependence on the composition of the synthetic biological media. Journal of Biomedical Materials Research Part A. 2009;90a(2):487-95.
271. Wang L, Shinohara T, Zhang BP. Influence of chloride, sulfate and bicarbonate anions on the corrosion behavior of AZ31 magnesium alloy. J Alloy Compd. 2010;496(1-2):500-7.
272. Xin Y, Huo K, Tao H, Tang G, Chu PK. Influence of aggressive ions on the degradation behavior of biomedical magnesium alloy in physiological environment. Acta biomaterialia. 2008;4(6):2008-15.
273. Yoshizawa S, Brown A, Barchowsky A, Sfeir C. Magnesium ion stimulation of bone marrow stromal cells enhances osteogenic activity, simulating the effect of magnesium alloy degradation. Acta biomaterialia. 2014;10(6):2834-42.

274. Yoshizawa S, Brown A, Barchowsky A, Sfeir C. Role of magnesium ions on osteogenic response in bone marrow stromal cells. Connective tissue research. 2014;55 Suppl 1:155-9.
275. Yang C, Yuan G, Zhang J, Tang Z, Zhang X, Dai K. Effects of magnesium alloys extracts on adult human bone marrow-derived stromal cell viability and osteogenic differentiation. Biomed Mater. 2010;5(4):045005.
276. Dou YN, Mujeeb A, Zheng YF, Ge ZG. Optimization of dual effects of Mg-1Ca alloys on the behavior of chondrocytes and osteoblasts in vitro. Prog Nat Sci-Mater. 2014;24(5):433-40.
277. Fujita T, Azuma Y, Fukuyama R, Hattori Y, Yoshida C, Koida M, et al. Runx2 induces osteoblast and chondrocyte differentiation and enhances their migration by coupling with PI3K-Akt signaling. The Journal of cell biology. 2004;166(1):85-95.
278. Birmingham E, Niebur GL, McHugh PE, Shaw G, Barry FP, McNamara LM. Osteogenic differentiation of mesenchymal stem cells is regulated by osteocyte and osteoblast cells in a simplified bone niche. European cells & materials. 2012;23:13-27.
279. Quarles LD, Yohay DA, Lever LW, Caton R, Wenstrup RJ. Distinct proliferative and differentiated stages of murine MC3T3-E1 cells in culture: an in vitro model of osteoblast development. J Bone Miner Res. 1992;7(6):683-92.
280. Mygind T, Stiehler M, Baatrup A, Li H, Zoua X, Flyvbjerg A, et al. Mesenchymal stem cell ingrowth and differentiation on coralline hydroxyapatite scaffolds. Biomaterials. 2007;28(6):1036-47.
281. Depprich R, Ommerborn M, Zipprich H, Naujoks C, Handschel J, Wiesmann HP, et al. Behavior of osteoblastic cells cultured on titanium and structured zirconia surfaces. Head & face medicine. 2008;4:29.
282. Langenbach F, Handschel J. Effects of dexamethasone, ascorbic acid and beta-glycerophosphate on the osteogenic differentiation of stem cells in vitro. Stem Cell Res Ther. 2013;4.
283. Ribeiro M, Monteiro FJ, Ferraz MP. Infection of orthopedic implants with emphasis on bacterial adhesion process and techniques used in studying bacterial-material interactions. Biomatter. 2012;2(4):176-94.

Appendix

Rights and Permissions

Figure 1

Order Completed

Thank you for your order.

This Agreement between Meduni Graz -- Sepideh Mostofi ("You") and Nature Publishing Group ("Nature Publishing Group") consists of your license details and the terms and conditions provided by Nature Publishing Group and Copyright Clearance Center.

Your confirmation email will contain your order number for future reference.

Printable details.

License Number	3985840081573
License date	Nov 11, 2016
Licensed Content Publisher	Nature Publishing Group
Licensed Content Publication	Nature Reviews Rheumatology
Licensed Content Title	Fracture healing: mechanisms and interventions
Licensed Content Author	Thomas A. Einhorn, Louis C. Gerstenfeld
Licensed Content Date	Sep 30, 2014
Licensed Content Volume	11
Licensed Content Issue	1
Type of Use	reuse in a dissertation / thesis
Requestor type	non-commercial (non-profit)
Format	electronic
Portion	figures/tables/illustrations
Number of figures/tables/illustrations	1
High-res required	no
Figures	Figure 2
Author of this NPG article	no
Your reference number	
Title of your thesis / dissertation	CELLULAR AND MOLECULAR REACTIONS OF PRE-OSTEOBLASTS TO DIFFERENT MAGNESIUM IMPLANTS
Expected completion date	Jan 2017
Estimated size (number of pages)	175
Requestor Location	Meduni Graz Stiftingtalstrasse 24 Graz, 8010 Austria Attn: Sepideh Mostofi
Customer VAT ID	ATU57511179
Billing Type	Invoice
Billing address	Meduni Graz Stiftingtalstrasse 2 Graz, Austria 8010 Attn: Sepideh Mostofi
Total	0.00 EUR

Figure 2

Copyright Clearance Center RightsLink®

Home | Account Info | Help

Title: Magnesium alloys for temporary implants in osteosynthesis: In vivo studies of their degradation and interaction with bone

Author: Tanja Kraus,Stefan F. Fischerauer,Anja C. Hänzi,Peter J. Uggowitzer,Jörg F. Löffler,Annelie M. Weinberg

Publication: Acta Biomaterialia

Publisher: Elsevier

Date: March 2012

Logged in as:
Sepideh Mostofi
Meduni Graz
Account #:
3001080030

LOGOUT

Order Completed

Thank you for your order.

This Agreement between Meduni Graz -- Sepideh Mostofi ("You") and Elsevier ("Elsevier") consists of your license details and the terms and conditions provided by Elsevier and Copyright Clearance Center.

Your confirmation email will contain your order number for future reference.

Printable details.

License Number	3985871111212
License date	Nov 11, 2016
Licensed Content Publisher	Elsevier
Licensed Content Publication	Acta Biomaterialia
Licensed Content Title	Magnesium alloys for temporary implants in osteosynthesis: In vivo studies of their degradation and interaction with bone
Licensed Content Author	Tanja Kraus,Stefan F. Fischerauer,Anja C. Hänzi,Peter J. Uggowitzer,Jörg F. Löffler,Annelie M. Weinberg
Licensed Content Date	March 2012
Licensed Content Volume	8
Licensed Content Issue	3
Licensed Content Pages	9
Type of Use	reuse in a thesis/dissertation
Portion	figures/tables/illustrations
Number of figures/tables/illustrations	2
Format	electronic
Are you the author of this Elsevier article?	No
Will you be translating?	No
Order reference number	
Original figure numbers	Figure 2, 3
Title of your thesis/dissertation	CELLULAR AND MOLECULAR REACTIONS OF PRE-OSTEOBLASTS TO DIFFERENT MAGNESIUM IMPLANTS
Expected completion date	Jan 2017
Estimated size (number of pages)	175
Elsevier VAT number	GB 494 6272 12
Requestor Location	Meduni Graz Stiftingtalstrasse 24 Graz, 8010 Austria Attn: Sepideh Mostofi
Customer VAT ID	ATU57511179
Total	0.00 EUR

Figure 3

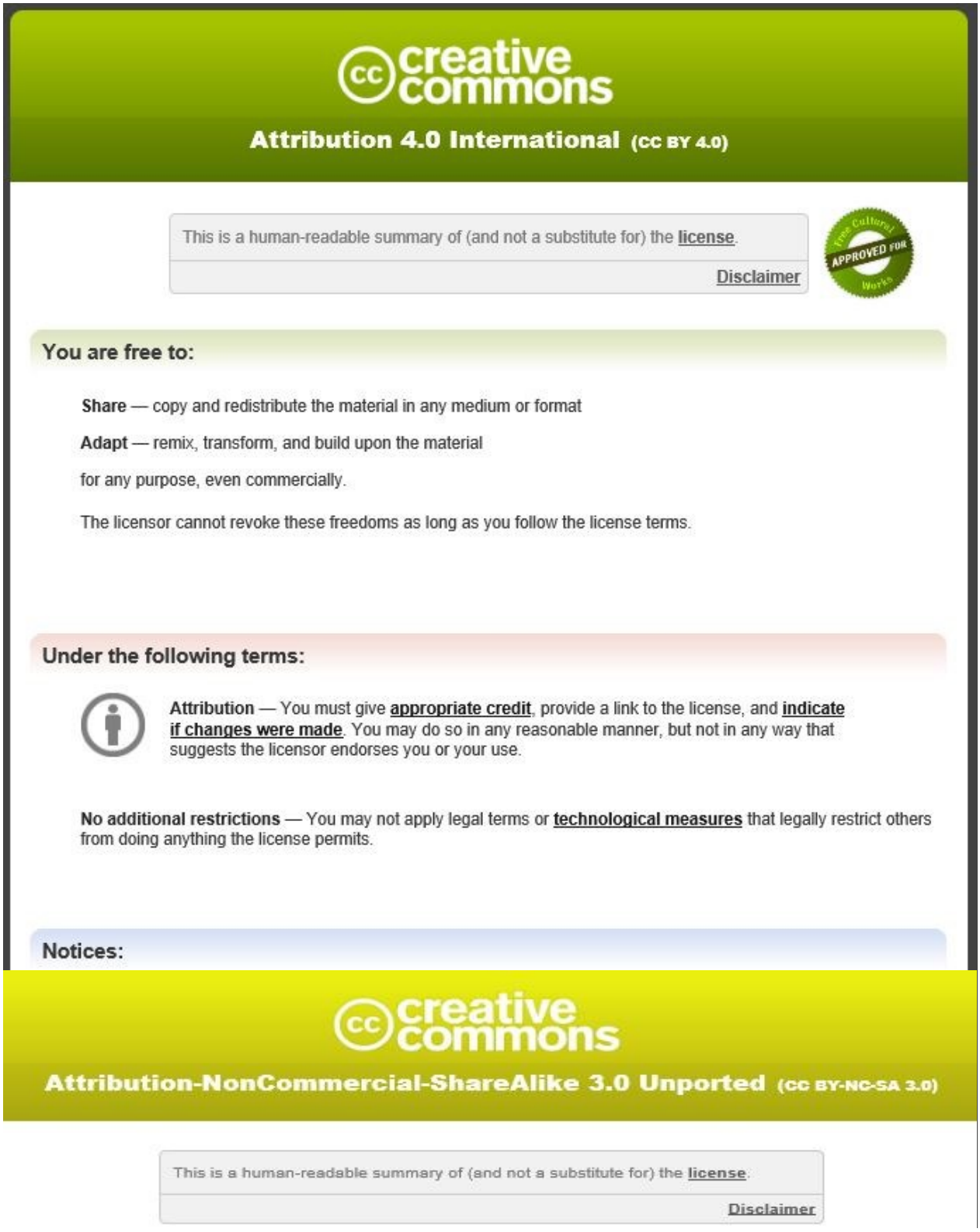
creative commons
Attribution 4.0 International (CC BY 4.0)
This is a human-readable summary of (and not a substitute for) the license.
Disclaimer
You are free to:
Share — copy and redistribute the material in any medium or format
Adapt — remix, transform, and build upon the material
for any purpose, even commercially.
The licensor cannot revoke these freedoms as long as you follow the license terms.
Under the following terms:
Attribution — You must give appropriate credit, provide a link to the license, and indicate if changes were made. You may do so in any reasonable manner, but not in any way that suggests the licensor endorses you or your use.
No additional restrictions — You may not apply legal terms or technological measures that legally restrict others from doing anything the license permits.
Notices:
creative commons
Attribution-NonCommercial-ShareAlike 3.0 Unported (CC BY-NC-SA 3.0)
This is a human-readable summary of (and not a substitute for) the license.
Disclaimer
You are free to:
Share — copy and redistribute the material in any medium or format
Adapt — remix, transform, and build upon the material
The licensor cannot revoke these freedoms as long as you follow the license terms.

Figures 5-8, 10-11, 13-14, 16-30, 33-39 & Tables 2, 5-7

Figures 5-8, 10-11, 13-14, 16-30, 33-39 & Tables 2, 5-7

Citation: Mostofi S, Bonyadi Rad E, Wiltsche H, Fasching U, Szakacs G, Ramskogler C, et al. (2016) Effects of Corroded and Non-Corroded Biodegradable Mg and Mg Alloys on Viability, Morphology and Differentiation of MC3T3-E1 Cells Elicited by Direct Cell/Material Interaction. PLoS ONE 11(7): e0159879. doi:10.1371/journal.pone.0159879

Editor: Donghui Zhu, University of North Texas, UNITED STATES

Received: March 17, 2016; **Accepted:** July 8, 2016; **Published:** July 26, 2016